INVESTIGATING THE STRUCTURE-FUNCTION RELATIONSHIP OF ANTI-MITOTIC NATURAL PRODUCTS IN CANADIAN PRAIRIE PLANTS

SHANNON HEALY KNIBB
B.Sc. Biological Sciences (Honours), University of Lethbridge

A Thesis
Submitted to the School of Graduate Studies
of the University of Lethbridge
in Partial Fulfilment of the
Requirements for the Degree

MASTER OF SCIENCE

Department of Biological Sciences
University of Lethbridge
LETHBRIDGE, ALBERTA, CANADA

INVESTIGATING THE STRUCTURE-FUNCTION RELATIONSHIP OF ANTI-MITOTIC NATURAL PRODUCTS IN CANADIAN PRAIRIE PLANTS

SHANNON HEALY KNIBB

Date of defense: April 3rd, 2024

Dr. Roy Golsteyn Thesis Supervisor	Professor	Ph.D.
Dr. Nehal Thakor Thesis Examination Committee Member	Professor	Ph.D.
Dr. Jean-Denys Hamel Thesis Examination Committee Member	Assistant Professor	Ph.D.
Dr. Dmytro Yevtushenko Chair, Thesis Examination Committee	Associate Professor	Ph.D.

ABSTRACT

This thesis investigates Canadian prairie plants as sources of natural product compounds capable of inhibiting human cell division. Natural products present an opportunity to identify novel anti-mitotic compounds to address the lack of known inhibitors for many mitotic regulatory proteins. By biology-guided fractionation, we purified the natural products anemonin from *Pulsatilla nuttalliana* and (+)-6-tuliposide A from *Erythronium grandiflorum*, and this is the first report of their anti-mitotic activities. We then conducted a comparative study between pulchelloid A (from *Gaillardia aristata*), anemonin and (+)-6-tuliposide A, and identified unique mitotic arrest profiles, suggesting distinct protein targets and mechanisms of action consistent with the widespread relationship between structure and function in biology. The discovery of natural product inhibitors from Canadian prairie plant species holds tremendous potential for advancing our understanding of mitotic regulation and contributes to the development of targeted treatments for precision medicine.

PREFACE

A version of Chapter 3 has been submitted to the journal "*Fitoterapia*" for publication. Healy Knibb, S. M., Yeremy, B., Williams, D. E., Andersen, R. J., Golsteyn, R. M. An anti-mitotic compound, (+)-6-tuliposide A, isolated from the Canadian Glacier Lily, *Erythronium grandiflorum*.

Contribution of Authors (Chapter 3):

Shannon M. Healy Knibb: Conceptualization, Biological Investigation, Writing

Benjamin Yeremy: Chemical Investigation

David E. Williams: Chemical Investigation

Raymond J. Andersen: Chemical Investigation

Roy M. Golsteyn: Conceptualization, Supervision, Funding Acquisition, Writing

ACKNOWLEDGEMENTS

I am extremely grateful for the incredible research experience I have gained throughout my master's degree, all made possible by the support of my supervisor Dr. Roy Golsteyn. Thank you for providing me with incredible opportunities, and for investing your time and energy into my professional development. Sharing your knowledge, advice, and passion for science, as well as your positivity, mentorship, and encouragement to aspire for greater heights have served as catalysts for a successful launch into my career as a scientist.

I extend my appreciation to my committee members Dr. Nehal Thakor and Dr. Jean-Denys Hamel for their support and advice throughout my graduate studies, Dr. Dmytro Yevtushenko for acting as chair and Dr. Angeliki Pantazi as an initial member of my committee. I am grateful to Dr. Raymond Andersen, Ben Yeremy, and Dr. David Williams for their collaboration in the isolation of the natural products investigated in this thesis.

Thank you to the past and present members of the Natural Product Laboratory Tanner Lockwood, Larissa Smith, David Witten, Brinnley Zanewich, Haley Allard, Araba Sagoe-Wagner, Nadia Hand, and Dr. Sophie Kernéis; their camaraderie and assistance in the lab made my graduate studies experience so much fun! I would also like to extend a thank you to all members of the Biological Sciences Department for their guidance, shaping me not only as a researcher, but as a teacher, leader, and colleague.

This achievement would not have been possible without the unwavering moral support and love of my family and friends. I will be forever grateful to my parents Lloyd and Kelly for always supporting my education, my sister Katelynn who I look up, my in-laws Parker, Jenn, Diane, and Jason, and my friends Keeley, Tamara, Madi and Hunter. And of course, to my husband and best friend Austin, thank you for supporting me every single day of this master's degree, for your unconditional love, and for believing in me.

TABLE OF CONTENTS

LIST OF TABLES

LIST OF FIGURES

LIST OF ABBREVIATIONS

6-OAP	6-O-angeloylplenolin
ANOVA	one-way analysis of variance
APC/C	anaphase-promoting complex/cyclosome
ATCC	American Type Culture Collection
ATM	ataxia telangiectasia mutated kinase
ATP	adenosine triphosphate
β-ME	beta-mercaptoethanol
BRT-1	bubristatin-1
BSA	bovine serum albumin
Bub3	budding uninhibited by benzimidazole protein 3
BubR1	budding uninhibited by benzimidazole related protein 1
Cdc20	cell division cycle protein 20
CDK	cyclin-dependent kinase
CENP-E	centromere-associated protein E
CENP-F	centromere-associated protein F
C-Nap1	centrosomal Nek2-associated protein 1
CPT	camptothecin
DAPI	4′,6-diamidino-2-phenylindole
DCM	dichloromethane
DMSO	dimethyl sulfoxide
DNA	deoxyribonucleic acid
DPT	4-deoxypodophyllotoxin
EDTA	ethylenediaminetetraacetic acid
EGTA	ethylene glycol bis-(2-aminoethylether)-*N*,*N*,*N*',*N*'-tetraacetic acid
EKA	*ent*-15-oxokaurenoic acid
EtOH	ethanol
FBS	fetal bovine serum
G0	resting phase
G1 phase	gap 1 phase
G2 phase	gap 2 phase
h	hour
HEPES	4-(2-hydroxyethyl)-1-piperazineethanesulfonic acid
HPLC	high-performance liquid chromatography
HRESIMS	high-resolution electrospray ionization mass spectrometry
HT-29	human colorectal adenocarcinoma cell line
IC_{50}	half-maximal inhibitory concentration
INCENP	inner centromere protein
Int	interphasic cell population
M phase	mitotic phase
Mad2	mitotic-arrest deficient protein 2
MCC	mitotic checkpoint complex
min	minute
Mit	mitotic cell population
MS	mass spectrometry
Msp-1	multipolar kinase-1

MTOC	microtubule-organizing centre
MTT	3-(4,5-dimethylthiazol-2-yl)-2,5-diphenyltetrazolium
Myr	million years
Nek2	never in mitosis-A related protein 2
NMR	nuclear magnetic resonance
NT	not-treated
OZ	13-hydroxy-15-oxozoapatlin
P	phosphate
PBS	phosphate buffered saline
PCM	pericentriolar material
PH3	phospho-histone H3
PLK-1	polo-like kinase 1
PLK-4	polo-like kinase 4
RanBP2	Ran binding protein 2
RanGAP1	Ran GTPase activating protein 1
RNA	ribonucleic acid
RNAi	RNA interference
S phase	DNA synthesis phase
SAC	spindle assembly checkpoint
SCF	Skp1-Cullin-F-box
SEM	standard error of the mean
SDS	sodium dodecyl sulfate
Skp-1	S-phase kinase-associated protein 1
Tot	total cell population
Ub	ubiquitin
U2OS	human osteosarcoma cell line
v	volume
WI-38	human non-cancerous lung fibroblast cell line

CHAPTER 1

General Introduction

This thesis investigates natural products from Canadian prairie plants with the ability to arrest human cancer cells in mitosis. The discovery of anti-mitotic compounds can help address the lack of known inhibitors for many mitotic regulatory proteins. Our laboratory launched the Prairie to Pharmacy program aiming to identify plant-derived chemical compounds that can be used as tools to investigate vital cellular pathways and potentially become medicines. Recent investigations have focused on the Asteraceae plant family, renowned for its sesquiterpene lactones, which led to the identification of two anti-mitotic compounds: pulchelloid A from *Gaillardia aristata* (Bosco et al., 2021) and hymenoratin from *Hymenoxys richardsonii* (Molina et al., 2021). Extending our exploration beyond the Asteraceae family, we discovered that *Pulsatilla nuttalliana* (Ranunculaceae) contained anemonin which exhibited anti-mitotic effects akin to pulchelloid A and hymenoratin. This prompted us to explore phylogenetic distance as an opportunity to identify chemically diverse anti-mitotic compounds. We then examined the most phylogenetically distant species relative to the Asteraceae family within our library of native Canadian prairie plants, *Erythronium grandiflorum* (Liliaceae), and identified (+)-6-tuliposide A which induced similar mitotic arrest phenotypes to the three compounds mentioned above. Finally, the relationship between structure and function in biology suggests that each compound targets a different cellular protein and thus may act via a unique mechanism of action. To investigate this, we conducted a comparative study of pulchelloid A, anemonin and (+)-6-tuliposide A to identify distinctions between their mitotic inhibition and the typical progression of mitosis. This is the first report to attribute anti-mitotic activities to anemonin and (+)-6-tuliposide A, and provide evidence to

distinguish the mitotic arrests induced by pulchelloid A, anemonin and (+)-6-tuliposide A. The discovery of natural product inhibitors, particularly those sourced from Canadian prairie plant species, holds tremendous potential for advancing our understanding of mitotic regulation and contributes to the development of targeted therapies for precision medicine.

1.1 Natural Products

Natural products encompass a large, structurally diverse class of organic compounds synthesized by plant, microbial and marine organisms, offering a rich repertoire of compounds with unique biological activities. These are typically secondary metabolites, which are not required for survival, but have evolved in organisms to confer a selective advantage in response to certain abiotic and biotic conditions (Hartmann, 1996; Pavarini et al., 2012). These compounds often exhibit biological activities, such as defense against herbivory or pathogens, which can be harnessed for therapeutic purposes beneficial to humans. An exemplary case is the antibiotic penicillin, produced by the fungus *Penicillium notatum*, discovered by Alexander Fleming in 1928 (Lobanovska & Pilla, 2017). In 1945, Fleming, alongside Sir Howard Florey and Sir Ernst Boris Chain, were awarded the Nobel Prize in Physiology or Medicine for their ground-breaking work on penicillin, acknowledging its profound impact in saving countless lives from bacterial infection, particularly during World War II (Lobanovska & Pilla, 2017). Upon examination of many natural products throughout history, scientists have identified numerous biological activities that can benefit human health, including anti-bacterial, anti-malarial, anti-inflammatory, anti-cancer properties.

These natural product compounds have evolved over time in response to both biotic and abiotic pressures to provide species with unique adaptations. The optimization of

chemical structures has led to a remarkable compatibility with various biological processes, from which significant shifts in secondary metabolite levels can occur in response to environmental condition (Pavarini et al., 2012). Recently, the polar fungus *Eutypella* sp. was selected for investigation specifically due to the harsh environmental conditions in which it grows, including extremely low temperatures, freeze-thaw cycles, and intense ultraviolet radiation, recognizing that this can lead to diverse and unique secondary metabolism (Ning et al., 2024). Fourteen sesquiterpene lactones, ten of which were novel, were identified from *Eutypella* sp. and exhibited anti-bacterial activity. This discovery provided support that natural products are a source of novel chemical compounds and bioactivities, and that chemical diversity can be driven by environmental pressures. Compared to tropical regions which have been extensively investigated for natural products, temperate and polar region investigations have been limited (dos Santos et al., 2021; Molina et al., 2022).

Whereas ideal environmental conditions allow species to thrive resulting in secondary metabolism adapted to combat competition, suboptimal environmental conditions force species to survive by adapting their secondary metabolism to abiotic stressors. In plants specifically, their sedentary nature requires secondary metabolites to also act as defense against pathogens and herbivory by producing compounds that affect bacterial and mammalian physiology. In summary, natural selection acts in response to various abiotic and biotic factors which, depending on the environmental region, shapes their secondary metabolism. Moreover, a targeted approach can then be employed to explore natural products from understudied regions, as these areas are likely to harbour additional stressors to confer a broader range of secondary metabolites. By identifying natural products from botanical sources, we shed light on relationships within ecosystems.

In the realm of medicinal applications, the advantage of evolutionary optimization becomes even more pronounced. Natural products often exhibit a level of specificity and selectivity in their interactions with cellular targets, which synthetic compounds may struggle to replicate and even cause unintended side effects (Swinney & Anthony, 2011). This evolutionary process has, in a sense, pre-screened these compounds as effective inhibitors since they were created to be compatible with biological processes. Additionally, the inherent diversity in natural products offers a vast pool of chemical structures with unique biological activities that have been shaped by natural selection (Hartmann, 1996). By studying the interactions between natural products and cellular targets, researchers gain invaluable insights into the connections of biological systems. Therefore, investigating natural products not only deepens our understanding of biological connections but also paves the way for the development of novel and effective therapeutic interventions (Newman, 2022).

The significance of natural products research is underscored by the realization that only a fraction of the 384,000 vascular plant species worldwide have been explored for their bioactive properties, with 60,000 having been screened for specific bioactivities and only 2000 being fully chemically described (Miller, 2011; Ulloa et al., 2017). Therefore, it is likely that an abundance of active compounds are still awaiting to be discovered in nature. In our pursuit of unraveling the potential of natural products, we are turning our attention to previously overlooked resources—Canadian prairie plants. By investigating the chemical composition and bioactivity of these plants, we aim to contribute to the expanding landscape of natural product discovery, recognizing their impact to enhance our understanding of the intricate connections between nature and human health.

1.2 Canadian Prairie Plants as a Source of Natural Products

The prairies represent one of fifteen ecological zones in Canada, stretching from the western border of Alberta to the eastern border of Manitoba. Despite harbouring diverse flora, the Canadian prairies remain underexplored for natural products (Molina et al., 2022; Thornburg et al., 2018). The United States National Cancer Institute's (NCI) Natural Product Repository houses one of the largest natural product extract libraries, encompassing marine, plant, and microbial species (Thornburg et al., 2018). However, the repository did not include collection sites in the Canadian prairies (Figure 1.1). These resilient and adaptable plants are well-suited to the challenging conditions of the prairie ecosystem, characterized by dry soils, intense solar irradiation, extreme fluctuations in temperatures and herbivory, by producing secondary metabolites (Erb & Kliebenstein, 2020; Jaakola & Hohtola, 2010; Molina et al., 2022; Yeshi et al., 2022). Exploring natural products in this geographically- and ecologically-varied region offers an opportunity to discover compounds with novel bioactivities, with potential applications as scientific tools or medicines (Newman, 2022). An excellent example of a Canadian natural product is paclitaxel (Taxol®) which was isolated from the Pacific yew tree, *Taxus brevifolia*, a species native to Canada growing in forests of the Pacific Northwest, and is utilized as one of the top breast cancer chemotherapy treatments (Gallego-Jara et al., 2020). The secondary metabolite activities of many Canadian plant species are unknown, presenting an avenue for further study (Kershaw & Allen, 2020).

To address this research gap, we initiated the Prairie to Pharmacy program, aiming to explore the potential of Canadian prairie plants yielding natural products with diverse biological activities, some of which may hold therapeutic benefits for human health. Since the program's inception, we have successfully identified four natural products from

Canadian prairie plant species, including luteolin from *Thermopsis rhombifolia* (Tuescher et al., 2020), pheophorbide A from *Symphoricarpos occidentalis* (Tuescher, 2018), hymenoratin from *Hymenoxys richarsonii* (Molina et al., 2021), and pulchelloid A from *Gaillardia aristata* (Bosco et al., 2021). This thesis contributes two natural products to this growing list, and more importantly these chemicals provide insight into a chemical structure and biological response.

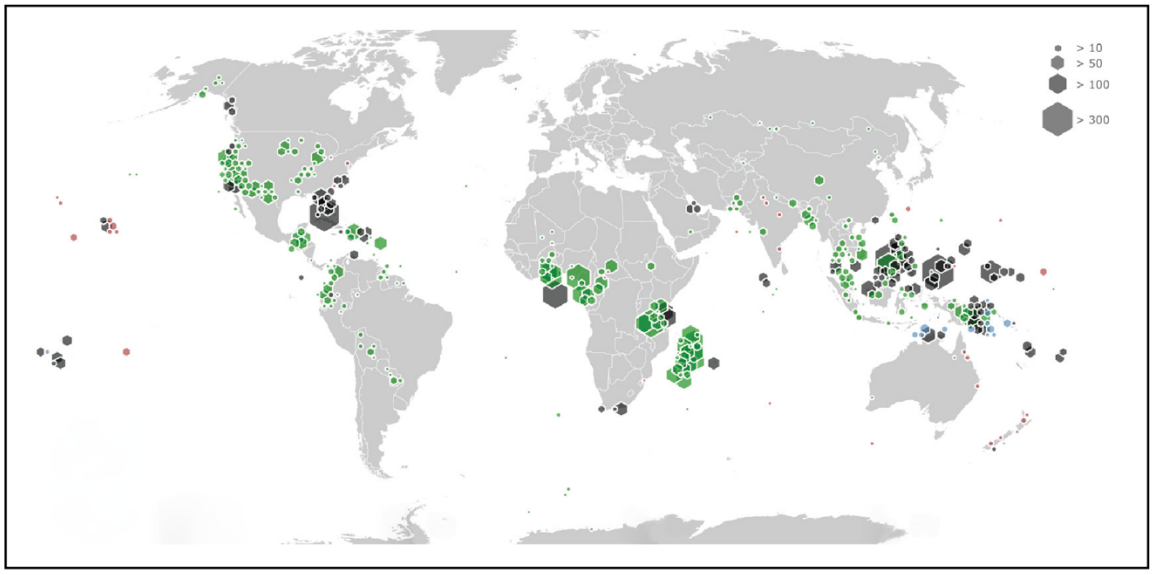

Figure 1.1. Collection sites of the United States NCI Natural Product Repository. The collection sites of species in the United States National Cancer Institute's Natural Product Repository from which a natural product extract library was created (adapted from Thornburg et al., 2018). The size of hexagon indicates the number of species per location including marine species (blue), plant species (green), microbial species (red) and more than one type of collected species (grey).

1.3 Identification of a Critical Chemical Functional Group and its Biological Activity

The natural products hymenoratin (**1**) and pulchelloid A (**2**) are both sesquiterpene lactones that are characterized by an α-methylene-γ-butyrolactone (**3**)—the moiety responsible for their anti-mitotic activity (Bosco et al., 2021; Cotugno et al., 2012; Molina et al., 2021; Sturgeon et al., 2005). Sesquiterpene lactones are part of a larger class of natural products known as terpenes and are produced by various plant species (Huang & Osbourn, 2019; Seaman, 1982). They are characterized by the repetition of isoprene units (C_5H_8), which serve as building blocks for larger terpenes: monoterpenes consist of two isoprene units, sesquiterpenes have three, diterpenes (including kaurenes) have four, and so on. The repetition, arrangement and modification of isoprene units contribute to a broad range of structures with diverse biological activities. Terpenes play a pivotal role in plant defense mechanisms (Ninkuu et al., 2021), pollinator attraction (Szenteczki et al., 2022), act as components in the biosynthesis of more complex molecules, such as steroids (Isah et al., 2018), and even exhibit anti-mitotic activities (Bosco & Golsteyn, 2017).

The shared α,β-unsaturated carbonyl among these compounds suggests a commonality in their mode of action, inducing mitotic arrest by binding to the reactive centre of proteins required for mitotic progression. This unveils a structure and function relationships where the α,β-unsaturated carbonyl can engage in Michael addition reactions with cellular cysteines (Berdan et al., 2019; Jackson et al., 2017). Michael addition is a type of nucleophilic reaction involving the addition of a nucleophile (such as the thiol (-SH) group in cysteine) to an α,β-unsaturated carbonyl (a carbonyl adjacent to an alkene) to produce a covalent adduct. Cysteines are commonly found in reactive centers of proteins due to the thiol group (Bak et al., 2019). Consequently, a compound with an α,β-unsaturated

carbonyl can inactivate these proteins by binding to cysteines within reactive centres. These α,β-unsaturated carbonyl compounds have previously been overlooked in the realm of drug discovery due to their perceived indiscriminate reactivity. However, there are examples of natural products that exhibit specific anti-mitotic activity without targeting all cysteine-containing proteins (Bosco & Golsteyn, 2017), indicating a high degree of specificity for a protein target to induce mitotic arrest rather than cytotoxicity, again reflecting the precise engineering of natural product evolution.

Although these compounds share a common reactive group, their phylogenetic characteristics, or evolutionary distance between each other's source species, would suggest diverse chemistry between the overall compounds. Investigating natural products provides an opportunity to explore the relationship between botanical phylogeny and chemical diversity (Hoffmann et al., 2018), and the phylogenetic relationships among plants offer predictive insights into their chemistry (Saslis-Lagoudakis et al., 2012; Wink, 2003). While phylogenetic proximity translates to similarities in metabolic pathways and, consequently, the biosynthesis of homologous compounds, phylogenetic distance can increase chemical diversity and help identify potentially novel bioactivities from unexplored members of taxa. This can lead to strategic bioprospecting to search for diverse chemical structures with similar bioactivities. For instance, when seeking natural products with anti-mitotic activity, diverse chemical structures will target different proteins but can accomplish the common goal of inhibiting mitosis via different mechanisms. This idea fits seamlessly with precision medicine, acknowledging that each proliferative disease is unique and demands a specific treatment, despite the commonality of uncontrolled cell growth.

In contrast, abiotic and biotic stressors within a shared ecological zone may drive phylogenetically diverse species to converge on similar biochemical pathways. An example of this convergent evolution is the similarity in appearance between African and American cacti driven by common abiotic stressors, such as arid environments, and possibly similar biotic stressors (Arakaki et al., 2011). Despite phylogenetic diversity, these plants have developed analogous adaptations, such as water-storing tissues and reduced leaves, highlighting how ecological factors can lead diverse species to converge on similar biochemical pathways for survival in comparable environments. The chemical diversity that can arise from plant secondary metabolism underscores the profound impact of natural products as a source of biologically active compounds.

1.4 Natural Products as Mitotic Inhibitors

Natural products have historically been sources of anti-mitotic compounds (Newman, 2022). Isolating biologically active natural products allows for the identification of specific protein targets in mitosis, many of which have no known inhibitors. Successful identification of precise targets and inhibition of cancer cell proliferation could lead to the development of medicines enhancing precision treatments for cancer patients. In fact, many FDA-approved anti-cancer drugs are natural products or natural product analogs (Newman & Cragg, 2020). Select examples of natural product mitotic inhibitors are discussed below and are accompanied by their chemical structures depicted in Figure 1.2.

1.4.1 Tubulin inhibitors

One class of anti-mitotic compounds are tubulin inhibitors which target microtubules and act by either the hyper-polymerization or depolymerization of their

tubulin subunits. These inhibitors have historically been used for cancer treatment since microtubules play a critical role in cell division. However, tubulin is also an important cytoskeletal protein. Therefore, tubulin-targeting compounds also affect interphasic cells as well as non-cancerous cells, which can result in severe side effects due to cytotoxicity. Despite this, tubulin inhibitors are highly effective and remain some of the top anti-cancer drugs.

Isolated from the Pacific yew tree, *Taxus brevifolia*, paclitaxel (Taxol ®) (**4**) is a natural product that stabilizes tubulin polymerization and is used to treat many types of cancer, including breast, ovarian, and lung cancer (Gallego-Jara et al., 2020). Similarly, docetaxel (Taxotere ®) (**5**) was isolated from the English yew, *Taxus baccata*, and acts in a similar manner to paclitaxel by stabilizing microtubules and inducing mitotic arrest (Guénard et al., 1993). Though these compounds are structurally and functionally related taxanes, they have different pharmacokinetic profiles in cancer patients (Kearns, 1997). Furthermore, although many effective chemotherapeutic treatments are Taxol-based, their clinical use is restricted when tumours acquire resistance, as in the case of triple negative breast cancer (Li et al., 2019). This highlights the importance of the discovery of novel inhibitors to provide alternative treatment options in precision medicine.

Other tubulin inhibitors include colchicine (**6**), an alkaloid isolated from *Gloriosa superba* (Srivastava et al., 2014) and *Colchicum autumnale* (Spasevska et al., 2017), which exhibits anti-inflammatory and anti-mitotic activities. Like the synthetic compound nocodazole (**7**) commonly used in cell biology research, colchicine depolymerizes microtubules to prevent the formation of the mitotic spindle and induce mitotic arrest. Colchicine has proven as an effective anti-cancer compound (Lin et al., 2013) and many colchicine derivatives have been created with anti-proliferative activities (Johnson et al.,

2017). Another microtubule depolymerizing compound is deoxypodophyllotoxin (**8**), isolated from *Pulsatilla koreana*, a tubulin toxin that blocks cells in mitosis (Kim et al., 2002) of which there are many isomers and derivatives also with anti-proliferative activities (Lazzarotto et al., 2019; Li et al., 2021; Wu et al., 2023). Lastly, coronopilin (**9**) is a sesquiterpene lactone isolated from *Ambrosia arborescens* that covalently binds to nucleophilic groups of tubulins, resulting in hyper-polymerization to induce mitotic arrest in cancerous cell lines (Cotugno et al., 2012; Sotillo et al., 2017). Interestingly, coronopilin was found to inhibit the proliferation of breast cancer and leukemia cell lines, while having low cytotoxicity on normal white blood cells (Cotugno et al., 2012; Sotillo et al., 2017).

1.4.2 Mitotic regulatory pathway inhibitors

Distinct from tubulin inhibitors, another group of anti-mitotic compounds target proteins that have specific roles in the regulation of mitosis. As previously mentioned, natural products have been optimized through evolution to interact in biological pathways, of which many are specialized to the highly regulated process of mitosis resulting in anti-mitotic activities. Many of these compounds, including those discovered in this thesis, fall under this category of mitotic inhibitors, and can lead to the identification of novel protein targets in mitosis.

Isolated from the plant *Centipeda minima*, 6-O-angeloylplenolin (6-OAP) (**10**) is a sesquiterpene lactone that induces mitotic arrest by presumably targeting Skp1 (S-phase kinase associated protein 1) to inactivate the ubiquitin ligase Skp1-Cullin-F-box (SCF) complex preventing the degradation of proteins critical for mitotic exit (Cheng et al., 2016; Liu et al., 2015). However, this inhibition does not occur via cysteine chemistry. It was also reported that 6-OAP supressed the proliferation of cell lines that are resistant to other

chemotherapies, indicating that 6-OAP may be a promising therapeutic option for resistant tumours (Liu et al., 2011). Two other anti-mitotic sesquiterpene lactones are psilostachyin A (**11**) and psilostachyin C (**12**), both isolated from *Ambrosia artemisiifolia* (Sturgeon et al., 2005). Their targets are unknown, but are likely proteins required for proper chromosome congression as they induce a prometaphase arrest with abnormal microtubule arrangement and unaligned chromosomes.

Compounds that induce mitotic arrests with phenotypes distinct from tubulin inhibitors should be further investigated, beyond cytotoxicity, for novel anti-mitotic mechanisms of action. An example is the sesquiterpene lactone pulchelloid A which was previously isolated from *Gaillardia pulchella* and described solely as cytotoxic (Inayama et al., 1982). Recently, extracts from *G. aristata* reported similar cytotoxicity, however further investigation revealed that pulchelloid A induced a mitotic arrest (Bosco et al., 2021), thus attributing an anti-mitotic activity to pulchelloid A after over 30 years. A subset of approximately a dozen sesquiterpene lactones have been reported to arrest cells in mitosis, including pulchelloid A and hymenoratin by our laboratory, although their precise targets or mechanism of action have not been identified (Bosco & Golsteyn, 2017; Bosco et al., 2021; Molina et al., 2021).

Of the studies detailing novel mitotic regulatory inhibitors, few have elucidated the precise mechanisms of action for each compound. These inhibitors induce mitotic arrest phenotypes resembling prometaphase, suggesting these compounds impact spindle assembly, chromosome congression, and/or centrosome duplication. The compounds identified in this thesis also exhibit this mitotic arrest phenotype, adding to this group of inhibitors. Unraveling their mechanisms of action holds promise for utilizing these compounds as valuable tools to enhance our comprehension of mitotic regulation and to

develop innovative drugs for precision medicine. To understand their potential mechanisms of action, we must first gain a comprehensive understanding of the normal progression and regulation of events during mitosis.

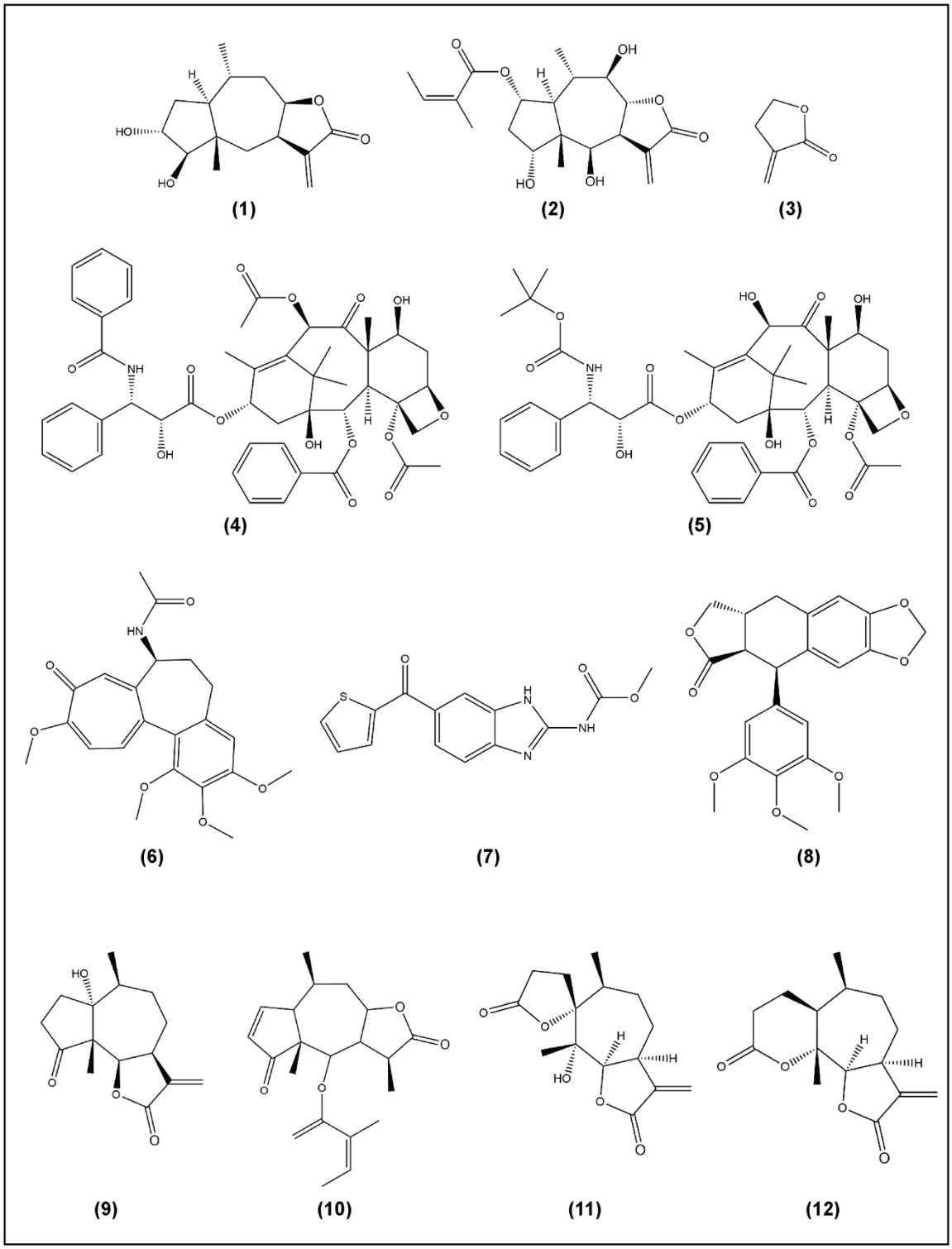

Figure 1.2. Chemical structure of anti-mitotic compounds. Hymenoratin **(1)**, pulchelloid A **(2)**, α-methylene-γ-butyrolactone **(3)**, paclitaxel **(4)**, docetaxel **(5)**, colchicine **(6)**, nocodazole **(7)**, deoxypodophyllotoxin **(8)**, coronopilin **(9)**, 6-O-angeloylplenolin **(10)**, psilostachyin A **(11)**, and psilostachyin C **(12)**.

1.5 Cell Cycle Regulation

The cell cycle is a fundamental biological process that governs the growth, replication, and division of eukaryotic cells. This highly regulated process consists of distinct phases, including interphase (comprising G1, S, and G2 phases) and mitosis (prophase, prometaphase, metaphase, anaphase, and telophase), each with its own set of crucial events. One eukaryotic cell division cycle takes approximately 24 hours to complete, with 11 hours in G1, 8 hours for DNA replication in S phase, 4 hours in G2 and 1 hour to complete mitosis and produce two identical daughter cells. Despite being the shortest phase in the cell cycle, mitosis is highly regulated by numerous proteins, checkpoints, and DNA repair mechanisms. The correct functioning of cell cycle regulation depends on post-translational modifications to regulate the synthesis, activation, inhibition, and degradation of all proteins. The following sections will provide an overview of the cell cycle and then delve into the specific mechanisms governing chromosome congression and centrosome duplication during mitosis (Figure 1.3).

1.5.1 Cell cycle overview

The cell cycle is regulated by three main checkpoints, each serving as a control mechanism to ensure the accuracy and integrity of cell division. The G1 checkpoint verifies favorable conditions for division and checks DNA integrity, while the G2 checkpoint ensures accurate DNA replication after synthesis (S phase) prior to the onset of mitosis. Finally, the M checkpoint ensures proper chromosome alignment and prevents the premature separation of sister chromatids during mitosis. These checkpoints are controlled by cyclin-dependent kinases (CDKs), a series of regulatory enzymes that orchestrate phosphorylation events to direct the progression of the cell cycle (Malumbres, 2014;

Vermeulen et al., 2003). These CDKs are activated by binding to cyclically synthesized proteins, aptly named cyclins, forming cyclin-CDK complexes which trigger the progression through each phase of the cell cycle. While the expression of CDKs is constant, the fluctuations of specific cyclins by additional regulatory proteins controls the progression through each phase of the cell cycle.

The onset of mitosis is marked by the activation of the cyclin B/CDK1 complex, and the expression of cyclin B can be used as a marker to detect cells in mitosis. The mitotic phase is further divided into five phases to ensure the precise distribution of replicated chromosomes. During prophase, chromatin condenses into chromosomes, the nuclear envelope breaks down, and the centrosomes move to opposite poles of the cell. The process of chromosome condensation is initiated by the phosphorylation of histone H3 (PH3) at the serine 10 residue by the kinase Aurora B (Goto et al., 2002; Hendzel et al., 1997). During prometaphase, the spindle fibers extend from the centrosomes and the kinetochore microtubules attach to the kinetochores of each chromosome. During metaphase, the chromosomes are aligned at the equatorial plane of the cell, called the metaphase plate, and this alignment is facilitated by the tension and balance of forces exerted by the kinetochore microtubules. The mitotic checkpoint, also known as the spindle assembly checkpoint (SAC), monitors the attachment of spindle fibers to the kinetochores of chromosomes and prevents the premature separation of sister chromatids. Once proper chromosome congression has occurred, the SAC is silenced, and prompts the migration of the sister chromatids toward opposite poles of the cell as the kinetochore microtubules shorten and the non-kinetochore microtubules elongate during anaphase. The metaphase to anaphase transition is critical to ensure the accurate distribution of genetic material from one generation of cells to the next. Finally, the cell undergoes telophase and cytokinesis where

the chromatids reach the poles and new nuclear envelopes form around each set of chromosomes, resulting in the formation of two identical daughter cells.

The progression of the cell cycle is dependent on the degradation of specific proteins for timely cell cycle transitions. This is orchestrated by the ubiquitin proteasome pathway where E3 ubiquitin ligases target proteins for degradation by the 26S proteasome. All cyclins are subjected to ubiquitin-mediated proteolysis to facilitate the transition between phases of the cell cycle once checkpoints are satisfied. These checkpoints are pivotal in preventing cell division in the presence of damaged DNA or other abnormalities, thereby maintain genomic stability. Detection of issues at any checkpoint prompts a temporary halt in the cell cycle, allowing for necessary repairs before advancing to the next phase.

1.5.2 Chromosome congression

Chromosome congression, a pivotal process in early mitosis, involves the precise positioning of chromosomes orchestrated by the dynamic and intricate mitotic spindle structure composed of centrosomes and microtubules. The SAC is a key regulatory mechanism that monitors the integrity of the mitotic spindle and the attachment of chromosomes to microtubules. It acts as a sentinel to ensure the proper alignment of all chromosomes before the metaphase to anaphase transition. Any error in spindle assembly or chromosome attachment prevents the silencing of the SAC, delaying progression to anaphase until all issues are resolved. This protective mechanism safeguards against the mis-segregation of chromosomes, a critical factor in preserving genomic stability. Targeting the SAC becomes an effective strategy to inhibit proliferation, particularly as the metaphase

to anaphase transition represents a point of no return in mitosis. Uncorrected errors at this stage can have detrimental effects on all subsequent generations of cells.

During prometaphase, the kinetochores located at the centromeres of sister chromatids establish either end-on or lateral attachments with microtubules to determine the mechanism of chromosome congression. Bi-orientation (amphitelic attachment) near the spindle center involves opposite kinetochore-pulling forces, whereas peripheral chromosomes use the motor proteins dynein and centromere-associated protein E (CENP-E) for transport towards the metaphase plate (Maiato et al., 2017; Prosser & Pelletier, 2017; Yu et al., 2019). CENP-E is responsible for stable kinetochore-microtubule attachment and tension, and its activity is regulated by post-translational modifications, including farnesylation (Ashar et al., 2000) and SUMOylation (Dasso, 2008). The centromere protein Aurora kinase B directs CENP-E to correctly associate with the kinetochores (Ditchfield et al., 2003) and is also responsible for the phosphorylation of histone H3 during early chromosome condensation (Goto et al., 2002; Hendzel et al., 1997). The kinase multipolar kinase-1 (Msp1) performs a similar role to Aurora B in the recruitment of SAC proteins to the kinetochores (Musacchio & Salmon, 2007). Inner centromere protein (INCENP) and RAN binding protein 2 (RanBP2) are required for the activation and SUMOylation of Aurora B to function properly in monitoring microtubule attachment to the HEC1 complex of the kinetochore (Di Cesare et al., 2023; Musacchio & Salmon, 2007; Samejima et al., 2015). Attachment is complete once the plus ends of kinetochore microtubules are attached to the Ndc80/HEC1 complex of the outer kinetochore. Attachment errors, including monotelic, syntelic and merotelic attachment, are quickly corrected by Aurora B. RanBP2 is involved in the proper localization of many kinetochore proteins, including CENP-E, CENP-F, and RanGAP1 (Ran GTPase activating protein 1) (Joseph et al., 2004). CENP-F

is a multifaceted protein involved in kinetochore-microtube attachment, chromosomal stability, dynein activity and centrosome maturation (Holt et al., 2005). Like CENP-E, the proper localization of CENP-F is regulated by farnesylation (Hussein & Taylor, 2002; Vergnolle & Taylor, 2007). These are just a few of the kinetochore- and centromere-associated proteins required for proper chromosome congression (Musacchio & Salmon, 2007).

During chromosome congression, the E3 ubiquitin ligase anaphase-promoting complex/cyclosome (APC/C) is inhibited by the mitotic checkpoint complex (MCC) until the SAC is satisfied. The MCC is composed of mitotic-arrest deficient 2 (Mad2), budding uninhibited by benzimidazole 3 (Bub3), budding uninhibited by benzimidazole related 1 (BubR1), and cell division cycle (Cdc20) proteins. Cdc20 is a co-factor of the APC/C, but it is inhibited when bound in the MCC. Once the SAC is satisfied, Cdc20 is released to activate the APC/C to ubiquitylate cyclin B and securin to promote sister chromatid separation, marking the onset of anaphase. In addition to their role in the MCC, BubR1 and Mad2 associate with unattached kinetochores and their signal remains strong until proper kinetochore microtubule attachment has occurred (Joglekar, 2016; Musacchio & Salmon, 2007). BubR1's activity can also be triggered by CENP-E at the kinetochores until proper kinetochore-microtubule attachment is achieved, upon which the BubR1 signal is silenced (Huang et al., 2019; Mao et al., 2005). This holds true for numerous mitotic regulatory proteins, as they often play multiple roles, contributing to the establishment of a robust regulatory network governing mitosis.

In parallel, the SAC can be activated upon the phosphorylation of histone H2AX by the protein kinase ataxia telangiectasia mutated (ATM), a response triggered after detection of a double-stranded break (Rogakou et al., 1998). DNA damage can occur during a

prolonged arrest and imbalanced tension at centromeres. This then exacerbates the length of the arrest since both poor chromosome congression and DNA damage can trigger the SAC, and both must be resolved for the APC/C inhibition to be released. This implies a crosstalk occurs between the DNA damage response and the SAC which strengthens the regulations of the metaphase to anaphase transition, again stressing its importance. This review highlights a few proteins from the extensive collection involved in regulating chromosome congression to preserve one of the most critical checkpoints of the cell division cycle.

1.5.3 Centrosome duplication

The centrosome is a cellular organelle comprised of two centrioles surrounded by pericentriolar material (PCM) containing various centrosomal-associated proteins. Centriole duplication is tightly regulated during the cell cycle, where the mother centriole acts as a template for assembling a new daughter centriole. In a fully mature centrosome, there is one "mother" centriole and one "daughter" centriole embedded in the pericentriolar material. This duplication process ensures that each daughter cell inherits the correct number of centrioles (Wang et al., 2014). During the G1/S transition, the PCM protein polo-like kinase 1 (PLK-1) initiates centrosome duplication. During S phase the centrioles undergo a semiconservative replication, and each centriole is now associated with a newly formed daughter centriole, resulting in the formation of two centrosomes. Centrosomes undergo maturation during G2 and separate by moving to opposite poles of the cell to prepare for mitosis, a process facilitated by the PCM proteins Nek2 (never in mitosis-A related 2) and PLK-1 (Schmucker & Sumara, 2014; van Vugt et al., 2004). Nek2 is involved in centrosome separation, maturation, and microtubule nucleation by phosphorylating C-

Nap1 (centrosomal Nek2-associated protein 1) to weaken centrosome cohesion. Nek2 and Aurora kinase B contribute to PCM organization during centrosome maturation, enabling the centrosomes to act as microtubule-organizing centres (MTOCs). These MTOCs, initiated with the help of the key ring complex protein γ-tubulin, nucleate microtubules to form the mitotic spindle (Prosser & Pelletier, 2017). Mature centrosomes ensure the formation of a bipolar spindle for accurate chromosome segregation.

To prevent centriole reduplication, the PCM protein PLK-4 (polo-like kinase 4) auto-phosphorylates, signaling its degradation by the E3 ubiquitin ligase SCF complex (Holland et al., 2010; Wang et al., 2014). Centrosomal abnormalities resulting from the overexpression of centrosomal-associated kinases can disrupt spindle assembly regulation, leading to the formation of multipolar spindles through overduplication or abnormal centrosome separation (Bühler & Stolz, 2022). The cycling of centrosomes involves numerous proteins, each regulated by enzymes to ensure accurate functionality and localization, and the interplay between centrosomes, spindle fibers, and kinetochores is crucial for achieving proper chromosome congression.

1.5.4 Loss of cell cycle regulation

Outside of embryonic development, growth and repair, eukaryotic cells remain in a resting state known as G0. The initiation of the cell cycle is meticulously regulated by external signals, such as growth factors, and within the cell cycle are mechanisms that often exhibit redundancy to prevent errors in division. A comprehensive understanding of the molecular mechanisms regulating cell division is imperative for developing targeted therapeutic strategies for intervention upon loss of cell cycle control. However, many mitotic regulatory proteins lack inhibitors, posing challenges when there is a breakdown in

cell cycle regulation. A loss of cell cycle control can result from sustained proliferative signalling or the evasion of regulatory mechanisms, and lead to the development of proliferative diseases such as cancer (Hanahan & Weinberg, 2011). The identification of novel inhibitors targeting specific proteins is crucial for advancing treatment strategies.

Historically, natural products have served as a rich source of anti-mitotic compounds (Newman & Cragg, 2020). Earlier, we reviewed previously identified natural product inhibitors that induce mitotic arrest, and this thesis adds two novel anti-mitotic compounds to expand this repertoire. Structure-activity relationships in biology underscore that different compounds target distinct proteins, highlighting the need for innovative compounds to address mitotic regulators lacking known inhibitors. Identifying such anti-mitotic compounds can enhance our understanding of mitosis and contribute to the development of novel therapies for precision medicine.

1.6 Methods to identify anti-mitotic natural products

There are several mitotic markers that can be utilized to identify anti-mitotic activities from complex plant extracts which can then lead to the purification of the active compound. Our approach involves cell-based assays to screen for a round cell morphology after exposure to a plant extract. This rounded phenotype is a characteristic of mitosis to ensure the equal division of cellular contents during the cell cycle. This assay allows an entire biochemical pathway, mitosis, to be investigated at once to screen plant extracts for inhibitory activity (Swinney & Anthony, 2011; Williams & Andersen, 2020). In addition to cell rounding, we consider the expression of cyclin B1 and PH3 as two other key mitotic markers to screen for anti-mitotic activity since both are highly expressed during mitosis.

Upon identification of anti-mitotic activity, we employ the technique of biology-guided fractionation to purify the active compound which involves a series of chemical fractionation steps alternated with phenotypic assays. This process continues until an active pure compound is isolated. Following the isolation of the pure compound, precise assays can be utilized to determine the mechanism of action and cellular target. This method was used to identify the anti-mitotic natural product paclitaxel, initially discovered from *T. brevifolia* extracts based on the observations of a rounded cell phenotype (Wani et al., 1971). The anti-mitotic activity of paclitaxel was confirmed by high levels of cyclin B1 and PH3 expression and it was found to bind tubulin as its cellular target. This method is employed in this thesis to identify two novel anti-mitotic compounds from Canadian prairie plants outlined in the following section.

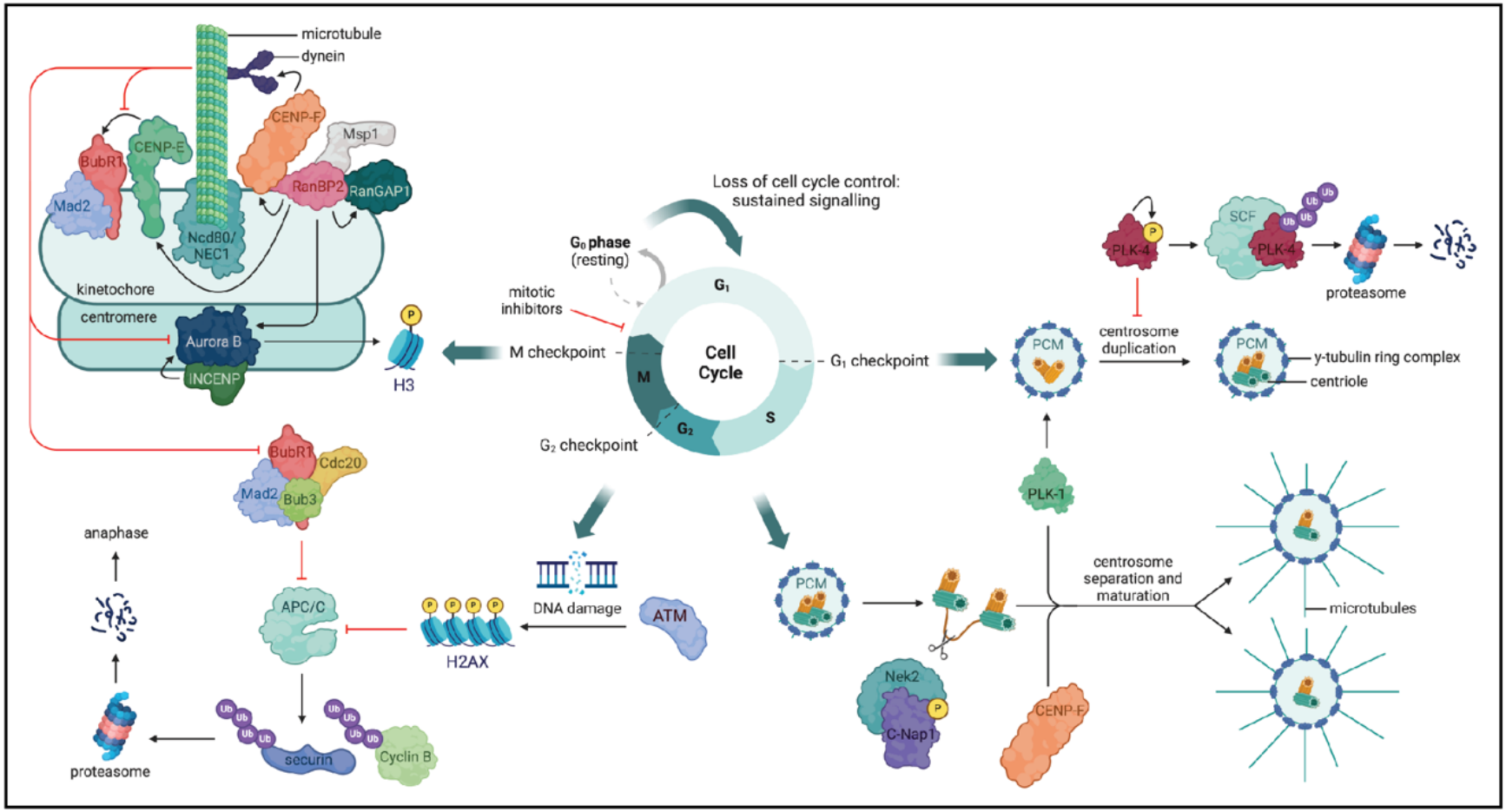

Figure 1.3. Eukaryotic cell cycle overview. Schematic summarizing the eukaryotic cell cycle highlighting centrosome duplication, DNA damage, kinetochore-microtubule attachment, and spindle assembly checkpoint pathways. Created with BioRender.com

1.7 Canadian Prairie Plant Species Under Investigation

This thesis focuses on the analysis of three natural products from species native to the Canadian prairies: *Gaillardia aristata* (Blanket Flower), *Pulsatilla nuttalliana* (Prairie Crocus), and *Erythronium grandiflorum* (Glacier Lily). *G. aristata*, a native perennial herbaceous plant, is the source of pulchelloid A (Bosco et al., 2021) and belongs to the Asteraceae family, which also includes sunflowers, daisies, and *Hymenoxys richarsonii*, the source of hymenoratin (Molina et al., 2021). The Asteraceae family is known for biologically active sesquiterpene lactone natural products (Molina et al., 2022). *P. nuttalliana* (Ranunculaceae) is a prominent spring prairie plant featuring striking purple flowers (Beaubien & Hamann, 2011), and *E. grandiflorum* (Liliaceae) is one of the first plants to emerge in the montane regions of the prairies (Kuijt, 1982). Figure 1.4 highlights the phylogenetic distance between the three species under investigation, where *G. aristata* and *P. nuttalliana* are separated by 147 ± 6 million years, and *E. grandiflorum* by 161 ± 7 million years (Wikström et al., 2001). In a phenotypic screen of extracts prepared from these plants, each exhibited anti-mitotic activities. Given the phylogenetic proximity between the source plants of pulchelloid A and hymenoratin, *G. aristata* and *H. richarsonii* respectively, it is unsurprising that the chemical structures of these two anti-mitotic compounds are similar. By contrast, it is reasonable to propose that an increase in the phylogenetic distance between species with anti-mitotic extracts, such as *P. nuttalliana* and *E. grandiflorum*, will result in increasingly diverse chemical structures of the active compounds.

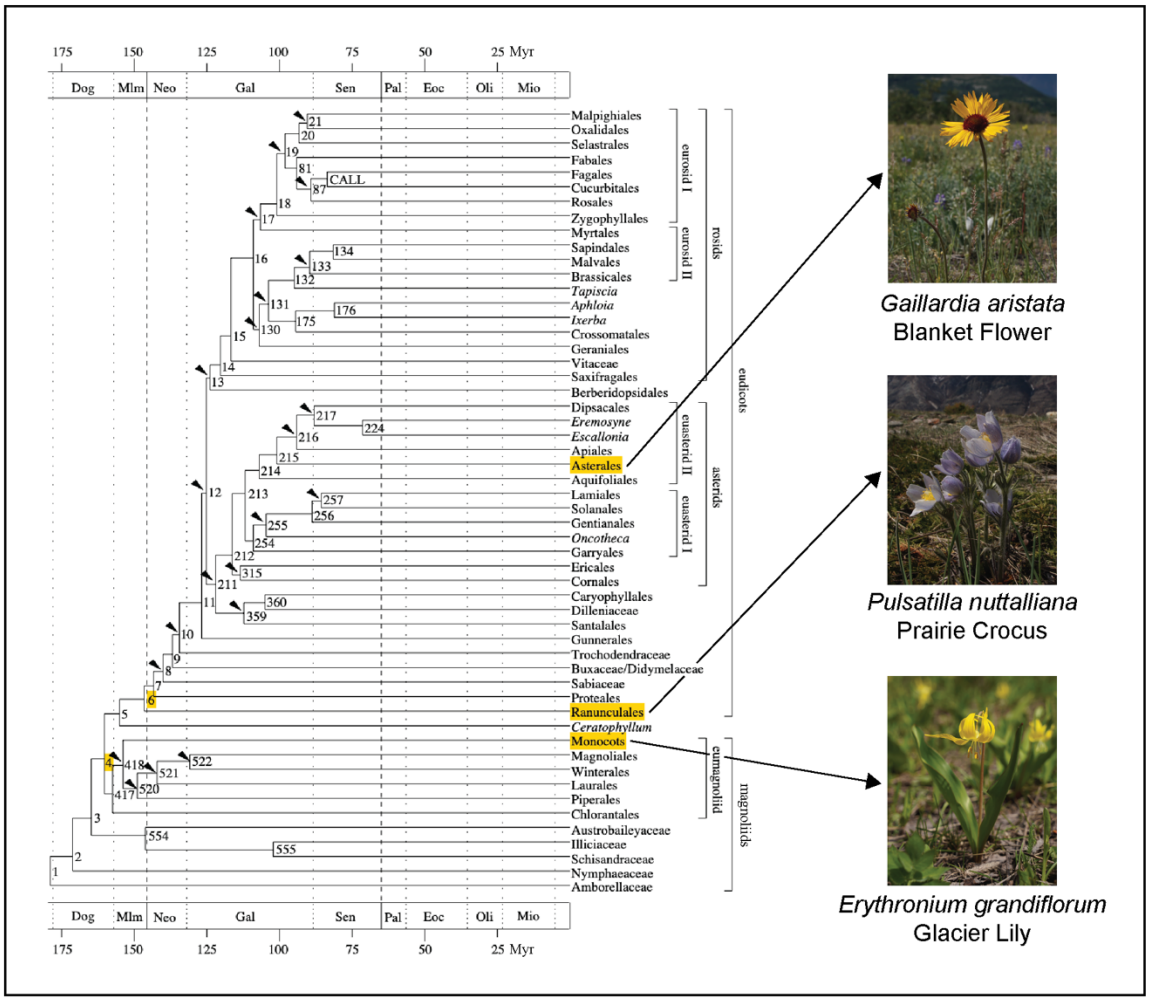

Figure 1.4. Phylogenetic relationship between *Gaillardia aristata*, *Pulsatilla nuttalliana*, and *Erythronium grandiflorum*. Phylogenetic chronogram of angiosperms, ages estimated using maximum parsimony by accelerated transformation optimization (adapted from Wikström et al., 2001). Species under investigation are the Blanket Flower, *Gaillardia aristata* (Asteraceae); the Prairie Crocus, *Pulsatilla nuttalliana* (Ranunculaceae); and the Glacier Lily, *Erythronium grandiflorum* (Liliaceae). Nodes of last common ancestor are highlighted in yellow, where node 4: 161 ± 7 Myr; and node 6: 147 ± 6 Myr.

1.8 Hypothesis and Objectives

The overarching goal of our research is to investigate Canadian prairie plants for natural products and identify their biological activities. Several of these compounds exhibit anti-mitotic activities that can advance our understanding of mitosis. Our approach is to investigate Canadian prairie plants, which are understudied, but have been proven as an abundant source of anti-mitotic compounds. We hypothesize that an increase in phylogenetic distance between plant species will lead to greater chemical diversity amongst anti-mitotic compounds with similar mitotic phenotypes. To test this hypothesis, we propose the following objectives:

- To characterize the biological activities of extracts from *Pulsatilla nuttalliana* and *Erythronium grandiflorum*.
- To identify the compounds responsible for the anti-mitotic activities by biology-guided fractionation.
- To distinguish the mitotic arrests of these novel anti-mitotic compounds through precise cell biology assays.

This is the first report to attribute anti-mitotic activities to the natural products anemonin, isolated from *P. nuttalliana*, and (+)-6-tuliposide A, isolated from *E. grandiflorum*. We also present evidence distinguishing the mitotic arrests induced by pulchelloid A, anemonin and (+)-6-tuliposide A, suggesting they inhibit mitosis by different mechanisms.

CHAPTER 2

Two anti-mitotic activities are present in extracts from the Canadian Prairie Crocus, *Pulsatilla nuttalliana*

2.1 Abstract

We are investigating plants from the prairie ecological zone of Canada to identify natural products that inhibit mitosis in cancer cells. Extracts prepared from the Canadian prairie plant species *Pulsatilla nuttalliana* (Ranunculaceae) exhibited anti-mitotic activity on human cancer cell lines. *P. nuttalliana* treated cells acquired a rounded morphology and were positive for phospho-histone H3, a mitotic protein. Further investigation revealed that some arrested cells displayed mitotic spindles, while others did not. Fractionation of the extract prepared from plant stems revealed two distinct anti-mitotic activities, each of which exhibited different effects on spindle organization. Using biology-guided fractionation, we isolated one of the anti-mitotic compounds as the natural product anemonin and are the first to report its anti-mitotic activity. This is the first report of two distinct anti-mitotic activities in one prairie plant and contributes to a growing body of evidence that select Canadian prairie plants have a range of anti-mitotic activities.

2.2 Introduction

The exploration of natural products helps us understand biological connections and advance the development of new treatments for diseases such as cancer. One approach is to discover natural products that interfere with the cell division cycle in human cells. A classic example is paclitaxel, a taxane compound isolated from *Taxus brevifolia*, which binds to tubulin resulting in the arrest of cells in mitosis (Schiff et al., 1979; Wani et al., 1971). The study of paclitaxel, also known as Taxol®, has provided detailed information about tubulin function and it has become one of the most widely used chemotherapeutic drugs to treat cancer (Cragg, 1998; Gallego-Jara et al., 2020; Kingston, 2021). Despite such discoveries, the potential of natural products from botanicals in Canadian ecological zones as scientific tools or medicines remains under explored (Molina et al., 2022; Thornburg et al., 2018).

We have undertaken a project to identify natural products from which to gather information about how human cells function and to identify chemical compounds with medicinal properties. A critical element in the discovery of inhibitors is the selection of sources from which to find such compounds (Wilson et al., 2020). We focus on investigating plant species from the prairie ecological zone in Canada because these plants grow under conditions that promote the production of special metabolites (Hartmann, 1996; Molina et al., 2022; Pavarini et al., 2012). The combination of biotic conditions, such as herbivory, and abiotic conditions, such as extreme temperature ranges, may contribute to the production of either abundant or novel special metabolites. In the province of Alberta, which harbours part of the prairie and montane ecological zones, 1636 vascular plant species from 123 botanical families have been catalogued (Kershaw & Allen, 2020). The

special metabolite activities of many of these plant species are unknown, presenting an avenue for further exploration.

The second component of identifying natural product inhibitors is the bio-assay. We utilized phenotypic assays, which is favourable in the discovery of novel inhibitory activities because an entire biochemical pathway can be tested at once (Swinney & Anthony, 2011; Williams & Andersen, 2020). This complements assays using purified systems, such as protein kinases, for which the precise target is known (Moffat et al., 2017; Perron-Sierra et al., 2012). We developed a cell-based assay for the detection of mitosis in HT-29 cells, which are particularly sensitive to mitotic arrest (Gascoigne & Taylor, 2008), in which the phenotype is the acquisition of a rounded morphology that is characteristic of mitosis (Kubara et al., 2012; Swift & Golsteyn, 2018). Identification of the molecular target requires additional study; however, the phenotypic approach is a critical first step that has successfully led to the purification and identification of inhibitory compounds (Bosco & Golsteyn, 2017; Bosco et al., 2021; Molina et al., 2021).

We created an extract library prepared from Canadian plant species and screened it using phenotypic assays for extracts that induced a mitotic arrest (Molina et al., 2022). Here, we report the characterization of an anti-mitotic activity of extracts prepared from the Prairie Crocus, *Pulsatilla nuttalliana* (Ranunculaceae), a prominent spring prairie plant (Beaubien & Hamann, 2011). The Pulsatilla genus, previously included in the Anemone genus (Mosyakin, 2016), is known by Traditional Knowledge in several First Nation communities in Canada (Moerman, 2009) and Chinese Traditional medicine (Wu et al., 2023). A species related to *P. nuttalliana*, *P. koreana*, is known to Korean Traditional knowledge (Park et al., 2013) and is a source of deoxypodophyllotoxin, a tubulin toxin that arrests cells in mitosis (Kim et al., 2002). We are the first to investigate *P. nuttalliana*,

whose distribution is limited to North America. By combining phenotypic assays with specific tests for mitotic function, we found that there were not one, but two distinct anti-mitotic activities present in this species. This is the first report of two anti-mitotic activities in extracts from one prairie plant species.

2.3 Materials and Methods

2.3.1 Plant Collection

Aerial plant parts of *P. nuttalliana* (Ranunculaceae) were collected by sustainable practice in southern Alberta, Canada at North 49°1 latitude and West -113°0 longitude, at approximately 850 to 1400 metres elevation during 2015 and 2019. Permits from provincial and local governments were acquired for collection. Plant taxonomy was confirmed to species (Kershaw & Allen, 2020; Moss & Packer, 1983) and verified by the University of Lethbridge Herbarium. A voucher specimen was provided to the herbarium as #Golsteyn080. Following harvest, the plants were dried at room temperature and stored in the dark in a dry environment at room temperature until extraction.

2.3.2 Preparation of Plant Extracts

Plant parts (whole aerial plant parts, leaves, stems, and flowers) were separated and ground into fine powders. Extracts were prepared by suspending powdered material in either 75% (v/v) ethanol in water (A extracts) or in 100% dichloromethane (B extracts) and stirring overnight at room temperature. The suspensions were filtered, dried, and stored in the dark at room temperature. The extracts were dissolved in dimethyl sulfoxide (DMSO) (Sigma-Aldrich, D2438) to a concentration of 50 mg/mL for use in biological assays.

2.3.3 Cell Culture

The human cell lines HT-29 (ATCC HTB-38) and U2OS (ATCC HTB-96) were obtained from the American Type Culture Collection (ATCC) and cultivated as previously described (Kubara et al., 2012; Lewis & Golsteyn, 2016). HT-29 cells were selected for further studies because of their capacity for prolonged mitotic arrest (Gascoigne & Taylor, 2008). HT-29

cells were plated at a density of 3.0 x 10^5 cells/25 cm^2 flask and cultured for 48 hours (h) prior to treatment. U2OS cells were plated at a density of 3.0 x 10^5 cells/25 cm^2 flask and cultured for 24 h prior to treatment. The compounds nocodazole (660 µM, Sigma-Aldrich, M1404), paclitaxel (1 mM, Sigma, T7402), 4-deoxypodophyllotoxin (125 µM, Cedarlane, D249500), hymenoratin (3.8 mM) and anemonin (10 mM, Millipore Sigma, PHL80346) were dissolved in DMSO and stored at -20°C. For not-treated cells, DMSO was added at a final concentration of 0.4% (v/v) as a solvent vehicle control. Light microscopy imaging was performed with an Infinity 1 camera operated by Infinity Capture imaging software (Lumenera Corporation, CA) on an Olympus CKX41 inverted microscope. Cells were manually scored for rounded or flat morphology. At least 200 cells were counted per treatment group.

2.3.4 Cell Viability (MTT) Assay

The 3-(4,5-dimethylthiazol-2-yl)-2,5-diphenyltetrazolium (MTT) assay (Sigma-Aldrich, M2128-1G) was used to measure plant extract cytotoxicity (Kubara et al., 2012). HT-29 cells were seeded at 5,000 cells per well in a 96-well culture plate and incubated at 37°C for 48 h prior to treatment. All experiments were carried out in triplicate, and the treatments were repeated at least three times. After 72 h of treatment, 20 µL of MTT solution (5 mg/mL MTT in phosphate-buffered saline (PBS:137 mM NaCl, 3 mM KCl, 100 mM Na_2HPO_4, 18 mM KH_2PO_4)) was added to the media in each well, and the plates were incubated at 37°C for 3.5 h. The medium was then aspirated and replaced with 150 µL of MTT solvent (4 mM HCl, 0.1% (v/v) octylphenoxypolyethoxyethanol, in isopropanol) in each well. The plates were left in the dark for 15 minutes with shaking, and a CytationTM 5 Cell Imaging Multi-Mode Reader (BioTek Instruments, USA) equipped with Gen5 software was used to

measure the absorbance at 590 nm. IC_{50} concentrations were calculated as the concentration of the compound or plant extract that reduced the absorbance of MTT by 50% compared to 0.1% (v/v) DMSO-treated cells. The normalized percent absorbance was calculated as follows:

Normalized percent absorbance = (absorbance/DMSO absorbance) x 100

The log concentrations of the compounds were plotted against the normalized absorbance percentage using Microsoft Excel. Analysis was performed with GraphPad Prism 5 software, using non-linear regression (log(inhibitor) versus normalized response) to estimate IC_{50} concentrations. Standard curves were plotted using the following equation:

$$Y = \text{maximum} + (\text{maximum} - \text{minimum}) / (1+10(X-\text{Log}IC_{50}))$$

Where Y is the percentage of viable cells, maximum is the percentage of viable cells after treatment with 0.1% DMSO, minimum is the percentage of viable cells after treatment with the highest concentration of the cytotoxic compound, and X is the $\log_{10}$ value of the treatment concentration.

2.3.5 Immunofluorescence Microscopy

HT-29 cells were seeded in 6 well culture plates on glass coverslips and incubated at 37°C for 48 h prior to treatment. After 24 h of treatment, the cells were fixed for 20 min at room temperature with 3% (v/v) paraformaldehyde (Fisher Scientific, 30525-89-4) in PBS. Fixation was halted with 50 mM NH_4Cl in PBS for 10 min, and then cells were permeabilized for 5 min with 0.2% (v/v) Triton X-100 in PBS and blocked with 3% (w/v) bovine serum albumin (BSA) in PBS-T (0.1% (v/v) Tween 20 diluted in PBS) for 30 min. Cells were then incubated overnight at 4°C with primary antibodies anti-phospho-Ser10 histone H3 (Millipore, 06-570(CH); 1:1000) and anti-α-tubulin (Santa Cruz Biotechnology,

sc-53030; 1:400). After incubation, cells were washed with PBS-T and incubated with secondary antibodies Alexa Fluor 594 AffiniPure goat anti-rabbit IgG (Jackson ImmunoResearch, 111-585-003; 1:300) and Alexa Fluor 488 rabbit anti-rat IgG (ThermoFisher, A11006; 1:200) for 45 min at room temperature. Nuclei were stained with 300 nM 4′,6-diamidino-2-phenylindole (DAPI) (Fisher, LSD1306) in PBS for 15 min. After staining, the coverslips were mounted onto microscope slides with ProLong Gold Antifade Mountant (Thermo Fisher; P36934). Cells were then observed and imaged with a CytationTM 5 Cell Imaging Multi-Mode Reader using the Gen5 software (BioTek Instruments, USA) and a Zeiss Axio Observer Z1 Motorized Inverted Fluorescence Microscope using AxioVision software (ZEISS, USA). A minimum of 200 cells were counted for each treatment, and the mean percentage and standard error of the mean of PH3-positive cells in at least three independent experiments were calculated. DMSO-treated mitotic cells were used as a reference for baseline mitotic spindle morphology.

2.3.6 Spectrophotometry

The extracts and fractions were diluted to 1 mg/mL in 100% methanol, and 75 µL of each sample was transferred to separate wells of a 96 well plate. The absorbance of each well was read on an Epoch microplate spectrophotometer (BioTek Instruments, USA) from 300 to 700 nm, with steps of 2 nm between reads. Absorbance data were blanked to a methanol negative control and normalized using the following equation:

$$\text{Normalized absorbance} = (\text{absorbance} - \text{minimum}) / (\text{maximum} - \text{minimum})$$

2.3.7 Cell Cycle Analysis

HT-29 cells were plated at 3.0 x 10^5 cells/25 cm^2 flask and incubated at 37°C for 48 h prior to treatment. Cells were collected by trypsinization, washed with cold PBS (0.8% FBS (fetal bovine serum), 1 mM EDTA (ethylenediaminetetraacetic acid)), and fixed in ice-cold 70% ethanol for 24 h. The fixed samples were stored at -20°C until use. For analysis, the samples were centrifuged at 300 × *g* for 5 min at 4°C, washed with PBS at room temperature, and resuspended in Muse Cell Cycle staining reagent. The cells were incubated for 30 min and analyzed using a Muse® Cell Analyzer (Luminex). Gating was set using a non-treated sample and experiments were performed three times.

2.3.8 LH-20 Column Chromatography

The extract PP-1631A was subjected to Sephadex LH-20 column chromatography in collaboration with Tanner Lockwood (University of Lethbridge). Two hundred microliters of a 100 mg/mL solution of PP-1631A in 100% methanol were loaded onto a Sephadex LH-20 column (225 mm length × 15 mm internal diameter) pre-equilibrated with 100% methanol. The column was then eluted with 100% methanol, yielding twelve 2 mL fractions (including a void volume fraction). The fractions were evaporated under vacuum and resuspended in 100% methanol to a concentration of 10 μg/mL.

2.3.9 Beta-mercaptoethanol Reduction Assay

HT-29 cells were either treated with nocodazole, 4-deoxypodophyllotoxin, hymenoratin, fraction 2, fraction 5, or anemonin alone, or treated in combination with beta-mercaptoethanol (β-ME) (MP BioMedical, 02194705-CF). Each compound was

preincubated with 0.1 mM β-ME for 1 h at 37°C prior to addition to media for cell culture treatment. After 24 h of treatment, light microscopy images were taken as described above.

2.3.10 Biology-Guided Fractionation and Isolation of Anemonin.

The biology-guided fractionation was completed in collaboration with Tanner Lockwood (University of Lethbridge), Benjamin Yeremy (University of British Columbia), Dr. David Williams (University of British Columbia) and Dr. Raymond Andersen (University of British Colombia).

2.3.10.1 General Experimental Procedures

The ^{1}H and ^{13}C NMR spectra were recorded on a Bruker AV-500 spectrometer with a 5 mm CPTCI cryoprobe. ^{1}H chemical shifts are referenced to the residual DMSO-d_6 (δ 2.49 (as used in Saidi et al., 2018) ppm) and ^{13}C chemical shifts are referenced to the DMSO-d_6 solvent peak to reference 1b (δ 39.5 ppm Merck Type 5554 silica gel plates were used for analytical thin layer chromatography. Reversed-phase HPLC purifications were performed on a Waters 1525 Binary HPLC pump attached to a Waters 2998 Photodiode Array Detector. All solvents used for HPLC were Fisher HPLC grade.

2.3.10.2 Isolation of Anemonin

Approximately 43 g of dried plant material was extracted twice with 200 mL methanol overnight at room temperature. The combined extracts were concentrated *in vacuo* and then taken up into 2:1 methanol:water and extracted 4 times with 100 mL of dichloromethane. The combined dichloromethane extracts were concentrated *in vacuo* to give 380 mg of

extract. Approximately 1/4 of the active dichloromethane soluble material was chromatographed on Sephadex LH20 using a 71 x 2.5 cm column with methanol as eluent. The fractions obtained were labelled RA205-241 and analyzed with the cell rounding assay. The bioactive fraction obtained was then purified by C_{18} reversed-phase HPLC using an InertSustain, 5µm, 25 x 1.0 cm column with a gradient transitioning over 60 minutes from 95% H_2O/acetonitrile to 5% H_2O/acetonitrile as eluent with a flow rate of 2 mL/min to give 0.4 mg of anemonin (RA223). The structure of anemonin was confirmed by analysis of standard 1D and 2D Nuclear Magnetic Resonance (NMR) spectra and comparison with the literature values (Saidi et al., 2018).

2.3.11 Statistical Analysis

Data were analyzed using Microsoft Excel 2016 and GraphPad Prism 5. Data are plotted as the mean of three independent experiments ± standard error of the mean. One-way analysis of variance (ANOVA) with Tukey's post hoc test was used to analyze the results from the light microscopy and immunofluorescence microscopy assays. Differences were considered statistically significant at $p < 0.05$.

2.4. Results

2.4.1 Extracts prepared from Pulsatilla nuttalliana induced a mitotic arrest in cancer cells

Pulsatilla nuttalliana (Ranunculaceae), commonly known as the Prairie Crocus, is a prominent herbaceous plant in the prairie ecological system. It is one of the first to emerge after winter, producing striking flowers before developing prominent leaves and stems approximately one month later (Figure 2.1A). We extracted the aerial parts of *P. nuttalliana* from post-flowering plants with either 75% ethanol (v/v) in water or 100% dichloromethane and analyzed their absorbance by spectrophotometry over a range of wavelengths. The ethanolic extract absorbance was highest at 410 nm, whereas the DCM extract absorbance was highest at 330 nm, indicating a different chemical mixture for each extraction (Figure 2.1B). We examined the properties of these extracts by adding them to the culture media of two cell lines (HT-29, Figure 2.1C; U2OS, Figure 2.1D). Cells were either not-treated, treated with nocodazole as a positive control for mitotic cell rounding, or treated with extracts at a concentration of 50 μg/mL for 24 h and observed by light microscopy. Few rounded cells were observed in the not-treated sample, whereas treatment with nocodazole induced cell rounding, indicative of mitosis. The ethanolic and DCM extracts of *P. nuttalliana* induced cell rounding in both HT-29 and U2OS cells. Additionally, we tested extracts prepared from *P. nuttalliana* collected at two different sites in southern Alberta and from plants collected in different years and found that all induced the rounded morphology (data not shown). We selected *P. nuttalliana* extracts for further investigation to determine whether the cell rounding activity was caused by a mitotic arrest.

We explored extracts prepared from plant parts of *P. nuttalliana* to characterize the cell rounding activity. Extracts were prepared from the leaves, stems, or flowers using either

75% (v/v) ethanol (labelled as A) or 100% DCM (labelled as B). HT-29 cells were either not-treated, treated with nocodazole, or treated with concentrations of each extract ranging from 15 to 500 μg/mL for 24 h and observed by light microscopy (Figure 2.2A). As expected, the not-treated cells had few rounded cells, whereas nocodazole induced nearly 100% cell rounding. Imaging (Figure 2.2A) and counting (Figure 2.2B) revealed that all extracts induced cell rounding at different concentrations. The stem fractions induced cell rounding at the lowest concentrations of any plant part: there were 50 ± 1% rounded cells at 150 μg/mL by ethanolic extraction and 81 ± 4% cell rounding at 50 μg/mL by DCM extraction.

We investigated *P. nuttalliana* stem extracts in more detail because they exhibited cell-rounding activity at the lowest concentration of all the extracts tested. Analysis by spectrophotometric absorbance readily distinguished the two extracts (Figure 2.3A), with stems A absorbing more strongly below 400 nm and less strongly at 670 nm than stems B. The two extracts were tested for toxicity in HT-29 cells using the MTT assay (Figure 2.3B). Stems A had an IC_{50} of 47.0 ± 15.5 μg/mL and stems B had an IC_{50} of 14.8 ± 4.6 μg/mL, which demonstrated that both extracts were moderately cytotoxic in addition to the cell-rounding activity. We noted that the values of cell viability for stems A were not easily fitted to a curve, which may reflect the activity described in later experiments. We next examined HT-29 cells by flow cytometry after treatment with stems A and B extracts to determine whether they underwent a cell cycle arrest, which would be consistent with the cell rounding effect. In a representative experiment, the number of cells with 4N DNA at 24 h was 26 ± 1% in not-treated cells and 94 ± 2% in nocodazole-treated cells, as expected (Figure 2.3C). Stems A- and stems B-treated cells showed similar 4N DNA profiles of 67

± 2% and 71 ± 1%, respectively. These data demonstrated that the two stem extracts were cytotoxic and caused cell cycle arrest.

To determine whether the cell rounding induced by *P. nuttalliana* extracts was caused by an arrest in mitosis, we used immunofluorescence microscopy to detect nuclei and the mitotic protein phospho-histone H3 (PH3) (Figure 2.4A). Cells were either not-treated or treated with nocodazole, paclitaxel, stems A or stems B extracts. The not-treated cells had relatively few nuclei stained positive for PH3, whereas the nuclei in cells treated with either nocodazole or paclitaxel were nearly all positive for PH3, as expected. Importantly, both extract treatments induced a PH3 signal whereas stems A induced 47 ± 2% of cells with a PH3 signal and stem B induced 83 ± 3% of cells with a PH3 signal, supporting the evidence that cell rounding was linked to an arrest in mitosis.

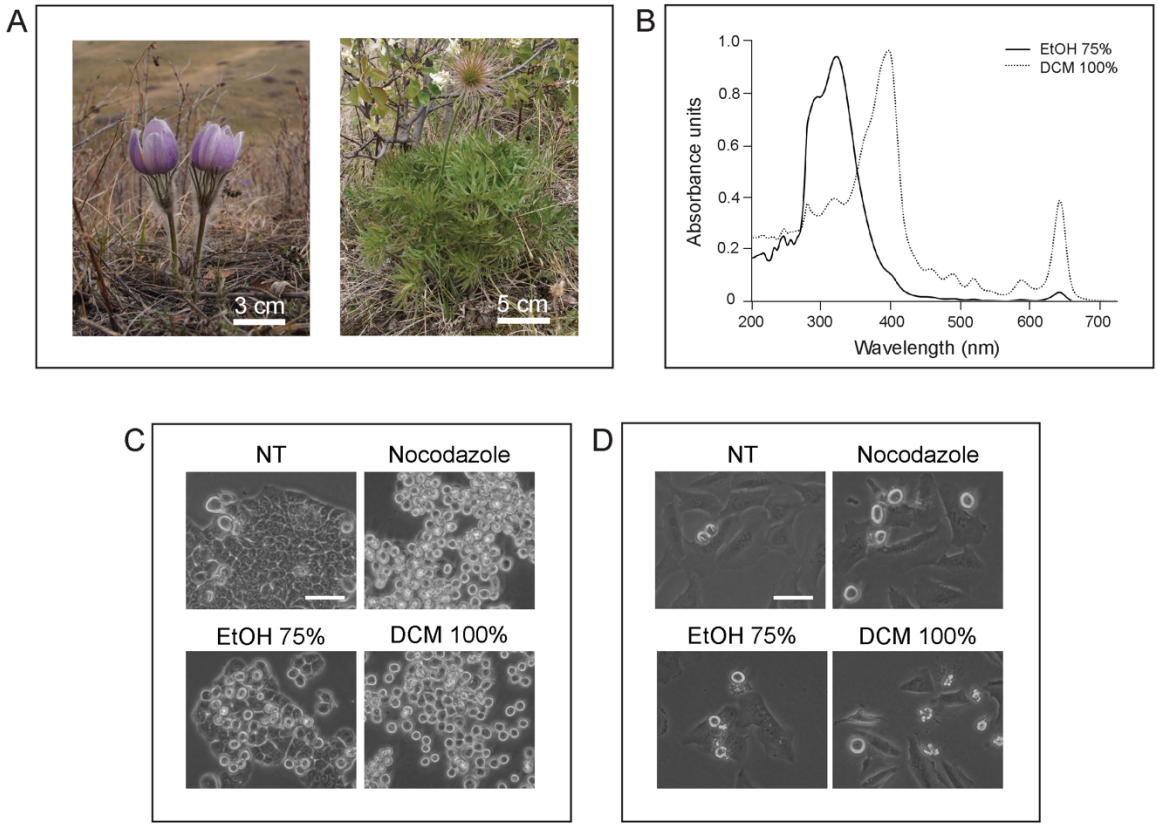

Figure 2.1. HT-29 and U2OS cells treated with *Pulsatilla nuttalliana* ethanolic and dichloromethane whole plant extracts acquire a rounded morphology. **A.** *Pulsatilla nuttalliana* (Ranunculaceae) in prairie habitat. Flowers (left); leaves and stems (right). **B.** UV/visible absorbance spectra of *P. nuttalliana* ethanolic (EtOH, solid line) and dichloromethane (DCM, dotted line) whole plant extracts. **C.** HT-29 cells and **D.** U2OS cells were either not-treated, treated with nocodazole, or treated with EtOH or DCM extract for 24 h. Images were taken by light microscopy and representative images are shown. Scale bar represents 50 µm.

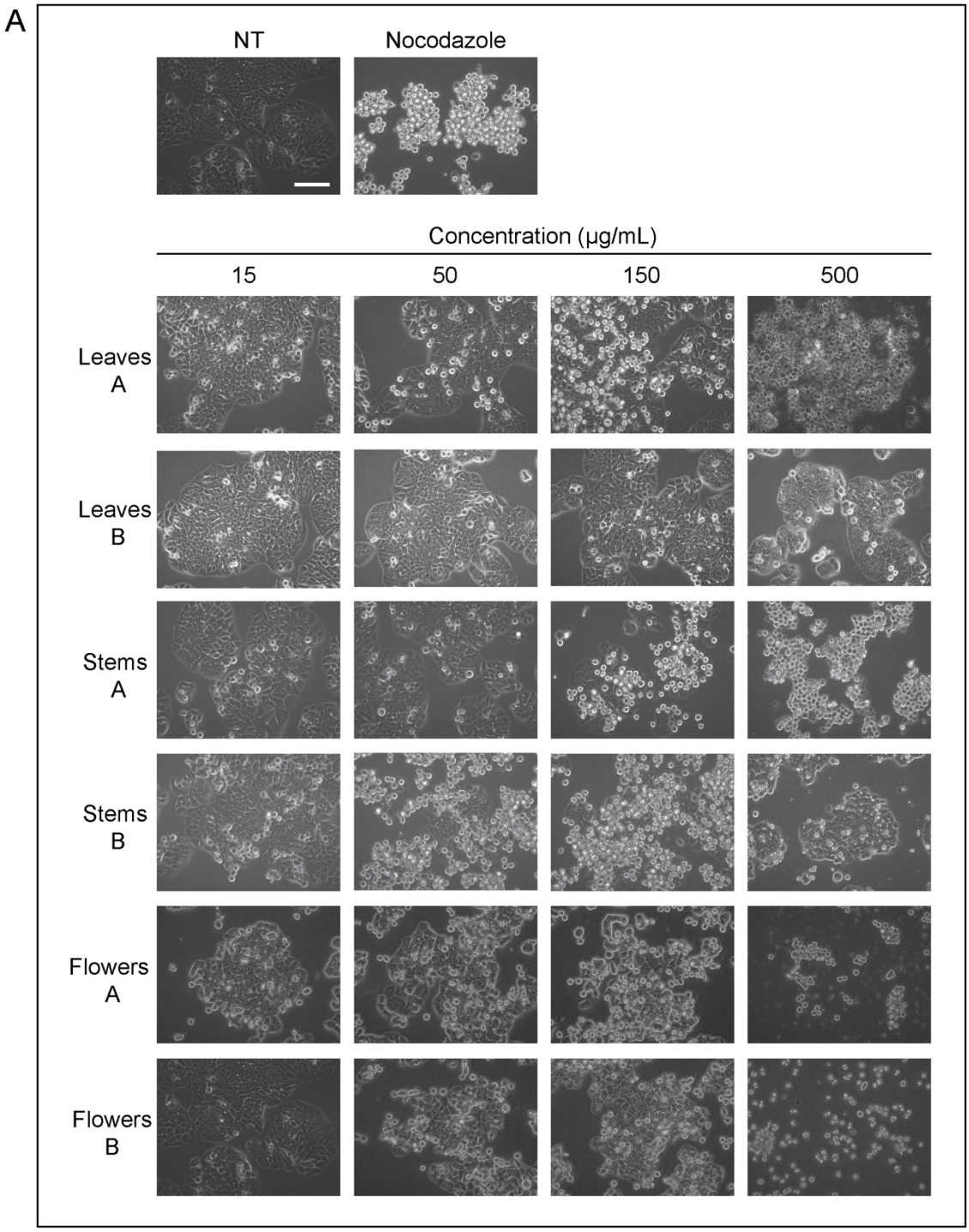
A
NT
Nocodazole
Concentration (µg/mL)
15
50
150
500
Leaves A
Leaves B
Stems A
Stems B
Flowers A
Flowers B

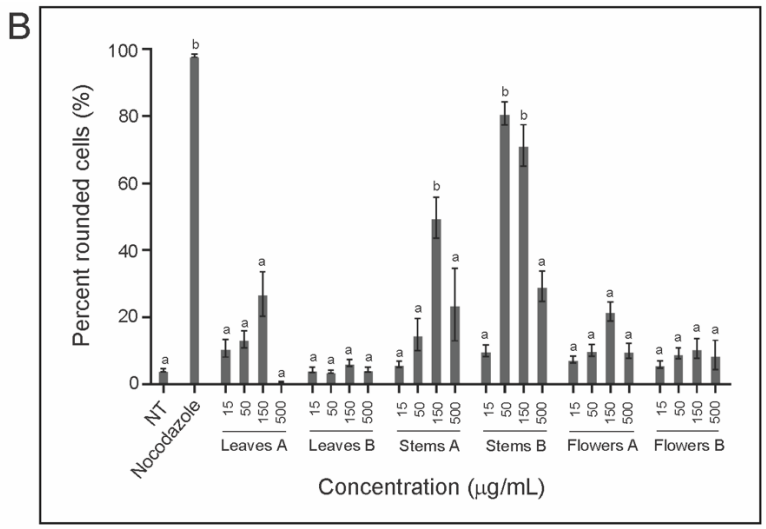

Figure 2.2. HT-29 cells treated with ethanolic or dichloromethane extracts of *P. nuttalliana* leaves, stems, or flowers acquire a rounded morphology. **A.** HT-29 cells were either not-treated or treated with nocodazole, *P. nuttalliana* ethanolic extracts (labelled as A) or dichloromethane extracts (labelled as B) of leaves, stems, or flowers for 24 h. Images were taken by light microscopy and representative images are shown. Scale bar represents 100 μm. **B.** The mean percentages of cells exhibiting a rounded morphology after treatment. Error bars represent the SEM of at least three independent experiments. Statistical significance was determined using one-way ANOVA followed by Tukey's post hoc test ($p < 0.0001$). Means that are significantly different from the mean of the not-treated control are represented with a different letter (a, b).

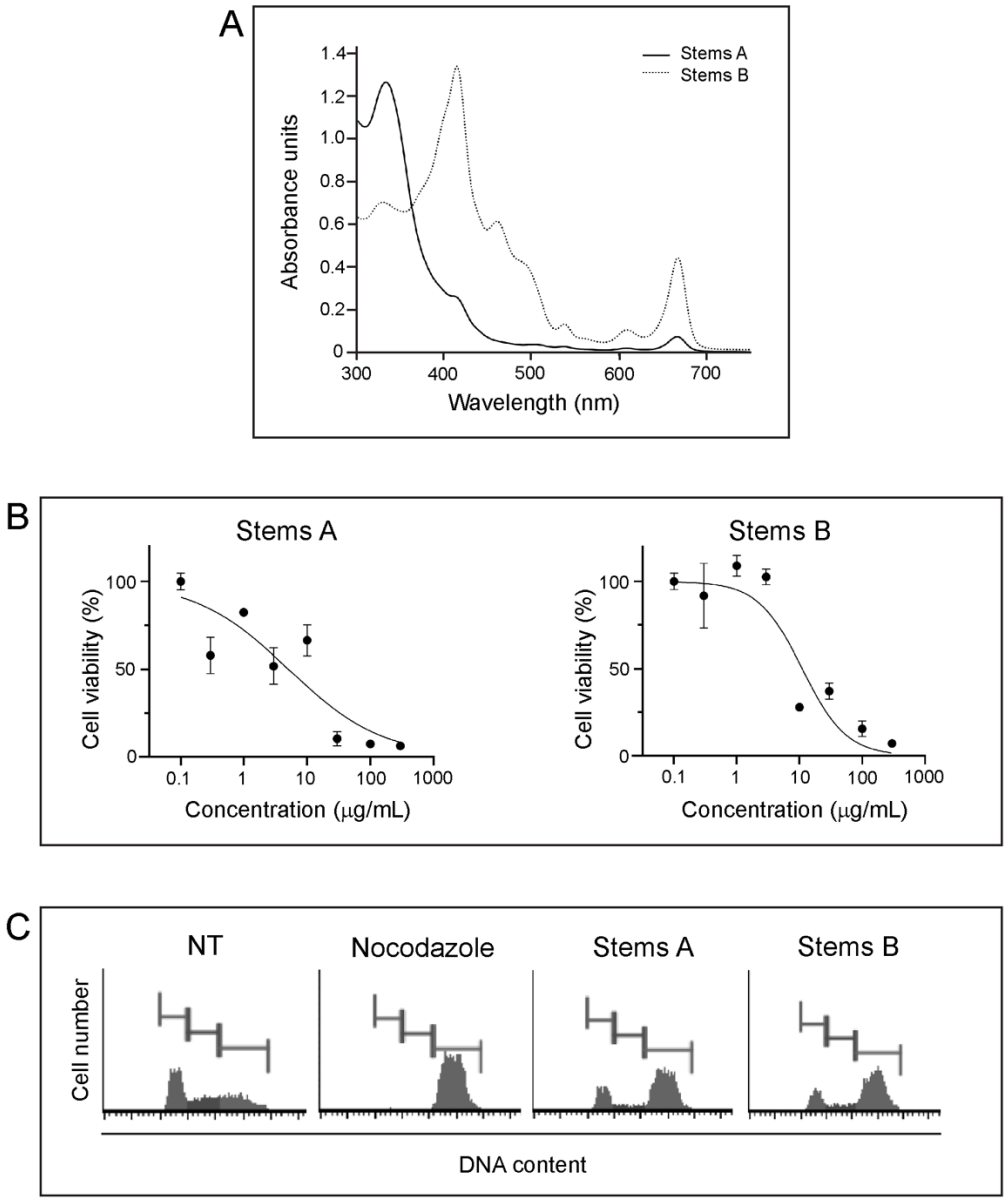

Figure 2.3. Plant extracts stems A and stems B are both moderately cytotoxic and cause a cell cycle arrest associated with the G2/M phase. **A.** UV/visible absorbance spectra of stems A (solid line) and stems B (dotted line). **B.** Percent cell viability of HT-29 cells was plotted as a function of the extract treatment concentration. **C.** HT-29 cells were either not-treated or treated with nocodazole, stems A or stems B and prepared for cell cycle analysis by flow cytometry. Histograms of representative experiments are shown with DNA content along the x-axis and cell count along the y-axis.

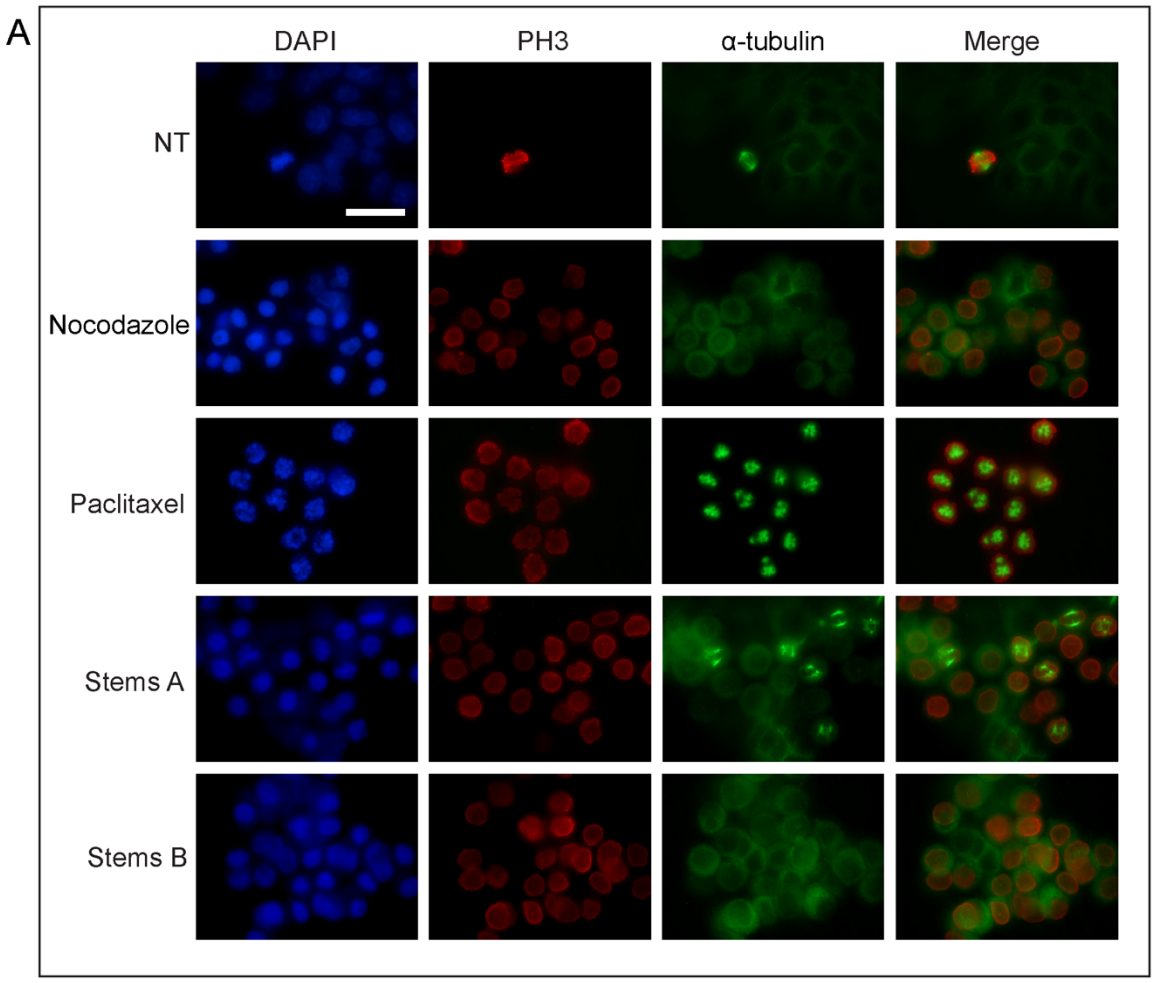
A
DAPI
PH3
α-tubulin
Merge
NT
Nocodazole
Paclitaxel
Stems A
Stems B

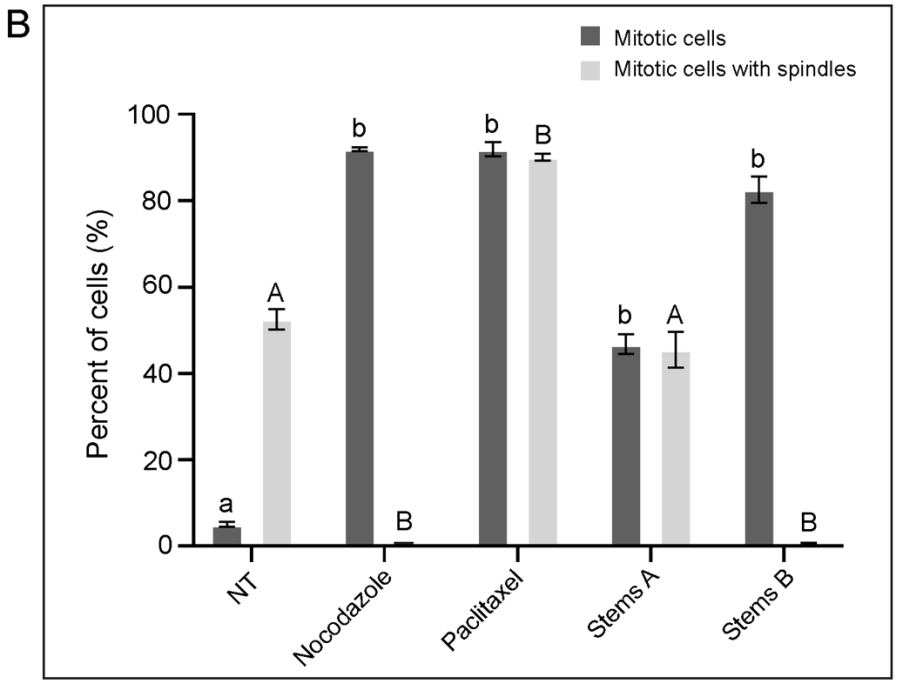
B
Mitotic cells
Mitotic cells with spindles
Percent of cells (%)
100
80
60
40
20
0
a
A
b
B
b
B
b
A
b
B
NT
Nocodazole
Paclitaxel
Stems A
Stems B

Figure 2.4. HT-29 cells treated with stems extracts exhibit a phospho-histone H3 signal with and without mitotic spindles. **A.** HT-29 cells were either not-treated or treated with nocodazole, paclitaxel, stems A or stems B extracts for 18 h. Cells were analyzed by immunofluorescence microscopy where DNA was detected with DAPI (blue), phosphorylated histone H3 with anti-phospho-histone H3 antibodies (red), and tubulin with anti-α-tubulin antibodies (green). The merge column is the combination of phospho-histone H3 and α-tubulin staining. Scale bar represents 50 μm. **B.** The mean percentages of cells exhibiting a phospho-histone H3 signal (mitotic cells, dark grey) and mitotic cells with a mitotic spindle (light grey) after treatment. Error bars represent the SEM of at least three independent experiments. Statistical significance was determined using one-way ANOVA followed by Tukey's post hoc test ($p < 0.0001$). Means that are significantly different from the mean of the not-treated control are represented with a different letter (a, b; A, B).

2.4.2 Pulsatilla nuttalliana extracts induced two distinct mitotic arrest phenotypes

We then observed the organization of tubulin in mitotic cells treated with each extract using immunofluorescence microscopy (Figure 2.4A). The few mitotic cells in the not-treated population showed bipolar spindles and these cells were co-stained with PH3 signals. Nocodazole prevents the formation of the mitotic spindle, leaving little or punctate staining, whereas paclitaxel stabilizes tubulin in spindle fibers, which increases signal intensity and co-localizes with PH3 signals. In cells treated with stems A, we made a striking observation of PH3 positive cells in which some contained tubulin spindle structures, whereas others did not. In contrast, stems B-treated mitotic cells did not contain spindles. We then calculated the percentage of cells in mitosis relative to the total population, and of those in mitosis, the percentage of cells that had a mitotic spindle (Figure 2.4B). The non-treated sample had 5 ± 1% of the cells in mitosis of which 53 ± 2% contained a bipolar spindle, which is consistent with the mitotic phases (prophase to telophase). None of the nocodazole-treated cells contained a spindle structure, whereas all of the paclitaxel-treated cells had a spindle structure, as expected. The stems A-treated mitotic cells showed 46 ± 4% with a spindle structure, and the remainder had no organized

tubulin structures. In contrast, only 1% of the stems B mitotic cells contained a spindle structure. We concluded that the *P. nuttalliana* extracts contained compounds with anti-mitotic activity; however, it appeared that there might be more than one type of activity present.

We then explored the possibility that the stems A extract might contain two distinct anti-mitotic activities by separating its complex chemical composition by column chromatography. The stems A extract was fractionated by LH-20 column chromatography, yielding 12 fractions (including a void volume fraction). Cells were then either not-treated or treated with nocodazole, stems A, or a fraction. After 24 h, the cells were observed by microscopy for cell rounding (Figure 2.5A). Not-treated cells had relatively few rounded cells, whereas treatment with nocodazole or stems A extract induced many rounded cells, as expected. Prominent cell rounding effects were observed in fractions 1 through 5 inclusive, and not in the void volume or fractions 6 through 11. We compared stems A, fraction 2 and fraction 5 using spectrophotometry and observed distinct spectra, suggesting that different compounds were eluted in each fraction (Figure 2.5B). We then tested whether fraction 2 or fraction 5 induced either of the two types of spindle profiles (spindle or no spindle) that were observed in the stems A whole extract again utilizing immunofluorescence microscopy (Figure 2.5C). Both fraction 2 and 5 treated cells had large numbers of PH3 positive cells, supporting the evidence that cell rounding was an arrest in mitosis. Close observation of fraction 2 treated cells revealed that 87 ± 1% of the cells positive for PH3 had a spindle structure. In contrast, fraction 5 treated cells were PH3 positive but did not display spindles (2 ± 1%) (Figures 2.5C, D). We concluded that *P. nuttalliana* contains two distinct anti-mitotic activities: one that arrests cells with mitotic spindles and another that arrests cells without spindles.

The two different biological responses (mitotic arrest with spindles and mitotic arrest without spindles) and the elution of these activities into separate fractions by chromatography suggest that this is the result of two distinct compounds. To assess this, we performed a chemical test by mixing fraction 2 or fraction 5 with the reducing agent beta-mercaptoethanol (β-ME) prior to treatment of cell cultures. In addition, cells were either not-treated or treated with nocodazole in the presence or absence of β-ME. Furthermore, we included two other mitotic-arresting compounds, 4-deoxypodophyllotoxin, which depolymerizes tubulin and is insensitive to β-ME, and hymenoratin, a natural product that induces mitotic arrest with spindles and is sensitive to reduction by β-ME. After 18 h of treatment, the cells were observed using light microscopy (Figure 2.6). β-ME did not induce mitosis in not-treated cells, nor did it reduce the cell rounding in nocodazole- or 4-deoxypodophyllotoxin-treated cells. In contrast, β-ME reduced the cell rounding activity of hymenoratin, demonstrating that different types of anti-mitotic compounds can be distinguished in this assay. Importantly, β-ME reduced the mitotic arrest activity of fraction 2 (mitotic arrest with spindles) but not the mitotic arrest activity of fraction 5 (mitotic arrest without spindles). These data support the conclusion that *P. nuttalliana* harbours two anti-mitotic activities that are both biologically and chemically distinct.

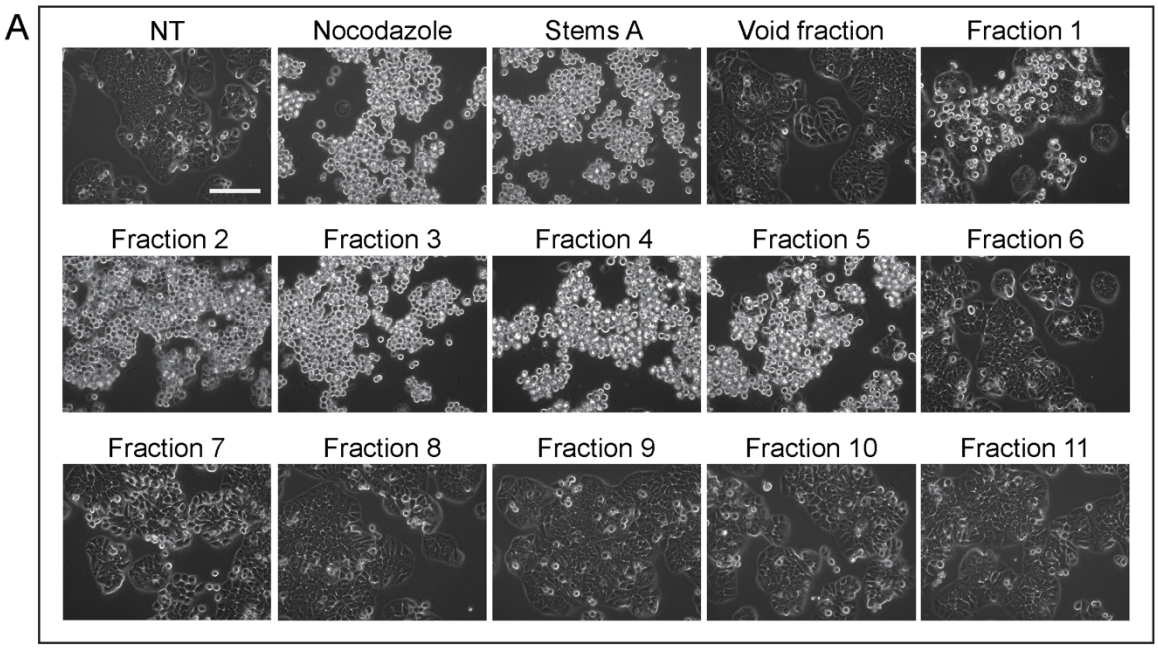
A
NT
Nocodazole
Stems A
Void fraction
Fraction 1
Fraction 2
Fraction 3
Fraction 4
Fraction 5
Fraction 6
Fraction 7
Fraction 8
Fraction 9
Fraction 10
Fraction 11

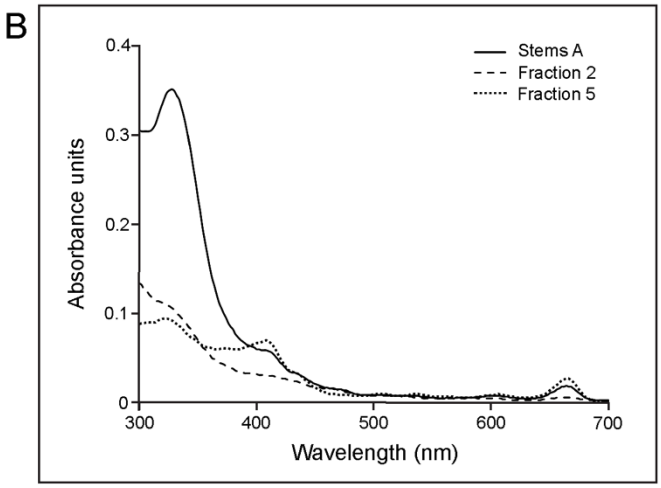
B
Stems A
Fraction 2
Fraction 5
Absorbance units
0.4
0.3
0.2
0.1
0
300
400
500
600
700
Wavelength (nm)

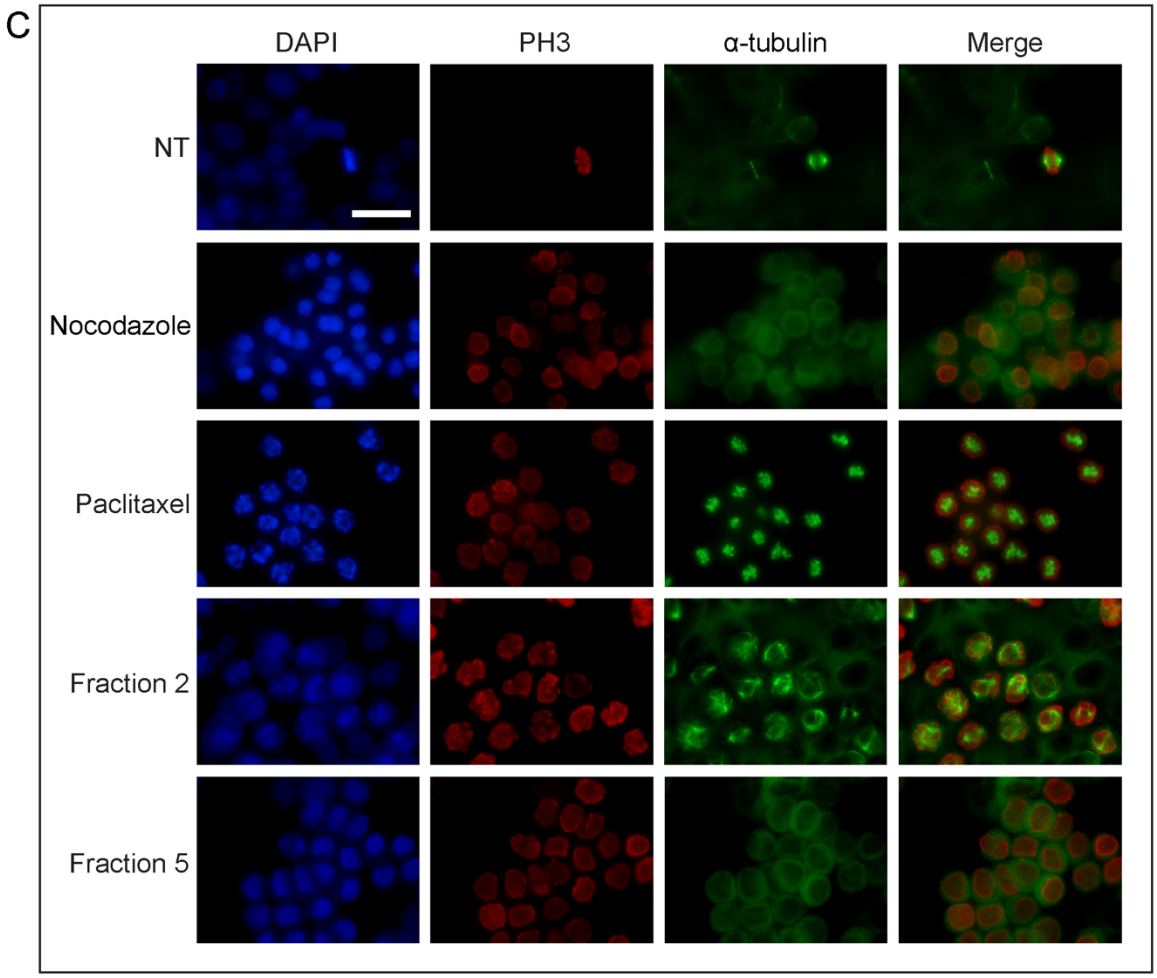
C
DAPI
PH3
α-tubulin
Merge
NT
Nocodazole
Paclitaxel
Fraction 2
Fraction 5

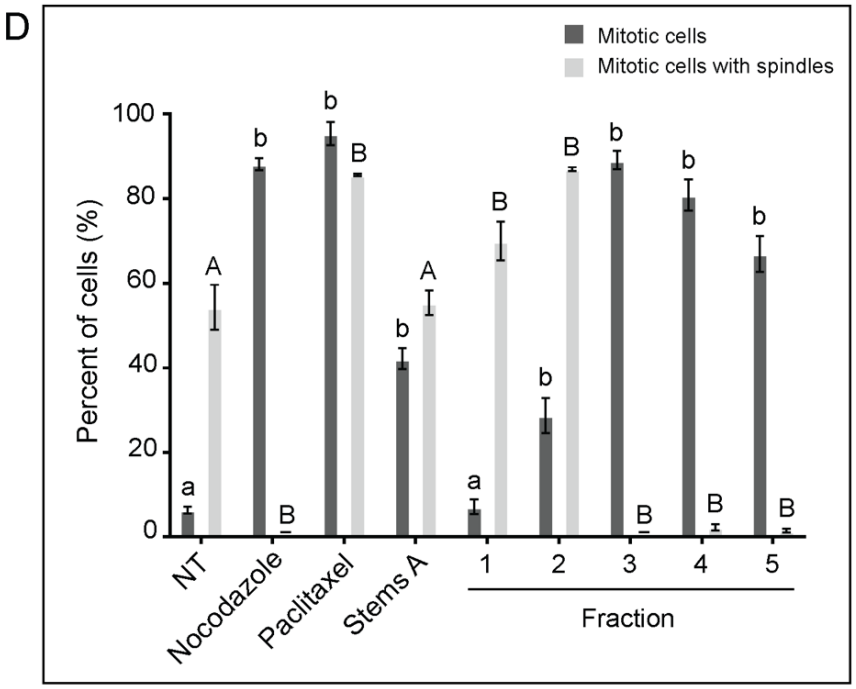

Figure 2.5. Fractionation distinguished mitotic spindle profiles of stems A extract between fraction 2 and fraction 5. **A.** HT-29 cells were either not-treated or treated with nocodazole, stems A, fractions 1 through 11, or void fraction for 24 h. Images were taken by light microscopy and representative images are shown. Scale bar represents 100 µm. **B.** UV/visible absorbance spectra of stems A whole extract (solid line), fraction 2 (dashed line) and fraction 5 (dotted line). **C.** HT-29 cells were either not-treated or treated with nocodazole, paclitaxel, stems A, fraction 2 or fraction 5 for 18 h. Cells were analyzed by immunofluorescence microscopy where DNA was detected with DAPI (blue), phosphorylated histone H3 with anti-phospho-histone H3 antibodies (red), and tubulin with anti-α-tubulin antibodies (green). The merge column is the combination of phospho-histone H3 and α-tubulin staining. Scale bar represents 50 µm. **D.** The mean percentages of cells exhibiting a phospho-histone H3 signal (mitotic cells, dark grey) and mitotic cells with a spindle structure (light grey) after treatment. Error bars represent the SEM of at least three independent experiments. Statistical significance was determined using one-way ANOVA followed by Tukey's post hoc test ($p < 0.005$). Means that are significantly different from the mean of the not-treated control are represented with a different letter (a, b; A, B).

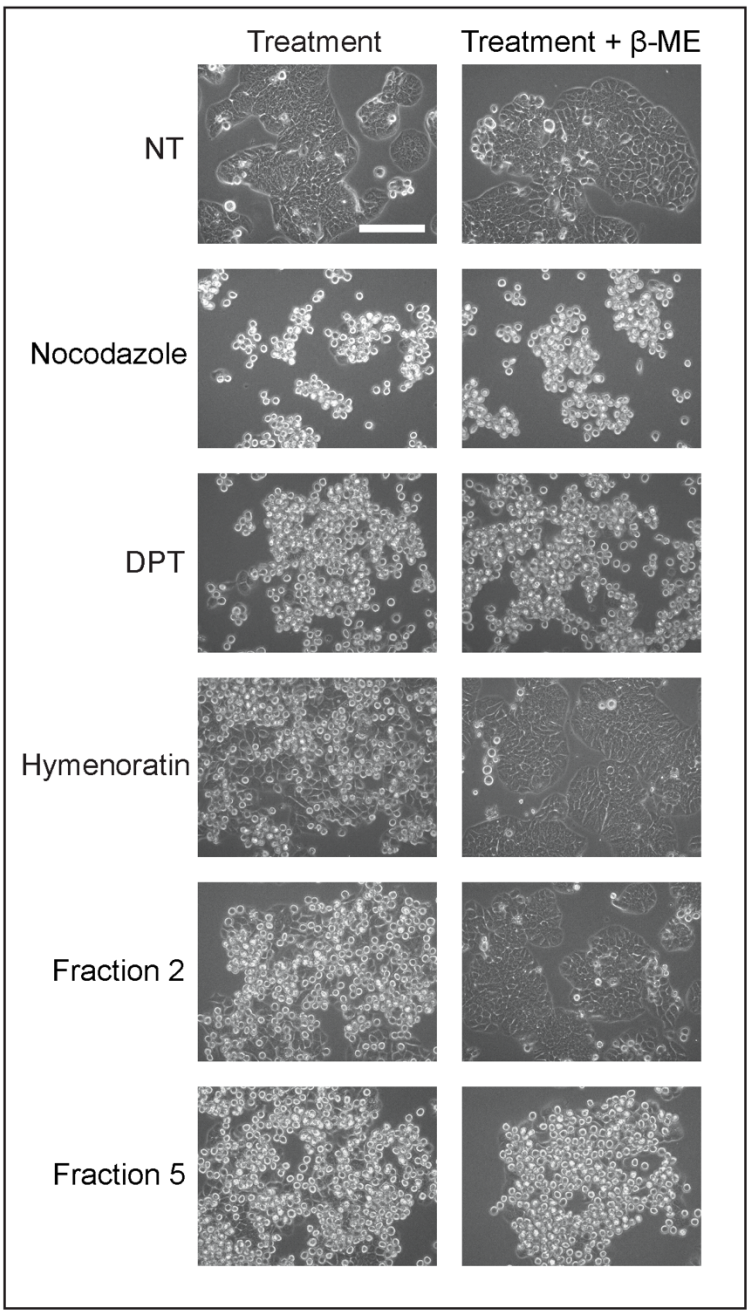

Figure 2.6. Cell rounding activity of fraction 2 was eliminated after reduction by beta-mercaptoethanol, whereas the cell rounding activity of fraction 5 was maintained. HT-29 cells were either not-treated or treated with nocodazole, 4-deoxypodophyllotoxin (DPT), hymenoratin, stems A fraction 2 or stems A fraction 5 for 24 h. Treatments were administered either alone or after preincubation with beta-mercaptoethanol (β-ME). Images were taken by light microscopy and representative images are shown. Scale bar represents 100 μm.

2.4.3 Isolation of anemonin from Pulsatilla nuttalliana and characterization of mitotic arrest

We used biology guided fractionation to isolate the compound that induced the mitotic arrest with spindles from *P. nuttalliana* stems. Through successive rounds of fractionation, we isolated a bicyclic butenolide known as anemonin ($C_{10}H_8O_4$) from *P. nuttalliana* (Figure 2.7A). The structure of anemonin was elucidated by analysis of 1D and 2D NMR data. The proton and carbon NMR data recorded for the sample in DMSO-d_6 exactly matched the literature values (Saidi et al., 2018).

We confirmed in cell rounding assays that anemonin induced 44 ± 4% cell rounding at 15 μM in HT-29 cells which, was similar to the effect of fraction 2 at 45 ± 3% cell rounding. An increase in the concentration of anemonin to 50 μM did not increase the percentage of cell rounding (Figures 2.7B, C). An independent source of anemonin was purchased and tested in a separate experiment and induced cell rounding, confirming its activity (data not shown). We then tested whether the cell rounding activity of anemonin could be reduced after incubation with β-ME, as observed in experiments using extract fraction 2. Cells were either not-treated, or treated with β-ME, anemonin, or anemonin that was preincubated with β-ME (Figure 2.7D). As we observed with various plant fractions, the cell rounding activity of anemonin was reduced by β-ME. Finally, we confirmed that anemonin was the compound responsible for the mitotic arrest with spindle structures by immunofluorescence microscopy (Figure 2.7E). These data provided evidence that *P. nuttalliana* harbours two distinct anti-mitotic compounds: one that arrests cells in mitosis without mitotic spindles, and another that arrests cells in mitosis with spindle structures which we identified as the natural product anemonin.

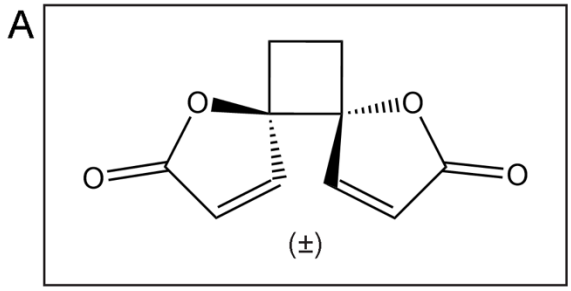
A
O
O
O
O
(±)

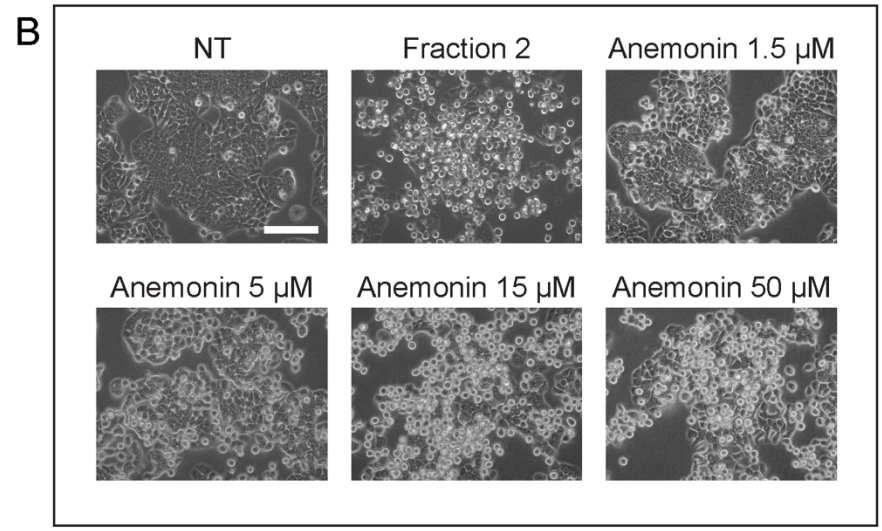
B
NT
Fraction 2
Anemonin 1.5 μM
Anemonin 5 μM
Anemonin 15 μM
Anemonin 50 μM

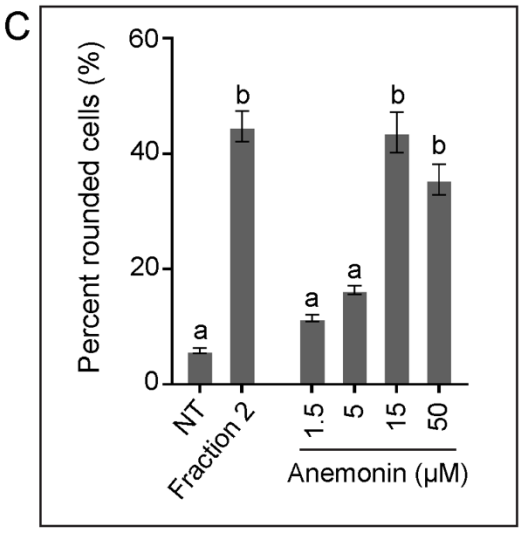
C
Percent rounded cells (%)
60
40
20
0
a
b
a
a
b
b
NT
Fraction 2
1.5
5
15
50
Anemonin (μM)

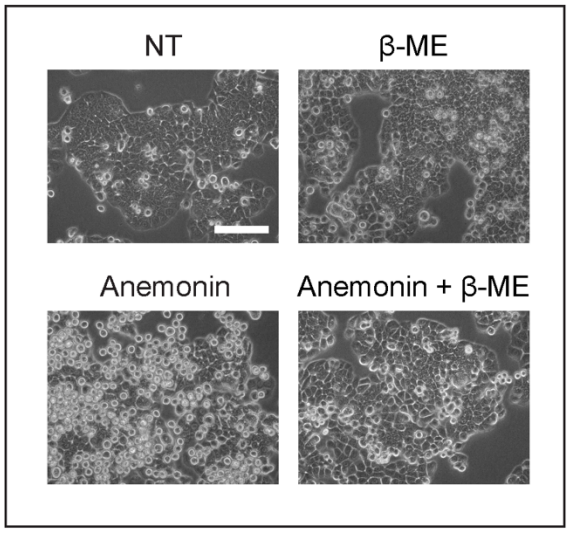
D
NT
β-ME
Anemonin
Anemonin + β-ME

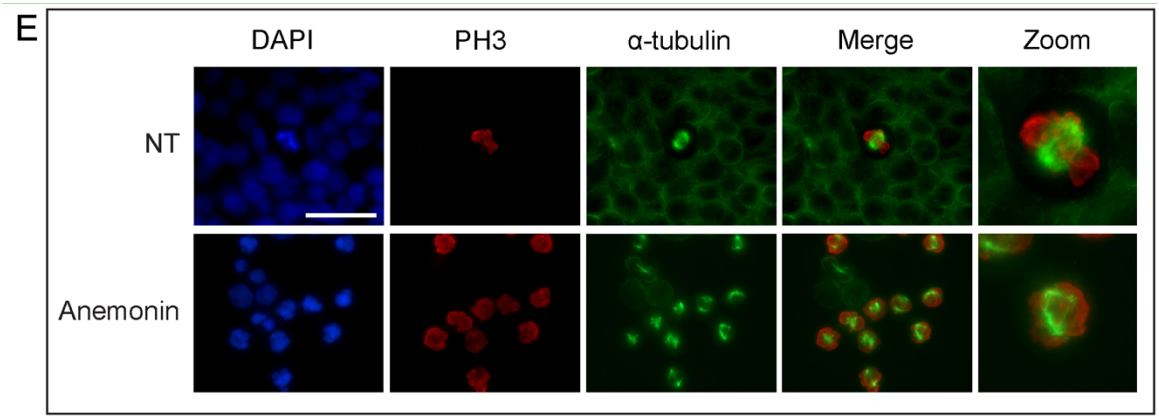

Figure 2.7. Anemonin, isolated by biology-guided fractionation of *P. nuttalliana*, induced cell rounding in HT-29 cells and its activity can be eliminated by beta-mercaptoethanol reduction. **A.** The chemical structure of anemonin. **B.** HT-29 cells were either not-treated or treated with fraction 2 or varying concentrations of anemonin for 24 h. **C.** The mean percentages of cells exhibiting a rounded morphology after treatment. Error bars represent the SEM of at least three independent experiments. Statistical significance was determined using one-way ANOVA followed by Tukey's post hoc test ($p < 0.0001$). Means that are significantly different from the mean of the not-treated control are represented with a different letter (a, b). **D.** HT-29 cells were either not-treated or treated with anemonin for 24 h, where treatments were either administered alone or after preincubation with beta-mercaptoethanol (β-ME). Images were taken by light microscopy and representative images are shown. Scale bar represents 100 µm. **E.** HT-29 cells were either not-treated or treated with 15 µM anemonin for 18 h. Cells were analyzed by immunofluorescence microscopy where DNA was detected with DAPI (blue), phosphorylated histone H3 with anti-phospho-histone H3 antibodies (red), and tubulin with anti-α-tubulin antibodies (green). The merge column is the combination of phospho-histone H3 and α-tubulin staining. Scale bar represents 50 µm.

2.5 Discussion

This study is the first to investigate the biological activities of *Pulsatilla nuttalliana* and identify the anti-mitotic activity of the natural product anemonin. *P. nuttalliana*, commonly known as the Prairie Crocus or American pasqueflower, is native to North America, whereas *P. patens* (the Eastern pasqueflower) is native to Europe and Asia (Mosyakin, 2016). The Pulsatilla genus harbours numerous biological activities (Łaska et al., 2019), including inhibition of cancer-related signalling pathways by *P. patens* extracts (Łaska et al., 2021), increased cancer cell death by *P. decoction* extracts (Jie et al., 2022), inhibition of cell proliferation by pulsatilla saponin D (Son et al., 2013) and inhibition of mitosis by deoxypodophyllotoxin (Kim et al., 2002) both isolated from *P. koreana*. Neither of the two North American species, *P. nuttalliana* and *P. occidentalis*, a have been investigated previously for biological activity.

After identifying two distinct anti-mitotic phenotypes from *P. nuttalliana* extracts, one with mitotic spindles and one without, we explored the possibility that the stems contained two different anti-mitotic compounds. By column chromatography, we reduced the chemical complexity of the extract as demonstrated by absorbance spectra and identified separate fractions that arrested cells in mitosis either with mitotic spindles or without spindles. The combination of two distinct anti-mitotic compounds, which may have different inhibitory concentrations, would explain the complex results of the cell viability assay from the whole stems A extract. An assay with β-ME distinguished the two anti-mitotic activities chemically, as the activity of fraction 2 was reduced after incubation with β-ME, whereas the activity of fraction 5 did not change after incubation with β-ME. This suggests that the two fractions contain different chemical compounds in support of their

distinct biological and chemical properties. Finally, we identified the natural product anemonin as the active compound within fraction 2.

Anemonin is a bicyclic symmetrical butenolide first isolated in 1792 (Moriarty et al., 1965) and is a natural product found in various species of the Ranunculaceae family, including *P. chinensis* (Duan et al., 2006), *P. wallichiana* (Ali et al., 2019), and *Clematis chinensis* (Y. H. Huang et al., 2008). It is recognised for its anti-inflammatory activity (Jiang et al., 2022; Wang et al., 2017) and has been reported to exhibit cytotoxicity against certain cancer cell lines (Ali et al., 2019; Y. H. Huang et al., 2008). Anemonin, however, has not been previously reported to arrest cells in mitosis. We have identified several features of anemonin that are similar to those found in previously identified sesquiterpene lactones isolated from the Asteraceae botanical family, including hymenoratin (Molina et al., 2021), pulchelloid A (Bosco et al., 2021), 6-O-angeloylplenolin (Liu et al., 2011) and psilostachyins A and C (Sturgeon et al., 2005). The anti-mitotic activity of anemonin was similar to that of hymenoratin, where both induced mitotic arrests with distorted mitotic spindle structures (Molina et al., 2021), and their activities were reduced after incubation with β-ME. The similarity in the biological and chemical responses between anemonin and select sesquiterpene lactones may be due to the shared α,β-unsaturated carbonyl functional group, as demonstrated in studies with coronopilin (Cotugno et al., 2012) and psilostachyin A (Sturgeon et al., 2005).

The Asteraceae family is phylogenetically distant from the Ranunculaceae family, however, diverging over 140 million years ago (Wikström et al., 2001). This may indicate that inhibitors with these similar mitotic arrest phenotypes are not solely localised to the Asteraceae family. Therefore, similarities between the anti-mitotic activities of sesquiterpene lactones and non-sesquiterpene lactones, such as anemonin, should be

considered. The natural product *ent*-15-oxokaurenoic acid (EKA) is another example of a compound that induces a 20-30% mitotic arrest with an abnormal spindle structure (Rundle et al., 2006). While not a sesquiterpene lactone, it contains an α,β-unsaturated carbonyl group. The discovery of anemonin may help bridge this gap in the literature for non-tubulin-binding anti-mitotic compounds and guide our research in identifying the molecular targets of these compounds.

The results of the bio-assays and chemical tests for fraction 5 were consistent with those of a 4-deoxypodophyllotoxin-like activity. 4-deoxypodophyllotoxin (DPT) is an anti-mitotic compound that inhibits microtubule polymerization (Desbène & Giorgi-Renault, 2002) and has been previously identified in *P. koreana* (Kim et al., 2002). β-peltatin, a podophyllotoxin isomer, was recently isolated from *P. decoction* and was found to induce a G2/M cell cycle arrest in PAC cell lines (Wu et al., 2023). Further investigation of fraction 5 may reveal that its chemical composition contains podophyllotoxin, β-peltatin, or a related compound characterized to depolymerize tubulin.

A growing number of natural products have been found to cause mitotic arrests similar to those of anemonin and hymenoratin, as opposed to those of tubulin-targeting compounds such as paclitaxel and podophyllotoxins. The results presented in this paper and others provide evidence that compounds which induce unique mitotic phenotypes should be further investigated, beyond cytotoxicity, for novel anti-mitotic mechanisms of action, as many mitotic pathways still have no known inhibitors. Identifying novel mitotic inhibitors will contribute to a deeper understanding of the complexities of mitosis and may lead to the development of new anti-cancer treatments. This is the first report of two biologically distinct and chemically distinct anti-mitotic activities identified from a single prairie plant species. Further investigations will include identifying the compound inducing

the podophyllotoxin-like activity, followed by the identification of the precise cellular targets for both compounds. The multifaceted biological activity of *P. nuttalliana* should continue to be explored, and anemonin may prove valuable as a natural product for pharmaceutical and scientific application.

CHAPTER 3

An anti-mitotic compound, (+)-6-tuliposide A, isolated from the Canadian Glacier Lily, *Erythronium grandiflorum*

Shannon M. Healy Knibb, Benjamin Yeremy, David E. Williams, Raymond J. Andersen and Roy M. Golsteyn

This chapter has been submitted for publication by the journal "Fitoterapia."

3.1 Abstract

The Canadian prairie ecosystem is subjected to a range of abiotic and biotic conditions that induce plants to produce secondary metabolites that affect mammalian physiology. Extracts prepared from certain plant species native to Canadian prairie and montane cordillera ecosystems have previously been shown to have anti-mitotic activity on human cancer cell lines. In this study, we investigated the Glacier Lily, *Erythronium grandiflorum* (Liliaceae), which was the most phylogenetically distant botanical extracts with anti-mitotic activity in our library. When added to cell lines, we found *E. grandiflorum* extracts induced a rounded cell morphology and arrested cells in the G2/M phase of the cell cycle. Of the cells that displayed a rounded phenotype, all were positive for phospho-histone H3 and contained a distorted mitotic spindle. This anti-mitotic activity was distinct from that of the compound colchicine, which had been previously isolated from the Liliaceae family. By biology-guided fractionation, we isolated the natural product (+)-6-tuliposide A and are the first to report its anti-mitotic activity. These results reveal a chemical motif in secondary metabolites and expand the range of Canadian prairie plants with anti-mitotic activity that can become new scientific tools or used in the development of anti-proliferative medicines.

3.2 Introduction

We are investigating natural products from Canadian botanical species to understand better the chemical relationships and potential medicinal compounds present in Canadian ecosystems (Kernéis et al., 2015; Tuescher et al., 2021; Tuescher et al., 2020). The 15 ecological zones within Canadian borders are vast and diverse regions that offer a comprehensive platform for exploring botanical natural products. Of these, the prairie and montane cordillera ecozones are largely understudied for natural products (Thornburg et al., 2018), yet they likely hold diverse biosynthetic potential, given the extremes of environmental stressors, including climate, solar irradiation, and herbivory (Erb & Kliebenstein, 2020; Jaakola & Hohtola, 2010; Molina et al., 2022; Yeshi et al., 2022). The exploration of natural products in this geographically and ecologically varied region presents an opportunity to uncover compounds with novel bioactivities that are produced by plants as ecological adaptations and may serve as guides for future pharmaceutical chemicals (Newman, 2022).

The botanical species in Canadian ecosystems also provide opportunities to explore the relationship between botanical phylogenetics and chemical diversity (Hoffmann et al., 2018). Notably, phylogenetic relationships among plants offer predictive insights into their chemistry (Saslis-Lagoudakis et al., 2012; Wink, 2003). This phylogenetic proximity translates to similarities in metabolic pathways and, consequently, the biosynthesis of homologous compounds. Thus, taxa-specific secondary metabolite biosynthesis may justify strategic bioprospecting within specific botanical families, extrapolating the chemical diversity and potential bioactivities from known entities to unexplored members of taxa. For example, the investigation of *Taxus baccata* and the consequent discovery of docetaxel was prompted only after the isolation of paclitaxel from *Taxus brevifolia*

(Guénard et al., 1993). Phylogenetic-guided bioprospecting is an important tool for drug discovery and has successfully led to the identification of natural products with antimalarial activity (Liana & Rungsihirunrat, 2021; Pellicer et al., 2018), potential cardiovascular drugs (Guzman & Molina, 2018), acetylcholinesterase inhibitors (Bay-Smidt et al., 2011; Larsen et al., 2010), and antibiotics (Culp et al., 2020). Furthermore, abiotic and biotic stressors in an ecological zone may drive phylogenetically diverse species to converge on similar biochemical pathways.

Prior research from our laboratory has identified a subclass of sesquiterpene lactones that induce mitotic arrest in human cancer cell lines (Bosco et al., 2021; Molina et al., 2021). These natural products were isolated from Canadian species in the Asteraceae taxonomic family, and these data were consistent with other reports of anti-mitotic activity of sesquiterpenes present in tropical Asteraceae species (Bosco & Golsteyn, 2017; Chadwick et al., 2013; Costantino et al., 2016; Cotugno et al., 2012; Fonrose et al., 2007; Ren et al., 2016; Rundle et al., 2006). We developed a robust and facile method for identifying botanical extracts with mitotic arrest activity (Kubara et al., 2012). From this screen, a species from the Liliaceae botanical family was identified. Liliaceae, a plant family with a rich history of ethnobotanical use and chemical exploration, is an important source of natural products. For instance, colchicine isolated from *Gloriosa superba* (Srivastava et al., 2014) exhibits anti-inflammatory and anti-proliferative (mitotic) activities. Another example pertains to steroidal saponins, such as diosgenin, isolated from various species within the Liliaceae family (Mimaki et al., 2001), which not only holds pharmacological interest but has been a precursor in the industrial synthesis of steroidal drugs.

We report the investigation of a natural product from *Erythronium grandiflorum*, a member of the Liliaceae family. *E. grandiflorum*, commonly known as the Glacier Lily, is a perennial herbaceous plant native to western North America with its range extending from Alberta and British Columbia in Canada to California in the United States (Moss & Packer, 1983). They are among the first flowers to bloom in spring, and their emergence is associated with the melting of snow which gives rise to their common name and reflects their ecological hardiness (Kuijt, 1982). We isolated the (+)-6-tuliposide A from *E. grandiflorum* and are the first to report that it has mitotic arrest activity. Our findings expand the catalogue of biologically active natural products isolated from Canadian botanical species.

3.3 Materials and Methods

3.3.1 Plant Collection and Preparation of Plant Extracts

Erythronium grandiflorum (Liliaceae) aerial plant parts were collected in southern Alberta, Canada at North 49°4 latitude and West -112°5 longitude, at an elevation of approximately 1400 metres during 2018 and 2022. Permits from provincial and local governments were acquired for collection, and plants were harvested by sustainable practice. Plant taxonomy was confirmed to species (Bain et al., 2014; Kershaw & Allen, 2020; Moss & Packer, 1983), and a voucher specimen was provided to the University Herbarium as #Golsteyn1850. The plants were dried in a dehydrator at 40°C for 72 hours (h) and then stored in a dark dry environment at room temperature until use. Extracts were prepared from either whole aerial plant parts, leaves, stems, or flowers by grinding the dried material into a fine powder. The powdered material was then suspended in either 75% (v/v) ethanol in water (A extracts) or in 100% dichloromethane (B extracts) and stirred overnight at room temperature on a shaking platform. The suspensions were filtered, dried, and stored in the dark at room temperature. Crude extracts were dissolved in dimethyl sulfoxide (DMSO) (Sigma-Aldrich, D2438) to a concentration of 50 mg/mL for use in biological assays.

3.3.2 Spectrophotometry

The extracts were diluted in 100% methanol to 1 mg/mL, and the absorbance was read from 300 to 700 nm with a step of 2 nm between reads on an Epoch microplate spectrophotometer and Gen5 software (BioTek Instruments, USA). Absorbance data were blanked to a methanol negative control and normalized using Microsoft Excel and the following equation:

Normalized absorbance = (absorbance - minimum) / (maximum - minimum)

3.3.3 Cell Culture

The human cell lines HT-29 (ATCC HTB-38), U2OS (ATCC HTB-96), and WI-38 (ATCC CCL-75) were obtained from the American Type Culture Collection (ATCC) and cultured as previously described (Kubara et al., 2012; Lewis & Golsteyn, 2016). HT-29 cells were plated at a density of 3.0 x 10^5 cells/25 cm^2 flask and cultured for 48 h prior to treatment. U2OS cells were plated at a density of 3.0 x 10^5 cells/25 cm^2 flask and cultured for 24 h prior to treatment. WI-38 cells were plated at a density of 1.5 x 10^5 cells/25 cm^2 flask and cultured for 24 h prior to treatment. HT-29 cells were selected for further study because of their capacity to sustain a mitotic arrest (Gascoigne & Taylor, 2008). The compounds nocodazole (660 µM, Sigma-Aldrich, M1404), paclitaxel (1 mM, Sigma-Aldrich, T7402), colchicine (100 mM, Sigma-Aldrich, C9754), and pulchelloid A (10 mM) were dissolved in DMSO and stored at -20°C. For not-treated cells, DMSO was added as a solvent vehicle control at a final concentration of 0.4% (v/v). Light microscopy images were captured using an Olympus CKX41 inverted microscope with an Infinity 1 camera operated by Infinity Capture imaging software (Lumenera Corporation, CA). Cells were manually scored for rounded or flat morphology and at least 200 cells were counted per treatment group.

3.3.4 Cell Viability Assay

The cytotoxicity of the extracts was measured using the 3-(4,5-dimethylthiazol-2-yl)-2,5-diphenyltetrazolium (MTT) assay (Sigma-Aldrich, M2128) (Kubara et al., 2012). HT-29 cells were seeded in a 96 well plate at 5,000 cells/well and incubated at 37°C for 48 h prior to treatment. After 72 h of treatment, 20 µL of MTT solution (5 mg/mL MTT in phosphate-

buffered saline (PBS:137 mM NaCl, 3 mM KCl, 100 mM Na_2HPO_4, and 18 mM KH_2PO_4)) was added to the media in each well, followed by a 3.5 h incubation at 37°C. The medium was then aspirated and replaced with 150 µL of MTT solvent (4 mM HCl, 0.1% (v/v) octylphenoxypolyethoxyethanol, in isopropanol) in each well. The plates were left in the dark for 15 min with shaking, and a CytationTM 5 Cell Imaging Multi-Mode Reader (BioTek Instruments, USA) equipped with Gen5 software was used to measure the absorbance of each well at 590 nm. IC_{50} values were calculated and represent the concentration of the compound or plant extract that reduced the absorbance of MTT by 50% compared with 0.1% (v/v) DMSO-treated cells. The normalized absorbance percentage was calculated as follows:

Normalized percent absorbance = (absorbance / DMSO absorbance) x 100

The log concentrations of the extracts were plotted against the normalized absorbance percentages using Microsoft Excel. Analysis was performed with GraphPad Prism 5 software using non-linear regression (log(inhibitor) versus normalized response) to estimate IC_{50} concentrations. The standard curves were plotted using the following equation:

$$Y = \text{maximum} + (\text{maximum} - \text{minimum}) / (1+10(X-\text{Log}IC_{50}))$$

Where Y is the percentage of viable cells, maximum is the percentage of viable cells after treatment with 0.1% DMSO, minimum is the percentage of viable cells after treatment with the highest concentration of cytotoxic compounds, and X is the $\log_{10}$ value of treatment concentration. All experiments were performed in triplicate and repeated at least three times.

3.3.5 Flow Cytometry

HT-29 cells were plated at 3.0 x 10^5 cells/25 cm^2 flask and incubated for 48 h at 37°C prior to treatment. After treatment for 18 h, cells were collected by trypsinization, washed with cold PBS (0.8% FBS (fetal bovine serum), 1 mM EDTA (ethylenediaminetetraacetic acid)), fixed in ice-cold 70% ethanol for 24 h, and stored at -20°C until use. The samples were centrifuged at 300 × *g* for 5 min at 4°C, washed with PBS, and resuspended in Muse Cell Cycle staining reagent for 30 min. The samples were analyzed using a Muse® Cell Analyzer (Luminex), and gating was set using a non-treated sample. All experiments were performed in triplicate.

3.3.6 Cell Extraction and Western Blotting

HT-29 cells were plated at 3.0 x 10^5 cells/25 cm^2 flask and incubated for 48 h at 37°C prior to treatment. After treatment for 18 h, total cell populations were collected by trypsinization. Rounded mitotic cells, which are weakly adherent, were collected by mechanical shake-off to separate them from interphasic cells that are strongly adherent (Swift & Golsteyn, 2016). Interphasic cells were collected by trypsinization. Cells were resuspended in ice cold lysis buffer (50 mM HEPES (4-(2-hydroxyethyl)-1-piperazineethanesulfonic acid), pH 7.4, 50 mM NaF, 10 mM EGTA (ethylene glycol bis-(2-aminoethylether)-*N*,*N*,*N*',*N*'-tetraacetic acid), 50 mM β-glycerophosphate, 1 mM ATP, 1 mM DTT (dithiothreitol), 1% Triton X-100 (v/v), 10 µg/mL RNase A (Sigma-Aldrich, R6513-250MG), 0.4 U/mL DNase I (Invitrogen, I354Ba), and protease inhibitor cocktail (Roche, 11836170001)) at a concentration of 20,000 cells/µL, passed through a 26-gauge needle five times to lyse the cells, and incubated on ice for 30 min. The suspension was centrifuged at 10,000 × *g* for ten minutes at 4°C and stored at -80°C until use. Extracts were

prepared for electrophoresis after being heated for ten minutes at 95°C in the presence of 2x SDS (sodium dodecyl sulfate) sample buffer (20% (v/v) glycerol, 10% (v/v) DTT, 6% (w/v) SDS, 500 mM Tris, pH 6.8). Western blots were performed as previously described (Swift & Golsteyn, 2016) using anti-cyclin B1 (Santa Cruz Biotechnology, sc-245; 1:200) and anti-actin (Santa Cruz Biotechnology, sc-58673; 1:200) primary antibodies, and alkaline phosphatase coupled anti-mouse IgG (Promega, PRS3721; 1:2500) secondary antibody. Western blot analyses were performed three times.

3.3.7 Immunofluorescence Microscopy

HT-29 cells were seeded on glass coverslips in 6-well culture plates and incubated for 48 h at 37°C, prior to treatment for 18 h. After treatment, the cells were fixed at room temperature with 3% (v/v) paraformaldehyde (Fisher Scientific, 30525-89-4) in PBS for 20 min. Fixation was quenched with 50 mM NH_4Cl in PBS for 10 min, followed by permeabilization for 5 min with 0.2% (v/v) Triton X-100 in PBS, and blocked with 3% (w/v) bovine serum albumin (BSA) in PBS-T (0.1% (v/v) Tween 20 diluted in PBS) for 30 min. The cells were incubated with primary antibodies anti-phospho-Ser10 histone H3 (Millipore, 06-570(CH); 1:1000) and anti-α-tubulin (Santa Cruz Biotechnology, sc-53030; 1:400) at 4°C overnight. After incubation, the cells were washed with PBS-T and incubated for 45 min at room temperature with secondary antibodies Alexa Fluor 594 AffiniPure goat anti-rabbit IgG (Jackson ImmunoResearch, 111-585-003; 1:300) and Alexa Fluor 488 rabbit anti-rat IgG (ThermoFisher, A11006; 1:200). Nuclei were stained with 300 nM 4′,6-diamidino-2-phenylindole (DAPI) (Fisher, LSD1306) in PBS for 15 min. Finally, the coverslips were mounted onto microscope slides with ProLong Gold Antifade Mountant

(Thermo Fisher, P36934) and imaged with a CytationTM 5 Cell Imaging Multi-Mode Reader using Gen5 software (BioTek Instruments, USA) and a Zeiss Axio Observer Z1 Motorized Inverted Fluorescence Microscope using AxioVision software (ZEISS, USA). DMSO-treated mitotic cells were used as a reference for baseline mitotic spindle morphology. At least three independent experiments were performed and at least 200 cells were counted for each treatment.

3.3.8 Beta-mercaptoethanol Reduction Assay

HT-29 cells were either treated with colchicine, pulchelloid A, PP1850A or (+)-6-tuliposide A alone, or treated with the compound in combination with beta-mercaptoethanol (β-ME) (MP BioMedical, 02194705-CF). Compounds of interest were preincubated with 0.1 mM β-ME for 1 h at 37°C prior to addition to media for cell culture treatment. After 18 h of treatment, light microscopy images were taken as described above. The cells were manually scored for rounded or flat morphology, and at least 200 cells were counted per treatment group.

3.3.9 Biology-Guided Fractionation and Isolation of (+)-6-Tuliposide A

3.3.9.1 General Experimental Procedures

Optical rotations were measured using a Jasco P-1010 Polarimeter with sodium light (589 nm). The ^{1}H and ^{13}C NMR spectra were recorded on a Bruker AV-600 spectrometer with a 5 mm CPTCI cryoprobe. ^{1}H chemical shifts are referenced to the residual DMSO-d_6 and D_2O (δ 2.49 and 4.70 (as used in Santucci et al., 1985) ppm, respectively) and ^{13}C chemical shifts are referenced to the DMSO-d_6 solvent peak and in D_2O to the C-4’ resonance

according to reference 1b (δ 39.5 and 35.0 ppm, respectively). Low and high resolution ESI-QIT-MS were recorded on a Bruker-Hewlett Packard 1100 Esquire–LC system mass spectrometer. Merck Type 5554 silica gel plates were used for analytical thin layer chromatography. Reversed-phase HPLC purifications were performed on a Waters 1525 Binary HPLC pump attached to a Waters 2998 Photodiode Array Detector. All solvents used for HPLC were Fisher HPLC grade.

3.3.9.2 Isolation of (+)-6-Tuliposide A

Approximately 40 g of dried plant material was extracted twice with 200 mL methanol overnight at room temperature. The combined methanol extracts were concentrated *in vacuo* to give 4.2 g of crude extract that was partitioned between water and ethyl acetate. These extracts were combined and dried. The active water fraction (2.1 g) was partitioned between 1-butanol and water. These extracts were also combined and dried. Approximately 1/4 of the 1-butanol soluble material was chromatographed on Sephadex LH20 using a 71 x 2.5 cm column with methanol as eluent. The fractions obtained were labelled RA242-RA281 and analyzed with the cell rounding assay. The bioactive fraction obtained was then purified by C_{18} reversed-phase HPLC using an InertSustain, 5µm, 25 x 1.0 cm column with a gradient transitioning over 60 minutes from 95% H_2O/acetonitrile to 55% H_2O/acetonitrile as eluent with a flow rate of 2 mL/min to give 7.6 mg of (+)-6-tuliposide A (RA278). The structure of (+)-6-tuliposide A was confirmed by analysis of standard 1D and 2D Nuclear Magnetic Resonance (NMR) spectra and High-Resolution Electrospray Ionization Mass Spectrometry (HRESIMS) and comparison with the literature values (Christensen, 1995; Ibrahim et al., 2017; Santucci et al., 1985).

3.3.10 Statistical Analysis

Microsoft Excel 2016 and GraphPad Prism 5 were used to analyze all data which were plotted as the mean of three independent experiments ± standard error of the mean. The results from light microscopy and immunofluorescence microscopy were analyzed by one-way analysis of variance (ANOVA) with Tukey's post hoc test. Differences were considered statistically significant at $p < 0.05$.

3.4 Results

3.4.1 Extracts prepared from Erythronium grandiflorum induced a mitotic arrest in cancer cells

Aerial parts of *E. grandiflorum* (Figure 3.1A) were collected by sustainable methods with permission on private and public lands in the prairie and montane cordillera ecological zone in southern Alberta, Canada. We prepared extracts in either 75% ethanol in water or 100% dichloromethane to extract polar and non-polar compounds, respectively, and they were given the code names PP1850A and PP1850B. Analysis by light spectrophotometry revealed that PP1850A had prominent absorbance peaks just above 400 nm, whereas PP1850B absorbed most strongly at 375 nm (Figure 3.1B), suggesting that the two extracts likely had different chemical compositions.

We assessed the cytotoxicity of each extract by measuring cell viability by the MTT assay. HT-29 cells were treated with either a solvent control of DMSO, a positive control (camptothecin, CPT) or with extracts at concentrations ranging from 0.1 to 300 μg/mL for 72 h. The half-maximal inhibitory concentration (IC_{50}) of each treatment was calculated. CPT exhibited an IC_{50} of 63 ± 1 nM, as expected (not shown). PP1850A had an IC_{50} of 150 ± 3 μg/mL whereas PP1850B had only 40% viable cells at the highest concentration tested of 300 μg/mL (Figure 3.1C). These values were used to guide subsequent experiments to identify pathways that reduced cell viability.

We tested whether *E. grandiflorum* extracts affected cell morphology by treating three human cell lines for 18 h: HT-29 (human colorectal adenocarcinoma), U2OS (human osteosarcoma), and WI-38 (human non-cancerous lung fibroblast). In addition to a solvent control (DMSO, not-treated), cells were treated with nocodazole, a positive control that

induces cell rounding by mitotic arrest. As expected, nocodazole treated cultures had 97 ± 1% cell rounding in HT-29 cells, whereas the not-treated control had only 5 ± 1% cell rounding, which is typical of a growing cell culture population. At a concentration of 150 µg/mL, PP1850A induced 31 ± 2% cell rounding in HT29 cells and was toxic at a concentration of 500 µg/mL with little change in morphology at 15 or 50 µg/mL (Figures 3.2A and B). In U2OS cell cultures, PP1850A induced 35 ± 4% cell rounding at a concentration of 150 µg/mL, with little cell rounding at lower concentrations (Figures 3.2C and D). By contrast, no cell rounding was observed after any extract treatment in the WI-38 cell line (Figures 3.2E and F). Treatment with PP1850B did not induce cell rounding in any of the cell lines tested (Figures 3.2); therefore, this extract was not selected for further investigation. We confirmed that *E. grandiflorum* extracts could be reliably investigated by preparing extracts (PP1850A) from plants collected in two different years at two different collection sites. HT-29 cells were treated with either solvent only (not-treated), nocodazole, or with 150 µg/mL of year 1 or year 2 extracts for 18 h. The number of rounded cells (38%) were similar under both conditions (Figure 3.3).

To determine whether the compound inducing cell rounding was localized to a specific plant organ, we prepared 75% ethanolic extracts from leaves, stems and flowers and tested them in HT-29 cells. Cells were either not-treated, treated with nocodazole, or treated with whole or plant organ extracts. Each extract induced cell rounding similar to that of the whole extract: PP1850A at 31 ± 2%, leaves at 34 ± 1%, stems at 38 ± 1%, and flowers at 31 ± 1% (Figure 3.4). This indicated that the compound inducing cell rounding is likely distributed throughout the entire aerial parts of *E. grandiflorum*.

A rounded cell morphology can be induced by mitotic arrest; therefore, we analyzed whether PP1850A treatment induced a cell cycle arrest by the technique of flow cytometry. HT-29 cells were either not-treated, treated with nocodazole, or treated with 150 μg/mL PP1850 then fixed at 18 h and analyzed by flow cytometry. The not-treated population of cells separated into 46 ± 2% in G0/G1, 24 ± 1% in S, and 30 ± 1% in G2/M phases, whereas 99 ± 1% of cells treated with nocodazole were in G2/M phase of the cell cycle (Figure 3.5A). Cells treated with PP1850A had a phase distribution of 42 ± 1% in G0/G1, 16 ± 1% in S, and 43 ± 1% in G2/M, which was different from that of not-treated or nocodazole treated cell populations. These data revealed that PP1850A treated cultures were arrested in the G2/M-phase of the cell cycle and there was a reduction in the number of cells arrested in S-phase.

To distinguish if the arrested cells were in the G2 or M-phase, we examined the levels of the mitotic protein cyclin B1 by western blotting. HT-29 cells were treated as described for analysis by flow cytometry. At 18 h, samples were prepared from total cell cultures of not-treated, nocodazole and PP1850A treated cells, and the PP1850A treated cells (total, Tot) were further processed by mechanical shake-off to isolate rounded cells (Mit) from adherent interphasic cells (Int). The samples were separated by SDS-PAGE and probed with anti-cyclin B1 and anti-actin antibodies. Cyclin B1 levels were significantly higher in nocodazole samples and in PP1850A rounded cells collected by mechanical shake-off as compared to adherent interphase cells or the not-treated cells (Figures 3.5B and C). These data revealed that the rounded cells induced by PP1850A treatment, which had accumulated in the G2/M-phase signal by flow cytometry, were arrested in mitosis.

Having demonstrated that PP1850A arrests cells in mitosis, we examined the organization of the mitotic spindle by immunofluorescence microscopy. Mitotic cells were identified using anti-phospho-histone H3 antibodies, and the organization of tubulin was probed with anti-tubulin antibodies. To understand better the type of mitotic arrest, we included cells that were treated with three tubulin toxins: nocodazole, which depolymerizes microtubules; paclitaxel, which stabilizes microtubules; and colchicine, a compound present in the Liliaceae family that depolymerizes microtubules. Cells were either not-treated, treated with one of the three toxins, or treated with PP1850A extract (Figure 3.6A). Immunofluorescence microscopy revealed that the not-treated cell population displayed a small number of cells that were positive for phospho-histone H3 with bipolar mitotic spindles, as expected (Figure 3.6B). Nocodazole treated cells were nearly all positive for phospho-histone H3 and did not contain mitotic spindles in contrast to paclitaxel treated cells, which displayed hyper polymerized spindle structures. Colchicine treated cells were similar to those treated with nocodazole and did not contain mitotic spindles. The rounded cells induced by PP1850A were positive for phospho-histone H3, which is consistent with the data demonstrating that they were in mitosis. Interestingly, these cells contained mitotic spindle structures, however they were distorted in shape, and readily distinct from those of either not-treated cells or cells treated with any of the three tubulin toxins tested.

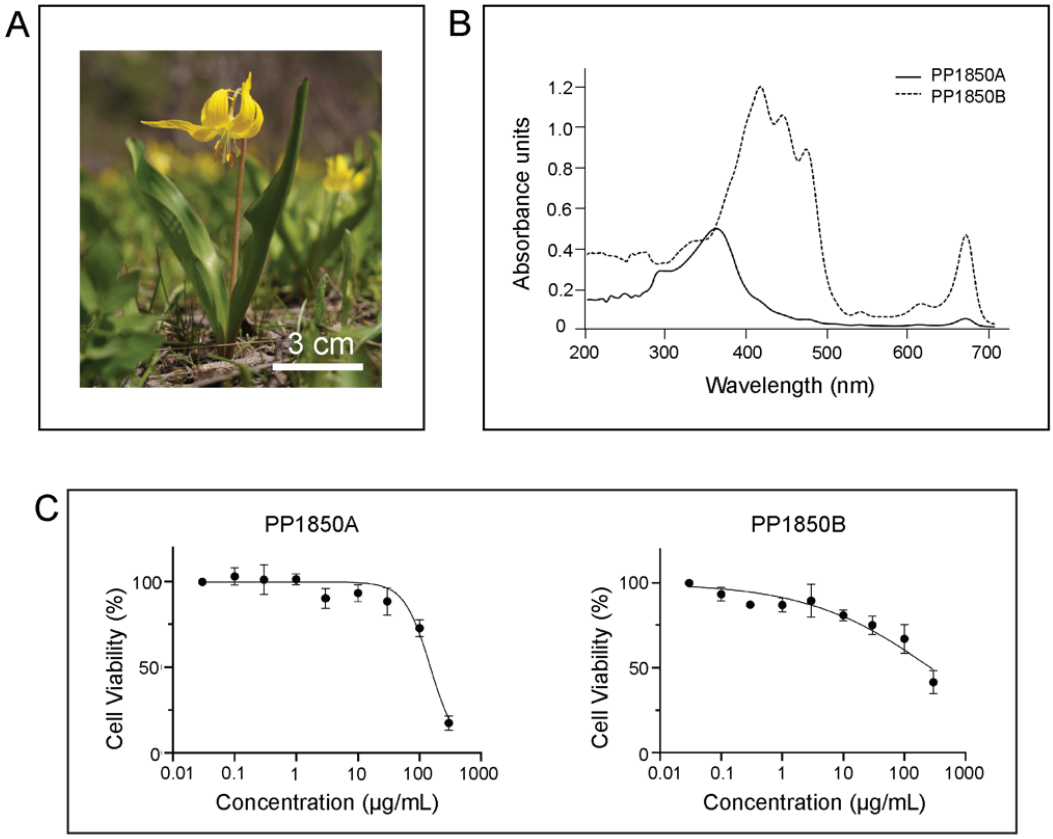

Figure 3.1. Extracts prepared from *Erythronium grandiflorum* are moderately cytotoxic to HT-29 cells. **A.** *Erythronium grandiflorum* (Liliaceae) in cordillera montane habitat. **B.** UV/visible absorbance spectra of *E. grandiflorum* ethanolic (PP1850A, solid line) and dichloromethane (PP1850B, dashed line) whole plant extracts. **C.** The percent cell viability of HT-29 cells plotted as a function of the $\log_{10}$ value of extract treatment concentration.

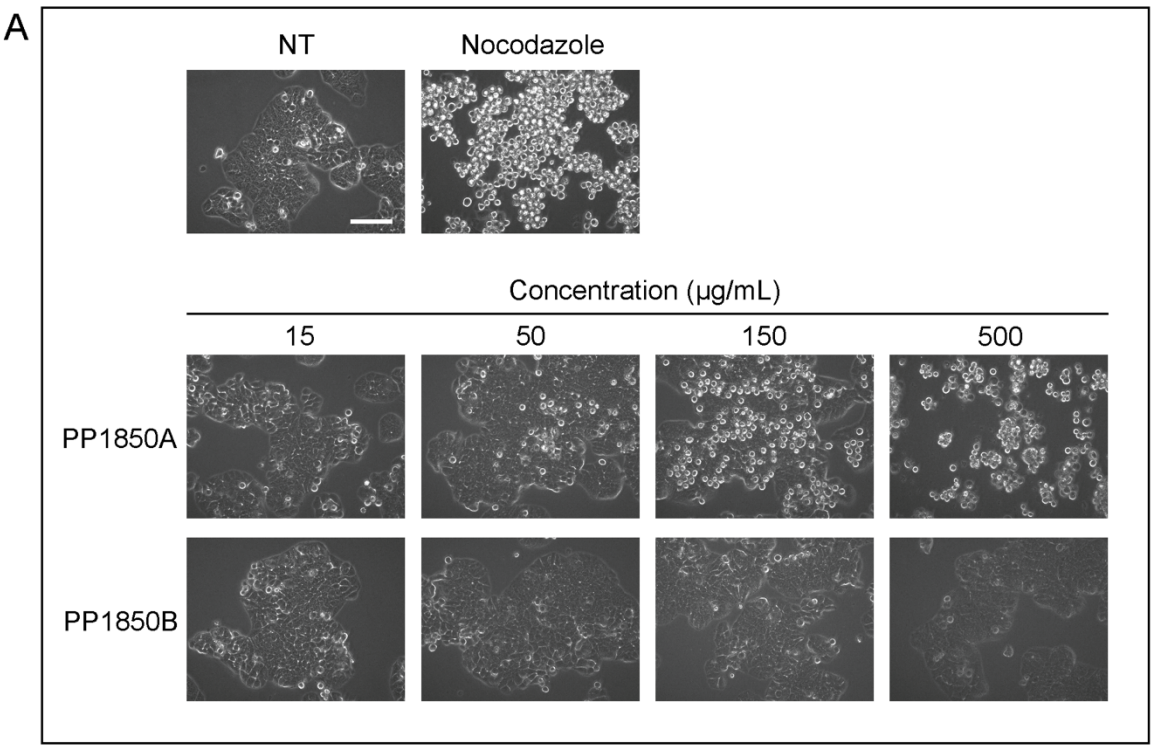
A
NT
Nocodazole
Concentration (μg/mL)
15
50
150
500
PP1850A
PP1850B

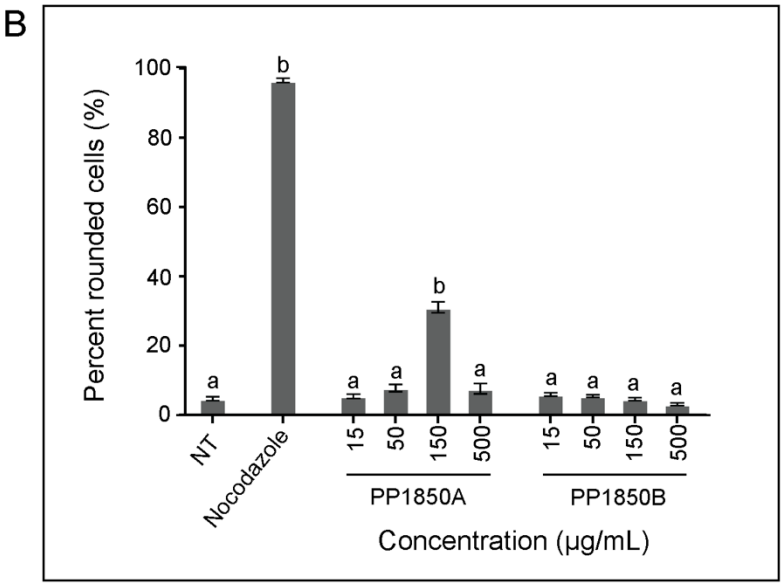
B
Percent rounded cells (%)
100
80
60
40
20
0
a
b
a
a
b
a
a
a
a
a
NT
Nocodazole
15
50
150
500
15
50
150
500
PP1850A
PP1850B
Concentration (μg/mL)

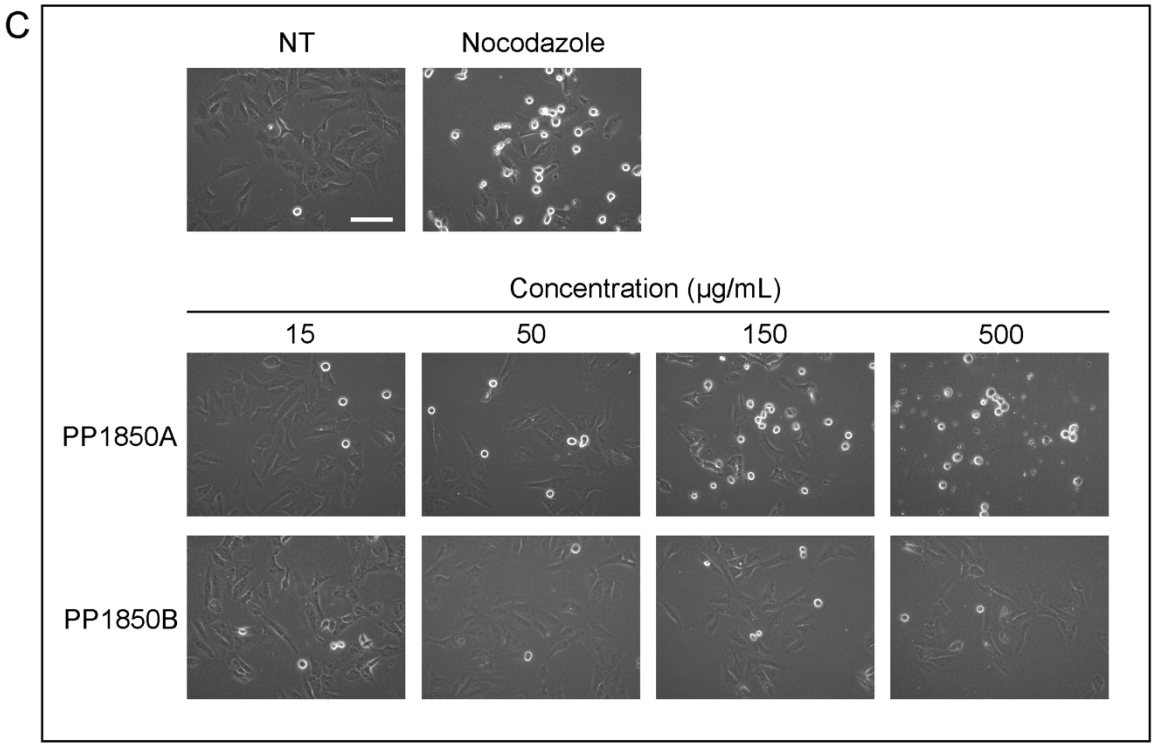
C
NT
Nocodazole
Concentration (μg/mL)
15
50
150
500
PP1850A
PP1850B

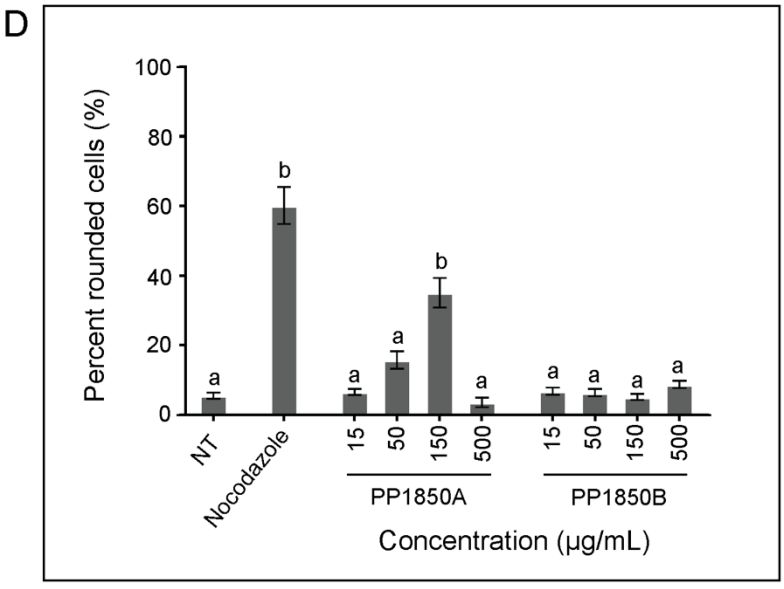
D
Percent rounded cells (%)
100
80
60
40
20
0
a
b
a
a
b
a
a
a
a
a
NT
Nocodazole
15
50
150
500
15
50
150
500
PP1850A
PP1850B
Concentration (μg/mL)

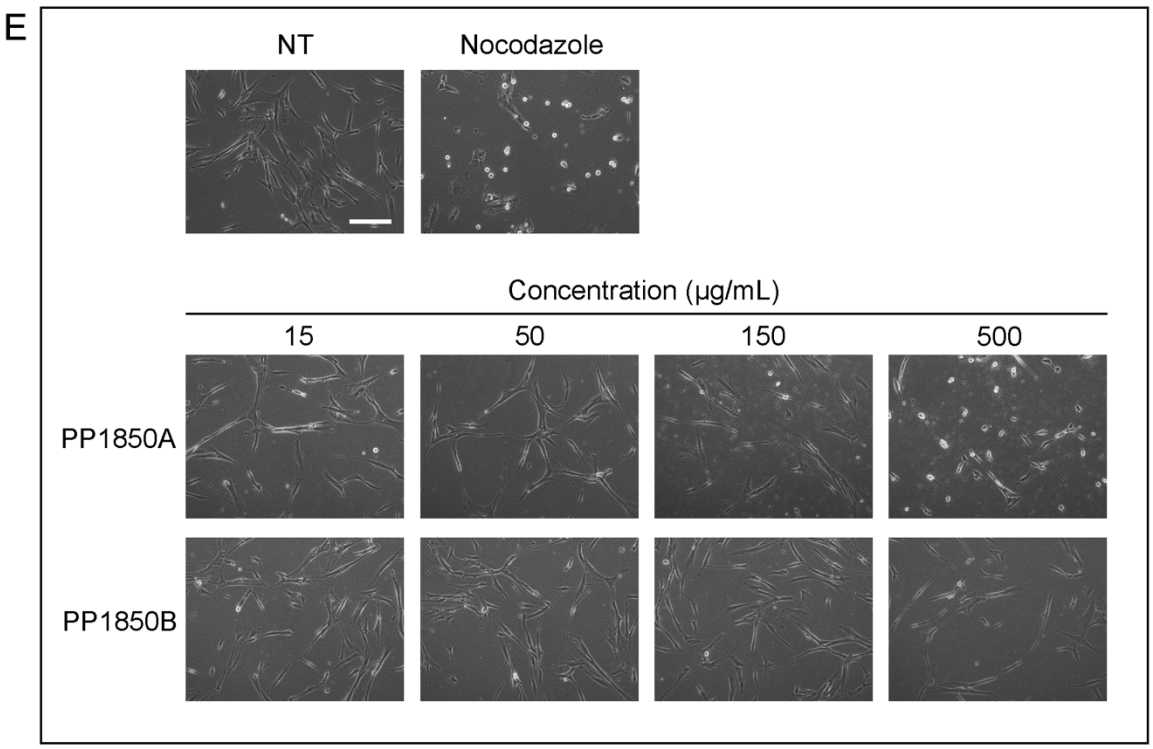
E
NT
Nocodazole
Concentration (μg/mL)
15
50
150
500
PP1850A
PP1850B

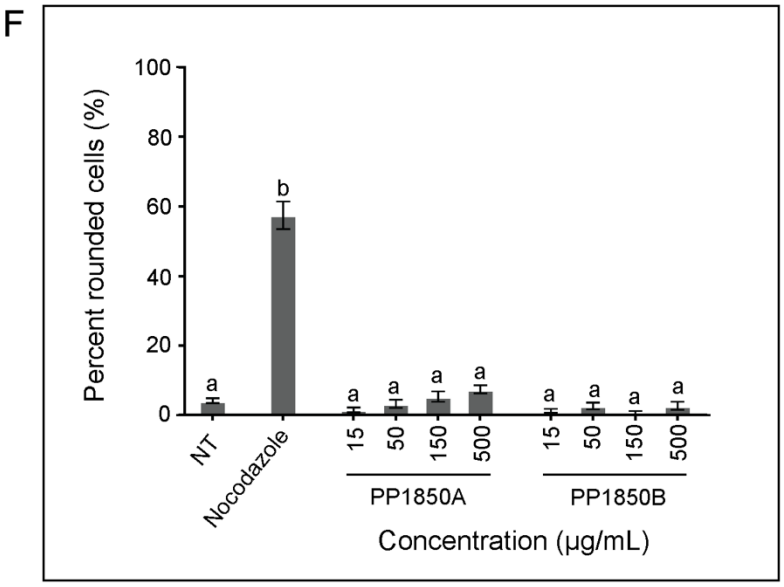
F
Percent rounded cells (%)
100
80
60
40
20
0
a
b
a
a
a
a
a
a
a
a
NT
Nocodazole
15
50
150
500
15
50
150
500
PP1850A
PP1850B
Concentration (μg/mL)

Figure 3.2. HT-29 and U2OS cells treated with ethanolic extracts of *E. grandiflorum* acquire a rounded morphology, whereas WI-38 cells do not acquire a rounded morphology. **A.** HT-29 cells were either not-treated or treated with nocodazole, *E. grandiflorum* whole plant ethanolic extracts (PP1850A) or dichloromethane extracts (PP1850B) for 18 h. Images were taken by light microscopy and representative images are shown. Scale bar represents 100 μm. **B.** The mean percentages of cells exhibiting a rounded morphology after treatment. **C.** U2OS cells were either not-treated or treated with nocodazole, *E. grandiflorum* whole plant ethanolic extracts (PP1850A) or dichloromethane extracts (PP1850B) for 18 h. Images were taken by light microscopy and representative images are shown. Scale bar represents 100 μm. **D.** The mean percentages of cells exhibiting a rounded morphology after treatment. **E.** WI-38 cells were either not-treated or treated with nocodazole, *E. grandiflorum* whole plant ethanolic extracts (PP1850A) or dichloromethane extracts (PP1850B) for 18 h. Images were taken by light microscopy and representative images are shown. Scale bar represents 100 μm. **F.** The mean percentages of cells exhibiting a rounded morphology after treatment. Error bars represent the SEM of at least three independent experiments. Statistical significance was determined using one-way ANOVA followed by Tukey's post hoc test ($p < 0.0001$). Means that are significantly different from the mean of the not-treated control are represented with a different letter (a, b).

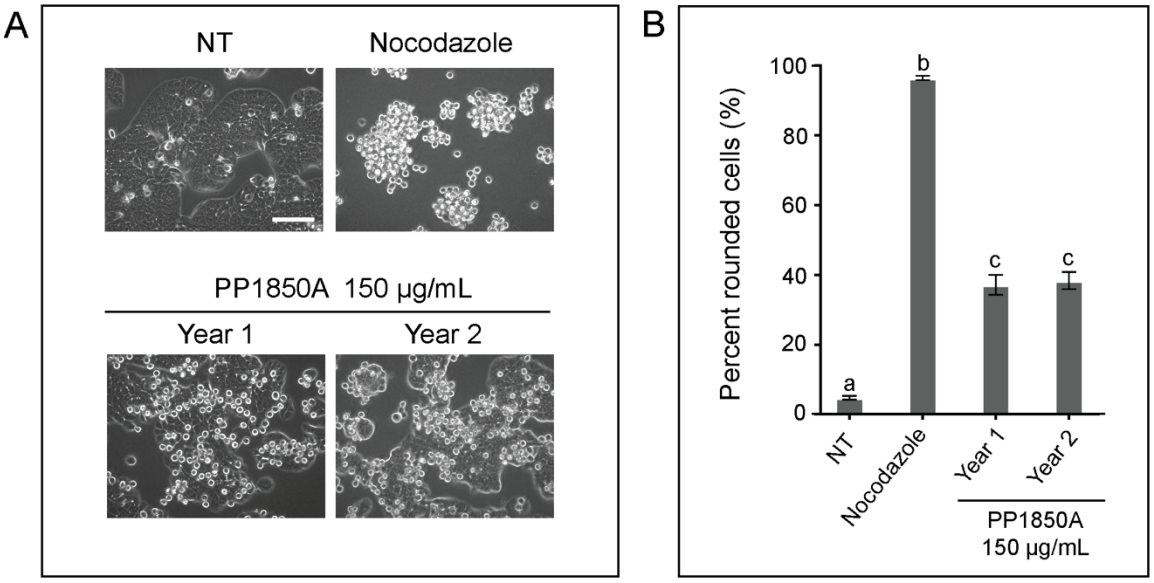

Figure 3.3. HT-29 cells treated with ethanolic extracts prepared from *E. grandiflorum* collected in different years and different sites acquire a rounded cell morphology. **A.** HT-29 cells were either not-treated or treated with nocodazole, *E. grandiflorum* ethanolic extract (PP1850A) year 1 or year 2 for 18 h. Images were taken by light microscopy and representative images are shown. Scale bar represents 100 µm. **B.** The mean percentages of cells exhibiting a rounded morphology after treatment. Error bars represent the SEM of at least three independent experiments. Statistical significance was determined using one-way ANOVA followed by Tukey's post hoc test ($p < 0.0001$). Means that are significantly different from the mean of the not-treated control are represented with a different letter (a, b).

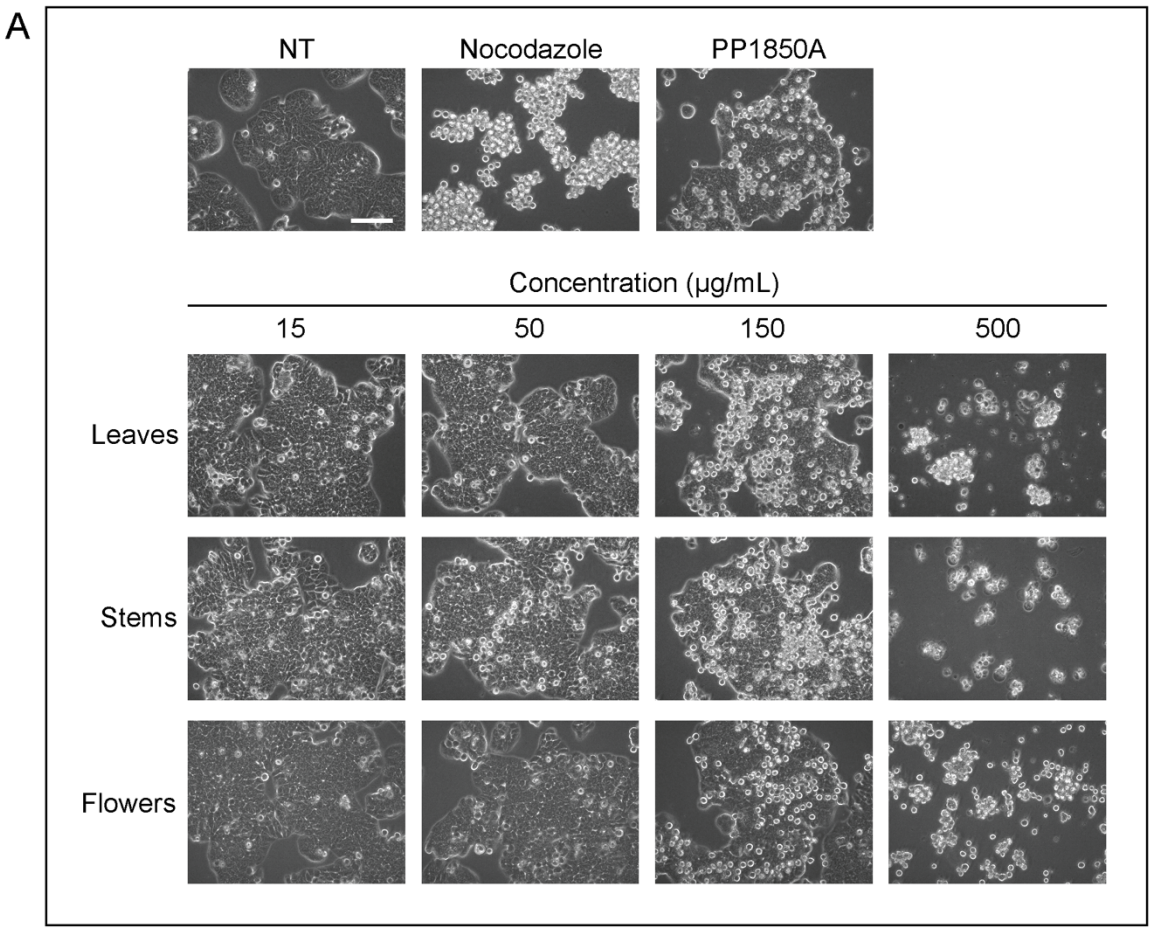
A
NT
Nocodazole
PP1850A
Concentration (µg/mL)
15
50
150
500
Leaves
Stems
Flowers

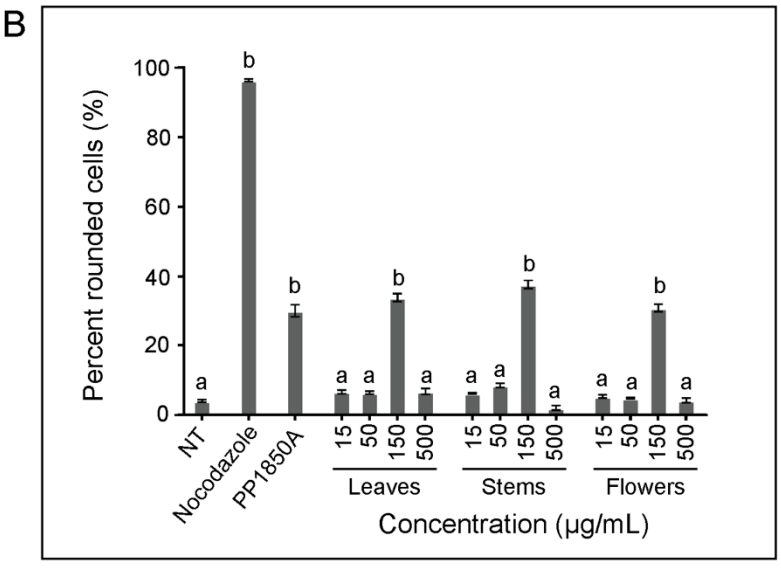
B
Percent rounded cells (%)
100
80
60
40
20
0
a
b
NT
Nocodazole
PP1850A
15
50
150
500
Leaves
Stems
Flowers
Concentration (µg/mL)

Figure 3.4. HT-29 cells treated with *E. grandiflorum* extracts from leaves, stems and flowers acquire a rounded cell morphology. **A.** HT-29 cells were either not-treated or treated with nocodazole, *E. grandiflorum* ethanolic whole extract (PP1850A) or ethanolic extracts of leaves, stems or flowers for 18 h. Images were taken by light microscopy and representative images are shown. Scale bar represents 100 µm. **B.** The mean percentages of cells exhibiting a rounded morphology after treatment. Error bars represent the SEM of at least three independent experiments. Statistical significance was determined using one-way ANOVA followed by Tukey's post hoc test ($p < 0.0001$). Means that are significantly different from the mean of the not-treated control are represented with a different letter (a, b).

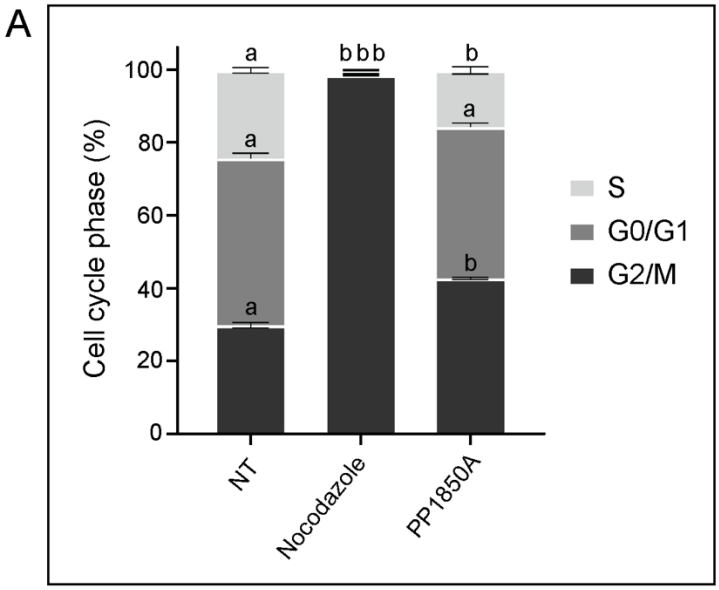
A
Cell cycle phase (%)
100
80
60
40
20
0
a
a
a
bbb
b
a
b
S
G0/G1
G2/M
NT
Nocodazole
PP1850A

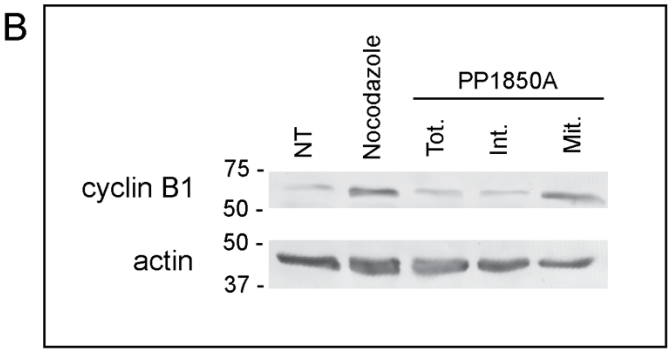
B
PP1850A
NT
Nocodazole
Tot.
Int.
Mit.
cyclin B1
75 -
50 -
actin
50 -
37 -

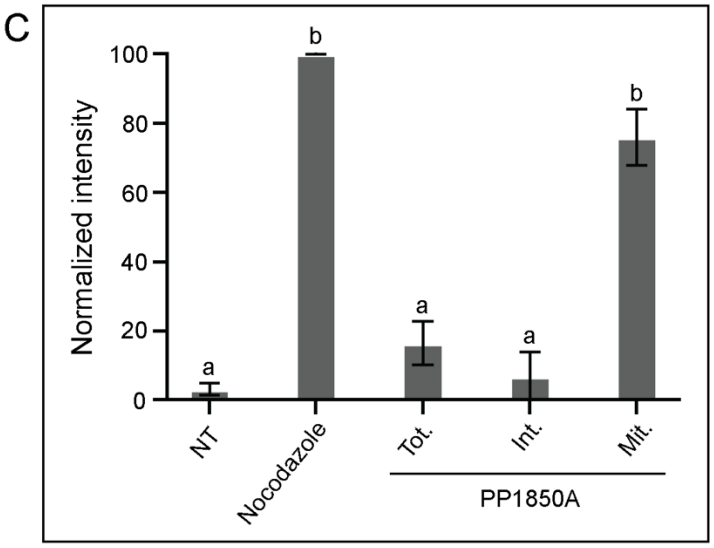
C
Normalized intensity
100
80
60
40
20
0
a
b
a
a
b
NT
Nocodazole
Tot.
Int.
Mit.
PP1850A

Figure 3.5. Rounded HT-29 cells treated with PP1850A exhibit a cell cycle shift and elevated levels of cyclin B1. **A.** HT-29 cells were either not-treated or treated with 500 nM nocodazole, or 150 µg/mL PP1850A and prepared for cell cycle analysis by flow cytometry. Statistical significance was determined using one-way ANOVA followed by Tukey's post hoc test ($p < 0.001$). Treatments that are significantly different from the not-treated control are represented with a different letter (a, b) and were determined for each cell cycle phase. **B.** After 18 h of treatment, cell extracts were prepared from a not-treated negative control, a nocodazole-treated positive control, and a total cell (Tot) population treated with PP1850A. Mitotic cells (Mit) were separated by mechanical shake-off from interphasic cells (Int) in a separate cellular protein extraction of HT-29 cells treated with PP1850A. Cell extracts were separated by SDS-PAGE and analyzed by western blotting for cyclin B1. For comparison of protein levels, the level of actin by western blotting is shown. **C.** Normalized band intensities (arbitrary units) for cyclin B1 western blots are shown. Error bars represent the SEM of at least three independent experiments. Statistical significance was determined using one-way ANOVA followed by Tukey's post hoc test ($p < 0.001$). Means that are significantly different from the mean of the not-treated control are represented with a different letter (a, b).

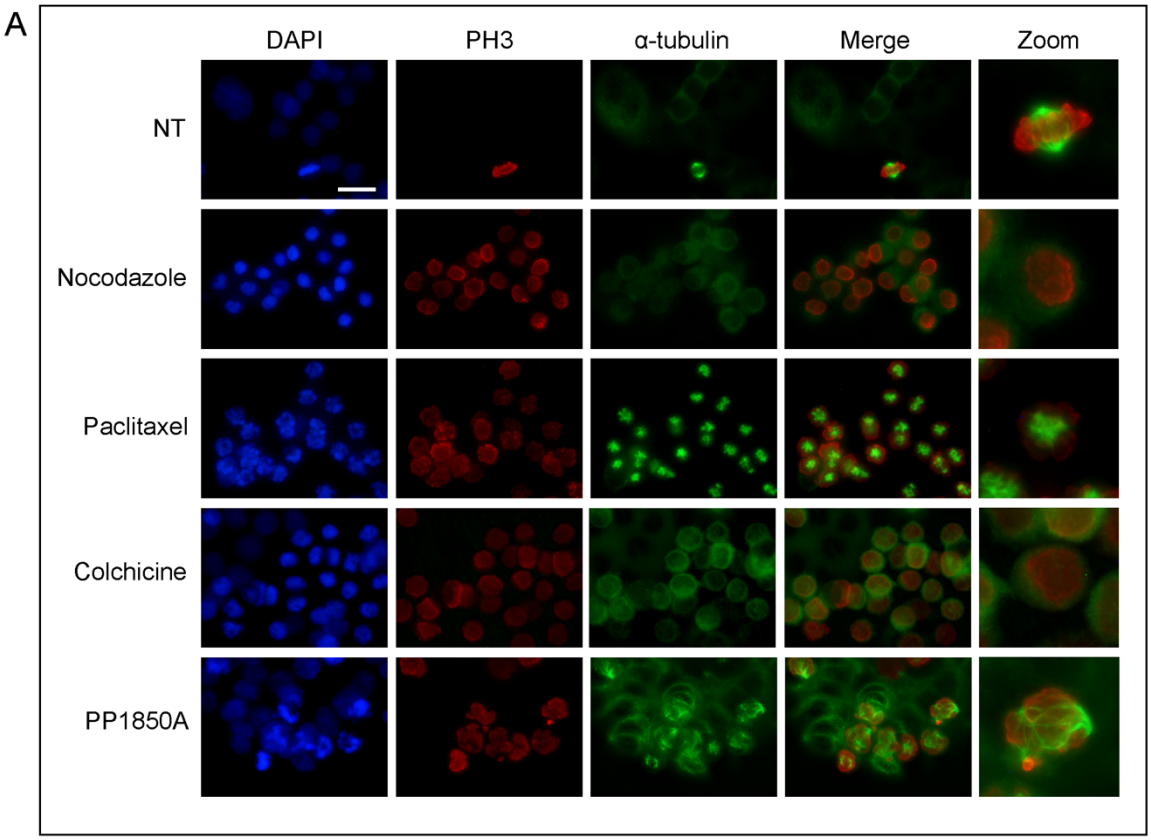
A
DAPI
PH3
α-tubulin
Merge
Zoom
NT
Nocodazole
Paclitaxel
Colchicine
PP1850A

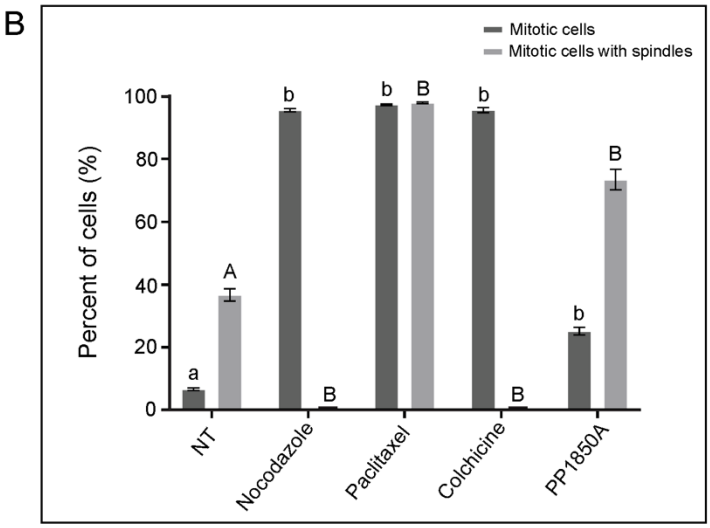
B
Mitotic cells
Mitotic cells with spindles
Percent of cells (%)
100
80
60
40
20
0
a
A
b
B
b
B
b
B
b
B
NT
Nocodazole
Paclitaxel
Colchicine
PP1850A

Figure 3.6. HT-29 cells treated with PP1850A exhibit a phospho-histone H3 signal and have a distorted mitotic spindle. **A.** HT-29 cells were either not-treated or treated with 500 nM nocodazole, 100 nM paclitaxel, 50 nM colchicine or 150 µg/mL PP1850A for 18 h. Cells were analyzed by immunofluorescence microscopy where DNA was detected with DAPI (blue), phosphorylated histone H3 with anti-phospho-histone H3 antibodies (red), and tubulin with anti-α-tubulin antibodies (green). The merge column is the combination of phospho-histone H3 and α-tubulin staining. Scale bar represents 50 µm. **B.** The mean percentages of cells exhibiting a phospho-histone H3 signal (dark grey) and mitotic cells with a spindle structure (light grey) after treatment. Error bars represent the SEM of at least three independent experiments. Statistical significance was determined using one-way ANOVA followed by Tukey's post hoc test ($p < 0.0001$). Means that are significantly different from the mean of the not-treated control are represented with a different letter (a, b; A, B).

3.4.2 Isolation of (+)-6-tuliposide A from Erythronium grandiflorum and confirmation of mitotic arrest activity

Through a series of biology-guided fractionation steps, using chemical fractionation and cell rounding phenotypic assays, we isolated (+)-6-tuliposide A ($C_{11}H_{18}O_8$) (Figure 3.7A) from *E. grandiflorum* as the compound that arrests cells in mitosis. The structure of (+)-6-tuliposide A was elucidated by analysis of high resolution mass spectrometry and 1D and 2D NMR data (supplemental data). The HRMS data for the sample of (+)-6-tuliposide A isolated from the *E. grandiflorum* extracts confirmed its molecular formula and the proton and carbon NMR data recorded for the sample in D_2O exactly matched the literature values (supplemental data) (Christensen, 1995; Ibrahim et al., 2017; Santucci et al., 1985).

We tested (+)-6-tuliposide A for its capacity to induce cell rounding. HT-29 cells were either not-treated, treated with a partially purified fraction RA262, or with increasing concentrations of (+)-6-tuliposide A (RA278), and examined by light microscopy. Not-treated populations had few rounded cells as did populations treated with either 10 or 50 µM of (+)-6-tuliposide A. However, 100 µM treatment induced 41 ± 2% cell rounding and

150 μM induced 38 ± 3% cell rounding (Figures 3.7B and C), which were numbers statistically similar to those of the initial extract PP1850A. We examined the organization of the mitotic spindle in cells treated with (+)-6-tuliposide A by immunofluorescence microscopy. The rounded cells induced by (+)-6-tuliposide A were positive for phospho-histone H3 and contained a distorted mitotic spindle (Figure 3.7D) which was consistent with the results for cells treated with PP1850A (Figure 3.6A).

The structure of (+)-6-tuliposide A revealed a methylene ester linkage, which was reminiscent of the methylene lactone structures that we and others have reported in natural products with similar mitotic arrest activity. The methylene functional group can be inactivated by reduction with beta-mercaptoethanol (β-ME), therefore we tested whether the activity of (+)-6-tuliposide A would be inactivated by incubation with β-ME. HT-29 cells were either not-treated or treated with colchicine (a mitotic arresting compound that does not have a methylene ester), pulchelloid A (a mitotic arresting compound with a methylene lactone), PP1850A, or (+)-6-tuliposide A. In parallel, cells were treated with β-ME alone, or treated with compounds preincubated with β-ME prior to addition to cells. After 18 h, the cells were analyzed by light microscopy and rounded cells were counted (Figures 3.7E and F). As expected, few rounded cells were present in not-treated cells, whereas many rounded cells were present in cultures treated with colchicine, pulchelloid A, PP1850A, or (+)-6-tuliposide A. The addition of β-ME did not change the number of rounded cells in the not-treated or colchicine treated cells. In contrast, the cell rounding activities of pulchelloid A, PP1850A and (+)-6-tuliposide A were greatly reduced after preincubation with β-ME (Figure 3.7E). These data led us to conclude that *E. grandiflorum* harbours (+)-6-tuliposide A, which arrests cancer cell lines in mitosis.

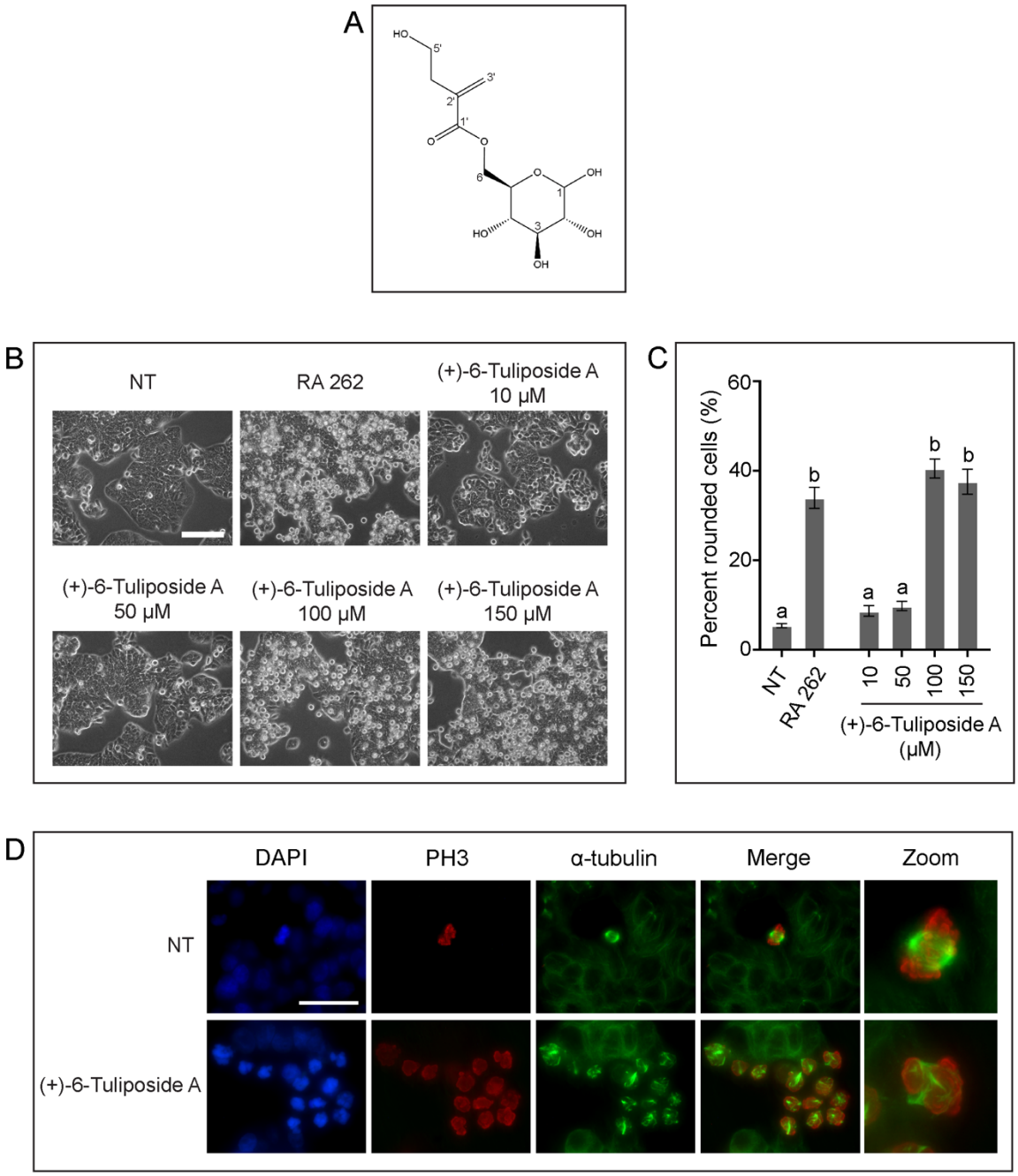
A
HO
5'
3'
2'
1'
O
O
6
O
1
OH
HO
3
OH
OH
B
NT
RA 262
(+)-6-Tuliposide A
10 μM
(+)-6-Tuliposide A
50 μM
(+)-6-Tuliposide A
100 μM
(+)-6-Tuliposide A
150 μM
C
Percent rounded cells (%)
60
40
20
0
a
b
a
a
b
b
NT
RA 262
10
50
100
150
(+)-6-Tuliposide A
(μM)
D
DAPI
PH3
α-tubulin
Merge
Zoom
NT
(+)-6-Tuliposide A

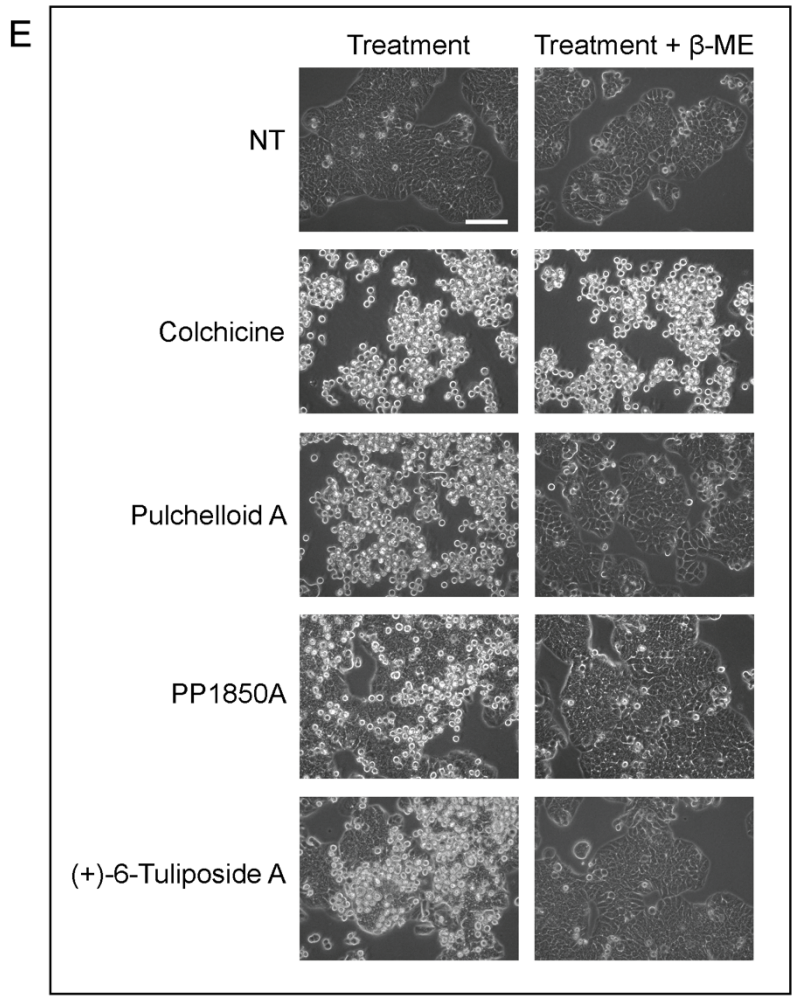
E
Treatment
Treatment + β-ME
NT
Colchicine
Pulchelloid A
PP1850A
(+)-6-Tuliposide A

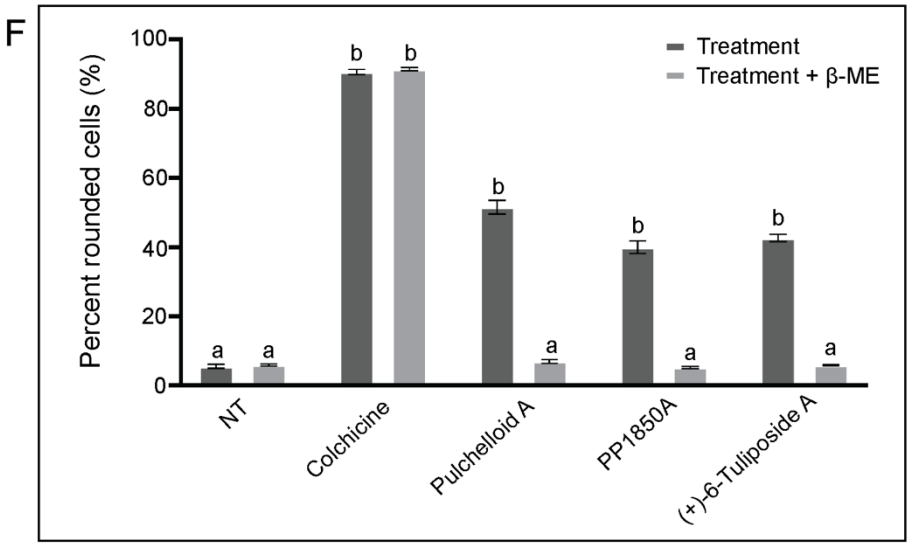
F
Percent rounded cells (%)
100
80
60
40
20
0
Treatment
Treatment + β-ME
a
a
b
b
b
a
b
a
b
a
NT
Colchicine
Pulchelloid A
PP1850A
(+)-6-Tuliposide A

Figure 3.7. (+)-6-tuliposide A, isolated by biology-guided fractionation of *E. grandiflorum*, induced cell rounding in HT-29 cells which exhibited a distorted mitotic spindle, and its activity can be eliminated by reduction with beta-mercaptoethanol. **A.** The chemical structure of (+)-6-tuliposide A. **B.** HT-29 cells were either not-treated or treated with varying concentrations of (+)-6-tuliposide A for 18 h. Images were taken by light microscopy and representative images are shown. Scale bar represents 100 µm. **C.** The mean percentages of cells exhibiting a rounded morphology after treatment. Error bars represent the SEM of at least three independent experiments. Statistical significance was determined using one-way ANOVA followed by Tukey's post hoc test ($p < 0.0001$). Means that are significantly different from the mean of the not-treated control are represented with a different letter (a, b). **D.** HT-29 cells were either not-treated or treated with 100 µM (+)-6-tuliposide A for 18 h. Cells were analyzed by immunofluorescence microscopy where DNA was detected with DAPI (blue), phosphorylated histone H3 with anti-phospho-histone H3 antibodies (red), and tubulin with anti-α-tubulin antibodies (green). The merge column is the combination of phospho-histone H3 and α-tubulin staining. Scale bar represents 50 µm. **E.** HT-29 cells were either not-treated or treated with 50 nM colchicine, 5 µM pulchelloid A, 150 µg/mL PP1850A extract or 100 µM (+)-6-tuliposide A for 18 h. Treatments were administered either alone or after a preincubation with beta-mercaptoethanol (β-ME). **F.** The mean percentages of cells exhibiting a rounded morphology after treatment. Error bars represent the SEM of at least three independent experiments. Statistical significance was determined using one-way ANOVA followed by Tukey's post hoc test ($p < 0.0001$). Means that are significantly different from the mean of the not-treated control are represented with a different letter (a, b).

3.5 Discussion

This is the first report describing the mitotic arrest activity of the natural product (+)-6-tuliposide A. We isolated (+)-6-tuliposide A from the Canadian plant species *Erythronium grandiflorum* (Liliaceae), commonly known as the Glacier Lily, which is a perennial herbaceous plant native to western North America. *E. grandiflorum* was identified in a phenotypic cell morphology screen as one of several botanical extracts in our library that induced cell rounding in cancerous cell lines. We selected *E. grandiflorum* for investigation because it was the most phylogenetically distant from other species identified by this assay in our laboratory. We previously characterized pulchelloid A from *Gaillardia aristata* (Asteraceae) (Bosco et al., 2021) and hymenoratin from *Hymenoxys richardsonii* (Asteraceae) (Molina et al., 2021), of which both compounds are members of the sesquiterpene lactone chemical class and arrest cells in mitosis (Bosco & Golsteyn, 2017). *E. grandiflorum* diverged from the Asteraceae family over 150 million years ago (Wikström et al., 2001). We hypothesized that increased phylogenetic distance might lead to chemical diversity in botanical natural products with mitotic arrest activity (Hoffmann et al., 2018).

Tuliposides are present in tulip plants which, like the Glacier Lily, are members of the Liliaceae family. (+)-6-tuliposide A is a relatively simple natural product composed of a five-carbon methylene carbonyl alcohol linked by an ester to a 6-carbon sugar derivative. We detected its activity in the 75% ethanolic extract of *E. grandiflorum* but not in the dichloromethane extract, which is consistent with the highly polar sugar component of the compound. It shares a biological activity with several other natural products, including pulchelloid A (Bosco et al., 2021), hymenoratin (Molina et al., 2021), psilostachyin A (Sturgeon et al., 2005), and *ent*-15-oxokaurenoic acid (Rundle et al., 2006). Like these

compounds, (+)-6-tuliposide A arrests cells in M-phase with phospho-histone H3 signals, and high levels of cyclin B1, a component of the Cdk1 complex. A select group of sesquiterpene lactones share a distinct type of mitotic arrest with (+)-6-tuliposide A, in which the frequency of arrest is 30-40% of the cell population (when applied to asynchronous cultures), and arrested cells exhibit a distorted mitotic spindle that is different from those observed in cells treated with tubulin binding compounds, including nocodazole, paclitaxel (Taxol®), and colchicine. Like pulchelloid A and hymenoratin, a cell cycle arrest was not detected when the non-transformed diploid human cell line WI-38 was treated with (+)-6-tuliposide A.

Despite that (+)-6-tuliposide A, *a priori*, appears to be different from sesquiterpene lactones, it harbours a methylene carbonyl group, which is common to some sesquiterpene lactones with anti-mitotic activity. We confirmed that the mitotic arrest activity of (+)-6-tuliposide A was sensitive to incubation with β-ME, which was predicted to reduce the methylene functional group of (+)-6-tuliposide A, thus eliminating its mitotic arrest activity. This result is consistent with the β-ME sensitivity of other sesquiterpene lactones such as psilostachyin A (Sturgeon et al., 2005). Methylenes adjacent to carbonyls can form adducts with cysteines via Michael-type addition reactions (Berdan et al., 2019). The distinction between (+)-6-tuliposide A and colchicine, shown herein by the type of mitotic spindle morphology and β-ME reactivity, is important because colchicine has previously been isolated from a member of the lily taxonomical family, the Flame Lily (*Gloriosa superba*) (Srivastava et al., 2014). There have been studies on the reactivity of various compounds containing α,β-unsaturated carbonyls and their potential in drug discovery (Jackson et al., 2017); however, their mitotic arrest activity has not been widely described. Although this is the first report of its mitotic arrest activity, (+)-6-tuliposide A is a precursor

of the biologically active compound tulipalin A, an allergen that can cause contact dermatitis in individuals who handle tulips (Christensen, 1995; Zwicker et al., 2016).

The discovery of (+)-6-tuliposide A and its mitotic arrest activity highlights several important features of the investigation of natural products from botanical sources. (+)-6-tuliposide A presents a previously unknown relationship between a simple chemical structure and a mitotic arrest phenotype, which can serve as a potential tool for drug development and mitotic regulators. The discovery of the bioactivity of (+)-6-tuliposide A also supports the continued investigation of botanical species in the ecological zones of Canada, a region distinguished by its exclusive and largely unexplored plant species. These flora, known to local agricultural sectors as being toxic to both human and livestock populations (Tannas, 2004), serve as a focal point of our research (Molina et al., 2022). Notably, our studies highlight the value of investigating plants with understudied natural products and limited global distribution. Continued research on flora from understudied ecological zones, such as those in Canada, highlights the significance of biologically rich ecosystems and thus the importance of their sustainable management (Tietje et al., 2022; Tietje et al., 2023). Through this approach, we identified the Glacier Lily, *Erythronium grandiflorum*, as a source of (+)-6-tuliposide A which increases the diversity of compounds with which to probe mitotic regulation. Additionally, understanding the structure-activity relationships of these compounds may help identify key mitotic regulatory proteins that previously have no known inhibitors. Future studies will include identifying the cellular targets of these compounds, which will open new avenues for drug development for the treatment of various proliferative diseases, such as cancer.

CHAPTER 4

Investigation of the structure and function relationship of three methylene carbonyl anti-mitotic natural products

4.1 Abstract

Mitotic regulation is governed by a network of molecular events to ensure the accurate segregation of chromosomes. Dysregulation of cell cycle control mechanisms can lead to uncontrolled cell growth—a hallmark of cancer. Botanically-derived natural products have emerged as promising candidates in the field of anti-cancer drug development. In this study, we conducted a comparative analysis of the anti-mitotic activities of the natural products pulchelloid A, anemonin, and (+)-6-tuliposide A, and identified distinct mitotic arrest profiles for each compound. A detailed analysis revealed these compounds induce prometaphase arrests characterized by disorganized spindle structures, damaged DNA, and activation of the spindle assembly checkpoint. Furthermore, the compounds differed in their effects on kinetochore proteins (CENP-E, BubR1) and centrosome organization (PLK-1, γ-tubulin), indicating that each compound acts via a unique mechanism despite sharing a methylene carbonyl moiety. Natural product inhibitors offer tremendous potential for advancing our understanding of mitotic regulation and provide insight in the development of targeted treatments for precision medicine.

4.2 Introduction

Mitosis—the fundamental process of cell division—is regulated by a system of molecular events to ensure the precise segregation of chromosomes from one parent cell into two identical daughter cells. Dysregulation of cell division mechanisms can lead to uncontrolled cell growth, which is a hallmark of proliferative diseases, notably cancer (Hanahan & Weinberg, 2011). Targeting the molecular events orchestrating cell division has been a cornerstone in drug development, and natural products derived from botanical sources have emerged as promising candidates with anti-cancer activity. The pursuit of natural products with anti-mitotic activity has led to the identification of a range of distinct chemical structures (Guo et al., 2022; Scaria et al., 2020). By analyzing data from several projects within the Natural Product Laboratory, we observed that compounds with different structures induced similar mitotic arrests. This observation appeared inconsistent with a foundational principle that asserts a strict relationship between structure and function, and raised the question of how diverse chemical structures could cause identical mitotic arrests.

Our collection of natural products with anti-mitotic activity uniquely positioned us to compare the biological effects of the compounds pulchelloid A, anemonin, and (+)-6-tuliposide A. All three induced mitotic arrests that have several features in common (Bosco et al., 2021; Chapter 2; Chapter 3) and prompted us to search for underlying cellular phenotypes that could differentiate their mechanisms of action. These compounds were selected for their positioning of unsaturated carbonyls: pulchelloid A contains an α-methylene-γ-butyrolactone which, as with many sesquiterpene lactones, is responsible for their activity (Sturgeon et al., 2005); anemonin contains endocyclic unsaturated carbonyls known as butenolides; and (+)-6-tuliposide A contains a linear α,β-unsaturated ester. The

methylene carbonyl moiety, known for its reactivity in Michael addition reactions (Jackson et al., 2017), is implicated in the anti-mitotic activity of these compounds and suggests a commonality in their mode of action. However, the diversity of the rest of the compound, outside of the methylene carbonyl function, would suggest more nuanced interactions with cellular components or signaling pathways. In this study, we asked whether one could distinguish the anti-mitotic activities of pulchelloid A, anemonin and (+)-6-tuliposide A. Our experiments revealed distinct characteristics by which each compound triggered an arrest during mitosis and provided support for different mechanisms of action.

Furthermore, this investigation revealed the breadth of mitotic inhibitors sourced from prairie botanicals and perhaps more expansively in nature. Whereas the structure-function relationship remains robust at the cellular biology level, it requires a refined perspective when diverse compounds culminate in similar cellular outcomes. This investigation not only identified tools to advance the understanding of mitotic regulation but also provided insights for the rational design of targeted anti-cancer strategies based on the unique features of these diverse compounds.

4.3 Materials and Methods

4.3.1 Cell Culture

The human cell line HT-29 (HTB-38, American Type Culture Collection) was cultivated as previously described (Kubara et al., 2012) and was selected because of their capacity to sustain a rounded phenotype during mitotic arrest (Gascoigne & Taylor, 2008). Cells were plated at a density of 3.0 x 10^5 cells/25 cm^2 flask and cultured for 48 hours (h) prior to treatment. The compounds nocodazole (660 µM, Sigma-Aldrich, M1404), paclitaxel (1 mM, Sigma-Aldrich, T7402), pulchelloid A (10 mM), anemonin (10 mM) and (+)-6-tuliposide A (10 mM) were dissolved in dimethyl sulfoxide (DMSO) (Sigma-Aldrich, D2438) and stored at -20°C until use. Pulchelloid A was isolated from *Gaillardia aristata* (Bosco et al., 2021), anemonin was isolated from *Pulsatilla nuttalliana* (Chapter 2) and (+)-6-tuliposide A was isolated from *Erythronium grandiflorum* (Chapter 3) by biology-guided fractionation in collaboration with Dr. Raymond Andersen (University of British Columbia). For not-treated cell groups, DMSO was added as a solvent vehicle control at a final concentration of 0.4% (v/v). An Olympus CKX41 inverted microscope with an Infinity 1 camera operated by Infinity Capture imaging software (Lumenera Corporation, CA) was used for light microscopy. Cells were manually scored for a flat or rounded morphology, and at least 200 cells were counted per treatment group.

4.3.2 Cell Viability Assay

The cytotoxicity of pulchelloid A, anemonin and (+)-6-tuliposide A was measured using the 3-(4, 5-dimethylthiazol-2-yl)-2, 5-diphenyltetrazolium (MTT) assay (Sigma-Aldrich, M2128) and carried out as previously described (Kubara et al., 2012; Molina et al., 2021). Absorbance was measured at 590 nm using a CytationTM 5 Cell Imaging Multi-Mode

Reader (BioTek Instruments, USA) with Gen5 software. An IC_{50} value was calculated for each compound and represent the concentration of the compound that reduced the absorbance of MTT by 50% compared to 0.1% (v/v) DMSO-treated cells. The normalized percent absorbance was calculated as follows:

Normalized percent absorbance = (absorbance / DMSO absorbance) x 100

The log concentrations were plotted against the normalized percent absorbance using Microsoft Excel and non-linear regression (log(inhibitor) versus normalized response) analysis was performed with GraphPad Prism 5 software to estimate IC_{50} concentrations. The standard curves were plotted using the following equation:

$$Y = \text{maximum} + (\text{maximum} - \text{minimum}) / (1+10(X-\text{Log}IC_{50}))$$

Where Y is the percentage of viable cells, maximum is the percentage of viable cells after treatment with 0.1% DMSO, minimum is the percentage of viable cells after treatment with the highest concentration of the compound, and X is the $\log_{10}$ value of treatment concentration. All experiments were performed in triplicate and repeated at least three times.

4.3.3 Beta-mercaptoethanol Reduction Assay

HT-29 cells were either not-treated or treated with nocodazole, pulchelloid A, anemonin or (+)-6-tuliposide A. In parallel, HT-29 cells were treated with each compound in combination with beta-mercaptoethanol (β-ME) (MP BioMedical, 02194705-CF). The compounds were preincubated with 0.1 mM β-ME for 1 h at 37°C prior to addition to media for cell culture treatment. After 18 h of treatment, light microscopy images were taken as described above. The cells were manually scored for rounded or flat morphology, and at least 200 cells were counted per treatment group. The mean percentage of rounded cells

and standard deviation of the mean were calculated from at least three independent experiments.

4.3.4 Timelapse Video Microscopy

HT-29 cells were plated at 1.0 x 10^4 cells/well in 12 well plates and culture for 48 h. Immediately after treatment, the 12-well plate was loaded into a CytationTM 5 Cell Imaging Multi-Mode Reader using Gen5 software (BioTek Instruments, USA) where the temperature and humidity were maintained at 37°C and 5% CO_2 throughout the experiment. In each well, three X,Y positions were selected for phase contrast imaging (with a 300-millisecond delay after plate movement) every hour for 24 h. Cells were manually scored for a flat or rounded morphology, and at least 200 cells were counted per treatment group and timepoint.

4.3.5 Cell Synchronization by Double Thymidine Block

HT-29 cells were synchronized by double thymidine block adapted from a previously described protocol (Chen & Deng, 2018). HT-29 cells were plated at 1.0 x 10^4 cells/well in 12 well plates and culture for 48 h. The cells were then subjected to the first 2 mM thymidine (Sigma, T1895-1G) treatment for 18 h followed by a warm 1x phosphate buffered saline (PBS) wash and release into fresh media for 9 h. A second 2 mM thymidine treatment was administered for 18 h to synchronize the cell population at the G1/S boundary. Cells were released from thymidine block by washing with warm 1x PBS followed by either not-treated media, or treatment with nocodazole, pulchelloid A, anemonin or (+)-6-tuliposide A.

4.3.6 Immunofluorescence Microscopy

4.3.6.1 PH3, α-tubulin, and γ-histone H2AX Immunofluorescence Microscopy

HT-29 cells were seeded at 2.0 x 10^5 cells/well on glass coverslips in 6-well culture plates and incubated for 48 h at 37°C, prior to treatment for 18 h. After treatment, the cells were fixed for 20 min at room temperature with 3% (v/v) paraformaldehyde (Fisher Scientific, 30525-89-4). Fixation was quenched with 50 mM NH_4Cl in PBS for 10 min, followed by permeabilization for 5 min with 0.2% (v/v) Triton X-100 in PBS, and blocked for 30 min with 3% (w/v) bovine serum albumin (BSA) in PBS-T (0.1% (v/v) Tween 20 diluted in PBS). The cells were incubated with primary antibodies anti-phospho-Ser10 histone H3 (Millipore, 06-570(CH); 1:1000), anti-α-tubulin (Santa Cruz Biotechnology, sc-53030; 1:400) or anti-γ-histone H2AX (Sigma, 05-636; 1:400) at 4°C overnight. The cells were then washed with PBS-T and incubated at room temperature for 45 min with secondary antibodies Alexa Fluor 594 AffiniPure goat anti-rabbit IgG (Jackson ImmunoResearch, 111-585-003; 1:300), Alexa Fluor 488 rabbit anti-rat IgG (ThermoFisher, A11006; 1:200) or Alexa Fluor 488 rabbit anti-mouse (ThermoFisher, A11059; 1:400). Nuclei were stained with 300 nM 4′,6-diamidino-2-phenylindole (DAPI) (Fisher, LSD1306) in PBS-T for 15 min. Finally, the coverslips were mounted onto microscope slides with ProLong Gold Antifade Mountant (Thermo Fisher, P36934). Cells were imaged with either a CytationTM 5 Cell Imaging Multi-Mode Reader using Gen5 software (BioTek Instruments, USA) or a Zeiss Axio Observer Z1 Motorized Inverted Fluorescence Microscope using AxioVision software (ZEISS, USA). Images were captured between treatment groups while maintaining identical intensity and wavelengths specified for each secondary antibody. At

least three independent experiments were performed and at least 200 cells were counted for each treatment.

4.3.6.2 γ-tubulin Immunofluorescence Microscopy

HT-29 cells were seeded at 2.0 x 10^5 cells/well on glass coverslips in 6-well culture plates and incubated for 48 h at 37°C, prior to treatment for 18 h. After treatment, the cells were washed for 90 seconds with IMF buffer (0.05% (v/v) Triton X-100, 0.5 mM $MgCl_2$, 1 mM EGTA (ethylene glycol bis-(2-aminoethylether)-*N*,*N*,*N*',*N*'-tetraacetic acid) in PBS) and then fixed for 20 min at -20°C with 100% ice-cold methanol. Fixation was quenched with 50 mM NH_4Cl in IMF for 10 min, followed by permeabilization for 5 min with 0.2% (v/v) Triton X-100 in IMF, and blocked for 30 min with 3% (w/v) BSA in IMF-T (0.1% (v/v) Tween 20 diluted in IMF buffer). The cells were incubated with the primary antibody anti-γ-tubulin (Sigma, T5326; 1:1000) at 4°C overnight. The cells were then washed with IMF-T and incubated at room temperature for 45 min with the secondary antibody Alexa Fluor 488 rabbit anti-mouse (ThermoFisher, A11059; 1:400). Nuclei were stained with 300 nM DAPI (Fisher, LSD1306) in IMF-T for 15 min. Cells were imaged as described in *4.2.6.1*.

4.3.6.3 CENP-E, BubR1, and PLK-1 Immunofluorescence Microscopy

Immunofluorescence was carried out as in 2.6.1 with the following additional step. Prior to fixation, the cells were permeabilized with 0.1% (v/v) cold Triton X-100 in PBS for 5 min. Primary antibodies are anti-CENP-E (Sigma, SAB3701429; 1:150), anti-BubR1 (ThermoFisher, 720297; 1:250) or anti-PLK-1 (ThermoFisher, PA528023: 1:1000). Secondary antibody is Alexa Fluor 488 goat anti-rabbit IgG (ThermoFisher, A11008;

1:300) or Alexa Fluor 488 rabbit anti-mouse (ThermoFisher, A11059; 1:400). Nuclei were stained with 300 nM DAPI (Fisher, LSD1306). Cells were imaged as described in *4.2.6.1*.

4.3.7 Plot Profile Analysis

Analysis of γ-tubulin fluorescent imaging was performed to generate plot profiles as follows. Each image was rotated until at least two γ-tubulin foci we aligned on the x-axis of the image and an area of 200 x 200 pixels was specified for gray value intensity analysis using ImageJ software. The gray values were normalized to cytoplasmic intensity and highest intensity across all treatments. GraphPad Prism 5 software was used to create plot profiles and the data represent a total of 15 cells from each treatment condition from at least three independent experiments.

4.3.8 Cell Extraction and Western Blotting

HT-29 cells were plated at 3.0 x 10^5 cells/25 cm^2 flask and incubated for 48 h at 37°C prior to treatment. After treatment for 18 h, total cell populations were collected by trypsinization. Rounded mitotic cells, which are weakly adherent, were collected by mechanical shake-off to isolate them from interphasic cells that are strongly adherent (Swift & Golsteyn, 2016), after which interphasic cells were collected by trypsinization. The samples were then resuspended in ice cold lysis buffer (50 mM HEPES, pH 7.4, 50 mM NaF, 10 mM EGTA, 50 mM β-glycerophosphate, 1 mM ATP, 1 mM DTT (dithiothreitol), 1% Triton X-100 (v/v), 10 µg/mL RNase A (Sigma-Aldrich, R6513-250MG), 0.4 U/mL DNase I (Invitrogen, I354Ba), and protease inhibitor cocktail (Roche, 11836170001)) to a concentration of 20,000 cells/µL, passed through a 26-gauge needle five times to lyse the

cells, and incubated on ice for 30 min. The suspension was centrifuged at 10,000 × *g* for ten minutes at 4°C and stored at -80°C until use. The samples were prepared for electrophoresis after being heated for ten minutes at 95°C in the presence of 2x SDS (sodium dodecyl sulfate) sample buffer (20% (v/v) glycerol, 10% (v/v) DTT, 6% (w/v) SDS, 500 mM Tris, pH 6.8). Western blots were performed as previously described (Swift & Golsteyn, 2016) using anti-CENP-E (Sigma, C7488-200UL; 1:200) and anti-actin (Santa Cruz Biotechnology, sc-58673; 1:200) primary antibodies, and alkaline phosphatase coupled anti-rabbit IgG (Promega, PRS3731; 1:2500) and alkaline phosphatase coupled anti-mouse IgG (Promega, PRS3721; 1:2500) secondary antibodies. Band intensity was analysed using ImageJ software. Western blot analyses were performed three times.

4.3.9 Statistical Analysis

Microsoft Excel 2016 and GraphPad Prism 5 software were used to analyze all data which were plotted as the mean of three independent experiments ± standard error of the mean (SEM). The results were analyzed by one-way analysis of variance (ANOVA) with Tukey's post hoc test. Differences were considered statistically significant at $p < 0.05$.

4.4 Results

4.4.1 Pulchelloid A, anemonin and (+)-6-tuliposide A induced similar mitotic arrest phenotypes in preliminary investigation

Pulchelloid A, anemonin and (+)-6-tuliposide A are distinct botanical natural products that share a methylene carbonyl functional group (Figure 4.1A) and arrest human cancer cells in mitosis. We assessed the cytotoxicity of each compound using the MTT assay and HT-29 cells. The IC_{50} for pulchelloid A was 12 ± 2 μM, 9 ± 2 μM for anemonin, and 73 ± 1 μM for (+)-6-tuliposide A after a 72-h treatment (Figure 4.1B). Pulchelloid A and anemonin displayed similar cytotoxicity and were both more cytotoxic than (+)-6-tuliposide A. Strikingly, all induced a maximum of about 40% cell rounding when applied to asynchronous populations of cells (Figure 4.1C). Pulchelloid A induced 39 ± 2% cell rounding at 5 μM, anemonin induced 41 ± 3% cell rounding at 15 μM, and (+)-6-tuliposide A induced 41 ± 2% cell rounding at 100 μM (Figure 4.1D). The three compounds induced cell rounding by 18 h, which was before the time that toxicity was detected at these concentrations.

We confirmed that the three compounds share a common reactive Michael addition centre that can be reduced by β-mercaptoethanol (β-ME) (Figure 4.2A). Cells were either not-treated (NT) or treated with nocodazole, pulchelloid A, anemonin or (+)-6-tuliposide A. In parallel, the compounds were each preincubated with β-ME prior to addition to HT-29 cells. In not-treated cells, the addition of β-ME did not change the percentage of rounded cells (Figure 4.2B). Nocodazole induced nearly 100% cell rounding independently of incubation with β-ME, as expected. By contrast, the percentage of rounded cells induced by pulchelloid A decreased from 45 ± 1% to 7 ± 1%, the percentage of rounded cells

induced by anemonin decreased from 43 ± 1% to 8%, and the percentage of rounded cells induced by (+)-6-tuliposide A decreased from 43 ± 1% to 6 ± 1%, values that were similar to those of the not-treated cells (6 ± 1%) (Figures 4.2A, 2B).

These data revealed that the three compounds harbour a common functional group that is required for their anti-mitotic (cell rounding) activity. It seemed surprising, however, that the non-methylene carbonyl functions would have little impact on the biological response of these compounds because they differ in their mass and chemical properties. We reasoned that if the compounds have the same target that interacts through a Michael addition reaction, they should generate the same results in experiments that examine mitotic machinery. We then designed a series of assays to determine whether the mitotic arrests induced by each of the three compounds were identical or not.

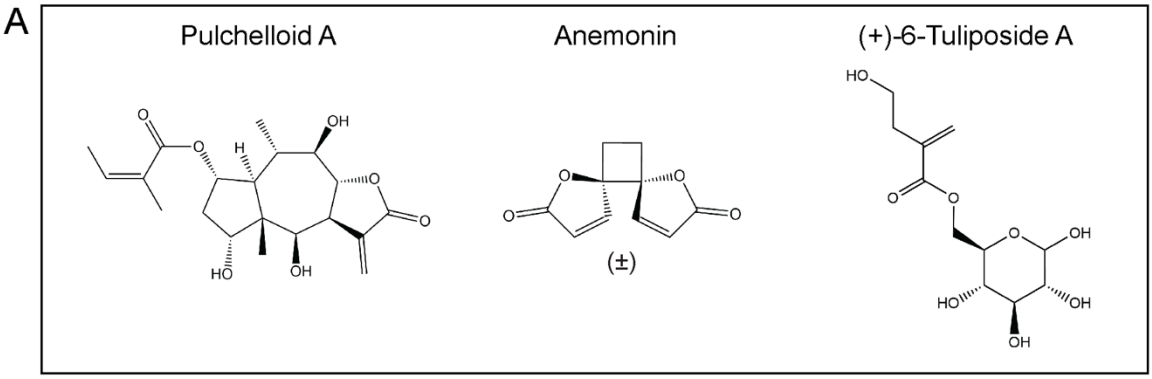
A
Pulchelloid A
Anemonin
(+)-6-Tuliposide A
(±)

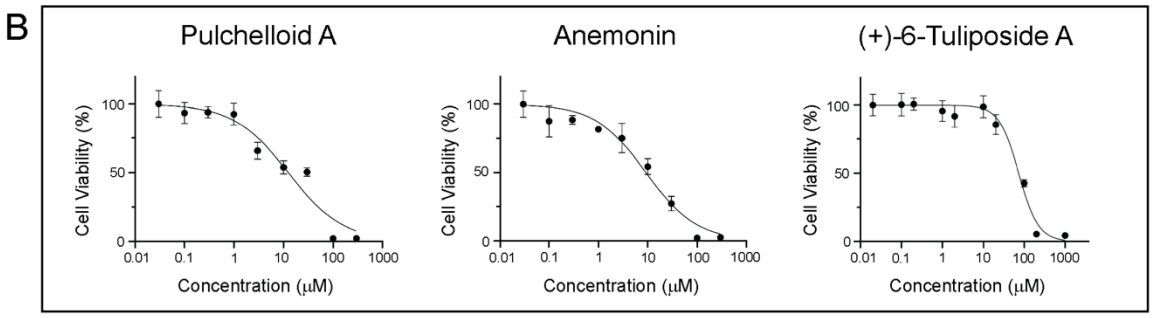
B
Pulchelloid A
Anemonin
(+)-6-Tuliposide A
Cell Viability (%)
Concentration (μM)

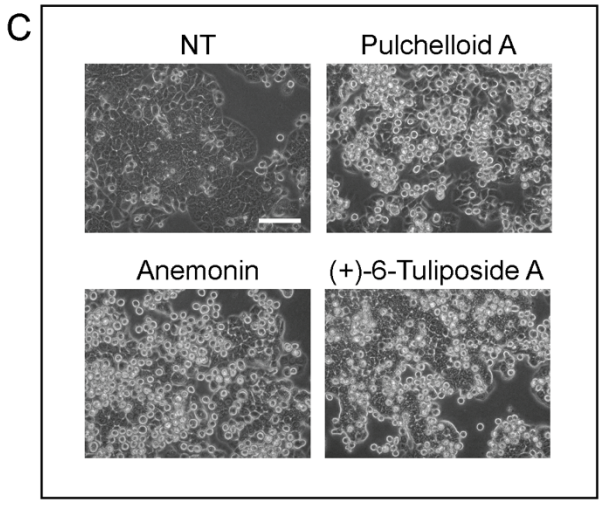
C
NT
Pulchelloid A
Anemonin
(+)-6-Tuliposide A

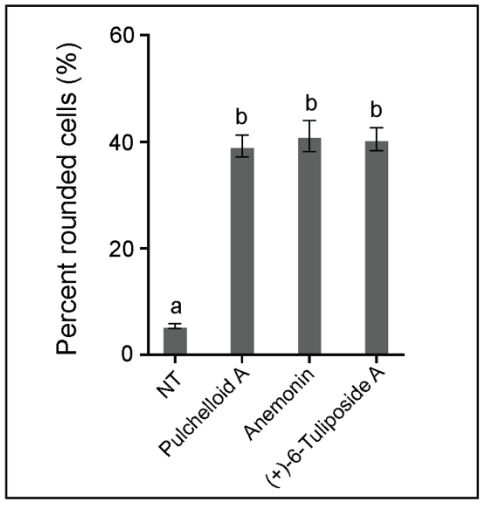
D
Percent rounded cells (%)
NT
Pulchelloid A
Anemonin
(+)-6-Tuliposide A

Figure 4.1. The compounds pulchelloid A, anemonin and (+)-6-tuliposide A were moderately cytotoxic and induced cell rounding in HT-29 cells. **A.** The chemical structures of pulchelloid A, anemonin and (+)-6-tuliposide A. **B.** The percent cell viability of HT-29 cells plotted as a function of the $\log_{10}$ value of compound treatment concentration. **C.** HT-29 cells were either not-treated or treated with pulchelloid A at 5 μM, anemonin at 15 μM or (+)-6-tuliposide A at 100 μM for 18 h. Images were taken by light microscopy and representative images are shown. Scale bar represents 100 μm. **D.** The mean percentages of cells exhibiting a rounded morphology after treatment. Error bars represent the SEM of at least three independent experiments. Statistical significance was determined using one-way ANOVA followed by Tukey's post hoc test ($p < 0.0001$). Means that are significantly different from the mean of the not-treated control are represented with a different letter (a, b).

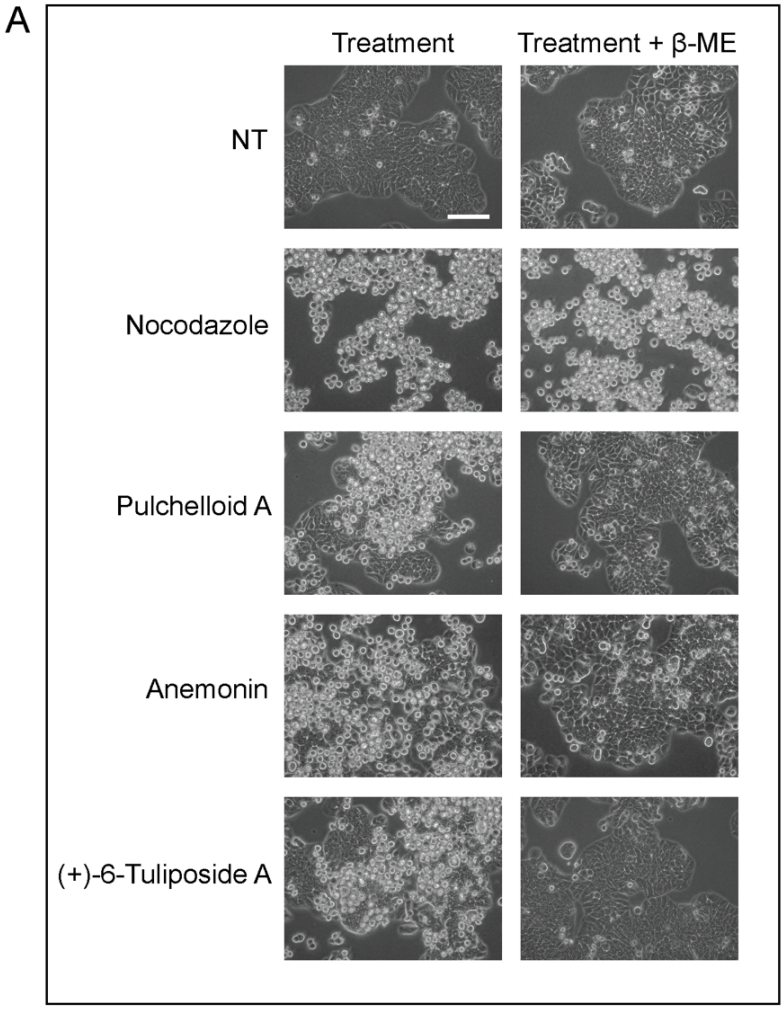
A
Treatment
Treatment + β-ME
NT
Nocodazole
Pulchelloid A
Anemonin
(+)-6-Tuliposide A

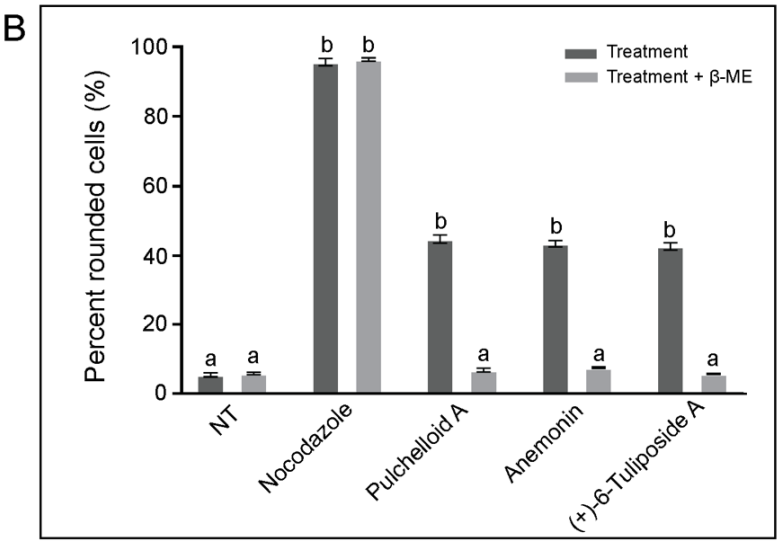
B
Percent rounded cells (%)
100
80
60
40
20
0
Treatment
Treatment + β-ME
a
a
b
b
b
a
b
a
b
a
NT
Nocodazole
Pulchelloid A
Anemonin
(+)-6-Tuliposide A

Figure 4.2. The cell rounding activities of pulchelloid A, anemonin and (+)-6-tuliposide A were eliminated after reduction by beta-mercaptoethanol. **A.** HT-29 cells were either not-treated or treated with nocodazole, pulchelloid A, anemonin or (+)-6-tuliposide A for 18 h. Treatments were administered either alone or after the compounds were preincubated with beta-mercaptoethanol (β-ME). Images were taken by light microscopy and representative images are shown. Scale bar represents 100 μm. **B.** The mean percentages of cells exhibiting a rounded morphology after treatment. Error bars represent the SEM of at least three independent experiments. Statistical significance was determined using one-way ANOVA followed by Tukey's post hoc test ($p < 0.0001$). Means that are significantly different from the mean of the not-treated control are represented with a different letter (a, b).

4.4.2 Pulchelloid A, anemonin and (+)-6-tuliposide A induced different effects on cell cycle progression

One of the mitotic arrest features common to the three compounds is their capacity to arrest approximately 40% of an asynchronous cell population whereas other compounds that target tubulin, such nocodazole, induce nearly 100% cell cycle arrest (Figure 4.3A). We then asked whether the compounds would have similar or different effects if applied to cultures that were synchronized in the G1/S-boundary of the cell cycle. Cells were synchronized by double-thymidine block and then released into media without further treatment, or released into media treated with nocodazole, pulchelloid A, anemonin or (+)-6-tuliposide A and analyzed by timelapse video microscopy for 24 h. Not-treated cells entered mitosis synchronously resulting in a peak of rounded cells at 10 h post-thymidine release. In the case of nocodazole, treated synchronized cells became 100% rounded by 10 h and remained so for the rest of the analysis. Pulchelloid A induced 91 ± 2% rounded cells for a duration of approximately 9 h, anemonin induced 81 ± 1% cell rounding for 8 h, whereas (+)-6-tuliposide A induced 90 ± 2% cell rounding for 11 h (Figure 4.3A). The duration of the arrest by (+)-6-tuliposide A was 20-30% longer than those of pulchelloid A

and of anemonin. These data revealed that the three compounds induced a mitotic arrest in the majority of cells when applied to synchronous cultures; however, the duration of each arrest was different between not-treated cells, or cells treated with nocodazole, pulchelloid A, anemonin or (+)-6-tuliposide A.

We continued the exploration of the relationship between the mitotic arrest and the chemical structure of the three compounds. Michael addition reactions in compounds that have methylene carbonyls are proposed to form covalent bonds with targets that contain thiols, such as cysteines in polypeptides. If these compounds form covalent bonds with their targets, then removing the compound after treatment should produce the same result as continuous exposure to the compound. Synchronized populations of cells were released from the double thymidine block into either media without further treatment, or media treated with nocodazole, pulchelloid A, anemonin, or (+)-6-tuliposide A for 6 h followed by release into media without these compounds. The percentage of rounded cells was determined by timelapse video microscopy over 24 h. Cells in the not-treated population achieved a peak of about 50 ± 4% cell rounding by 10 h (Figure 4.3B). Nocodazole, which does not covalently bind to its tubulin target, had little effect upon cells once removed from the culture at 6 h. Pulchelloid A arrested cells to a similar level whether continuously treated or removed from the culture. The removal of anemonin permitted the cells to exit mitosis rather than maintain the arrest and the time of mitotic onset peaked at 13 h instead of 10 h. After the removal of (+)-6-tuliposide A, the time of mitotic onset and exit was like that of a not-treated synchronized population, and readily distinguishable from that of the continuous treatment of (+)-6-tuliposide A.

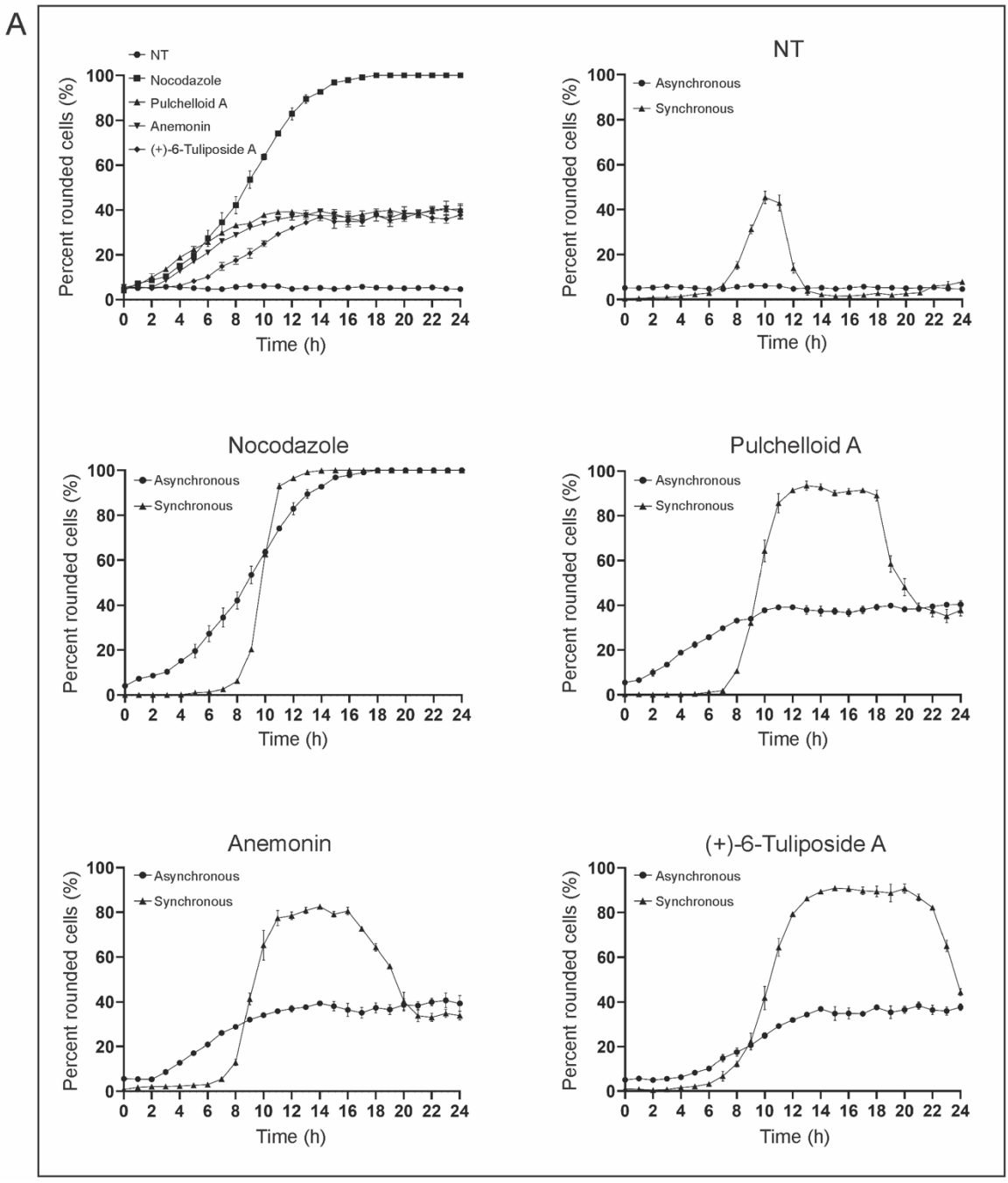
A
NT
Nocodazole
Pulchelloid A
Anemonin
(+)-6-Tuliposide A
Percent rounded cells (%)
Time (h)
NT
Asynchronous
Synchronous
Nocodazole
Pulchelloid A
Anemonin
(+)-6-Tuliposide A

B

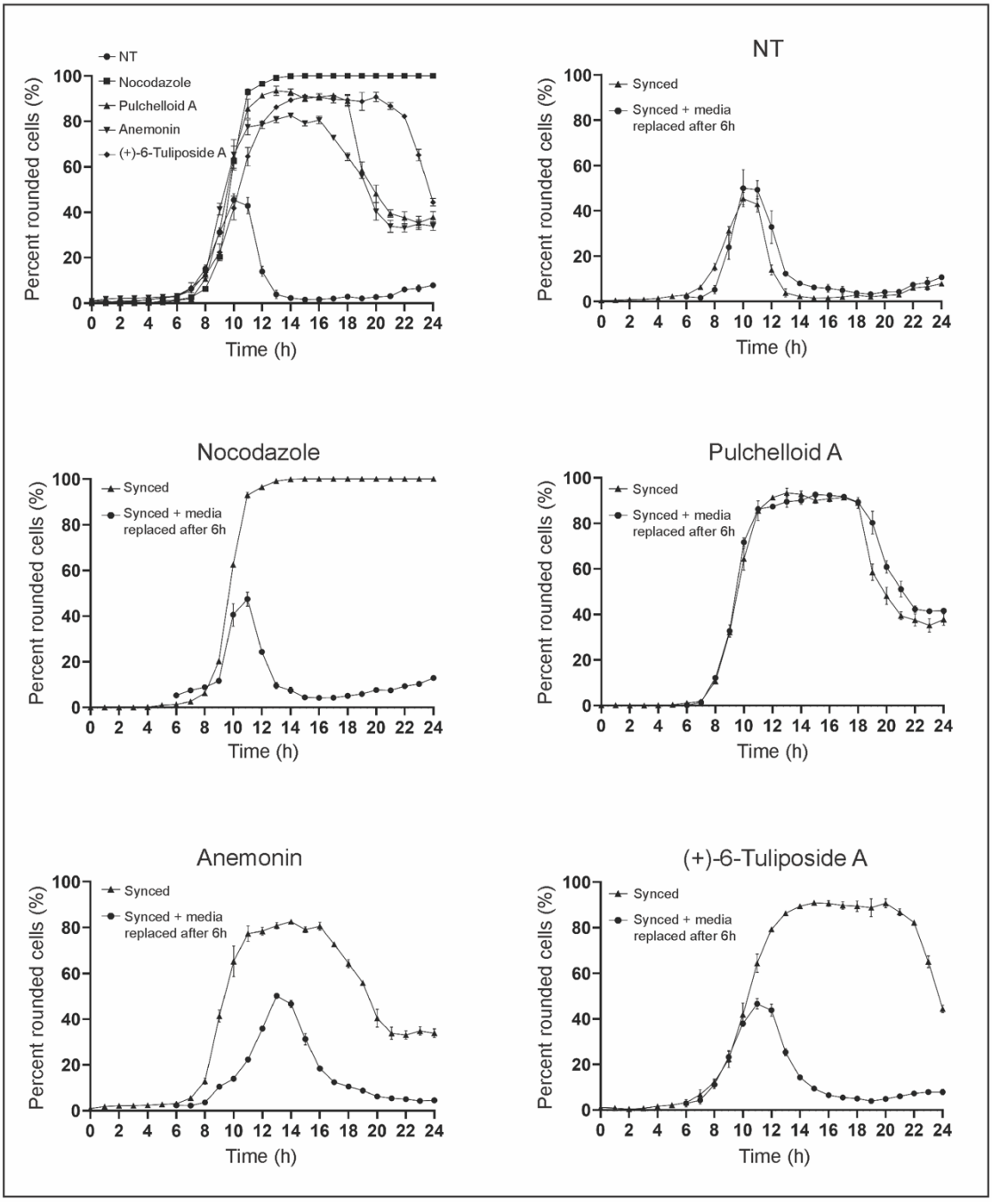
NT
Nocodazole
Pulchelloid A
Anemonin
(+)-6-Tuliposide A
Percent rounded cells (%)
Time (h)
NT
Synced
Synced + media replaced after 6h
Nocodazole
Pulchelloid A
Anemonin
(+)-6-Tuliposide A

Figure 4.3. The compounds pulchelloid A, anemonin and (+)-6-tuliposide A induced 40% cell rounding in asynchronous populations of HT-29 cells, but induced mitotic delays in nearly all cells of synchronized populations of HT-29 cells. Synchronized cells maintained a mitotic arrest after removal of pulchelloid A from treatment. **A.** The mean percentages of cells exhibiting a rounded cell morphology after treatment with nocodazole, pulchelloid A, anemonin, (+)-6-tuliposide A or not-treated in asynchronous and synchronous cell populations. HT-29 cells were synchronized by double thymidine block before being released into treatment. Images were taken by timelapse video microscopy for 24 h. Error bars represent the SEM of at least three independent experiments. **B.** The mean percentages of cells exhibiting a rounded cell morphology after treatment with nocodazole, pulchelloid A, anemonin, (+)-6-tuliposide A or not-treated in synchronous cell populations. HT-29 cells were synchronized by double thymidine block before either being released into treatment continuously or being released into treatment for 6 h followed by removal of treatment into not-treated media. Images were taken by timelapse video microscopy for 24 h. Error bars represent the SEM of at least three independent experiments.

4.4.3 Pulchelloid A, anemonin and (+)-6-tuliposide A induced different effects on spindle distortion and centrosome protein organization

We then examined whether the three compounds affected the organization of the mitotic spindles in a similar or different manner. Asynchronous populations of cells were either not-treated or treated with each compound for 18 h. Cells were then fixed for immunofluorescence microscopy and observed for phosphorylated histone H3 (anti-phospho-histone H3 antibodies), the organization of tubulin (anti-α-tubulin antibodies), and DAPI staining. In not-treated cells, bipolar mitotic spindles were readily observed (Figure 4.4A). Of the total number of cells that were in mitosis (4 ± 1%, PH3 staining), 50 ± 5% contained a bipolar spindle (Figure 4.4B). Each of the three compounds under investigation induced PH3 staining consistent with cell rounding observations with pulchelloid A at 38 ± 2% mitotic cells, anemonin at 41 ± 4% mitotic cells and (+)-6-tuliposide A at 38 ± 3% mitotic cells. Of these mitotic cells, pulchelloid A treated cells had 90 ± 1% containing a spindle structure, anemonin treated cells had 87 ± 2%, and (+)-6-

tuliposide A treated cells had 80 ± 3%, values that were statistically similar (Figure 4.4B). We then asked whether the cells with spindles had either a bipolar spindle or non-bipolar (distorted) spindle. In the mitotic cells induced by pulchelloid A, 84 ± 2% of the spindles were distorted, anemonin induced 40 ± 1% cells with a distorted spindle, and (+)-6-tuliposide A induced a distorted spindle in 74% of cells, values that were statistically dissimilar (Figure 4.4C).

We next tested whether the distorted spindle was assembled in an unorganized manner, or if it first arose from a prior bipolar spindle structure. To assess this, cells were synchronized by a double thymidine block and then released into media treated with pulchelloid A, anemonin, or (+)-6-tuliposide A. At times from 10 to 20 h post release, cells were fixed and analyzed by immunofluorescence microscopy to assess the organization of tubulin in the mitotic spindle over the course of the arrest (Figure 4.5A). Not-treated cells formed a bipolar spindle that aligned the chromosomes in a time of about 2 h as demonstrated by PH3 staining (representative images from asynchronous cells). Pulchelloid A treated cells appeared to form an organized spindle structure by 10 h, followed by an increase in the numbers of cells with distorted spindles by 14 h. The frequency of distorted spindles increased until nearly 98% of cells contained a distorted spindle by 20 h. The number of cells with a distorted spindle during anemonin treatment increased from 13 ± 3% to 58 ± 4%; whereas cells with spindle distortion after (+)-6-tuliposide A treatment increased from 15 ± 2% to 95 ± 1%. These results revealed that the mitotic arrests of these three compounds affected spindle organization, including the placement of phospho-histone H3 signals.

Having observed that the mitotic spindle was organized differently in cell treated by either of the three compounds, we then examined whether centrosome organization was altered or not under these treatments. We used immunofluorescence microscopy and anti-γ-tubulin antibodies to evaluate cells that were either not-treated, or treated with paclitaxel, pulchelloid A, anemonin, or (+)-6-tuliposide A for 18 h. Individual cells were photographed (Figure 4.5A) and subjected to plot profile analysis to obtain a graphical representation of the intensity, proximity, and number of γ-tubulin structures, typically centrosomes (Figure 4.5B). Not-treated cells displayed centrosomes that were organized on either side of the metaphase chromosomes, which were graphically shown as two distinct and spaced peaks of similar intensity on the plot profile. Plot profile analysis of paclitaxel treated cells revealed that centrosomes remain organized while being slightly closer than those in not-treated cells. Analysis of pulchelloid A treated cells revealed four peaks of different intensities of γ-tubulin. Whereas anemonin treated cells display two peaks that were less organized as represented by the breadth of the peaks. This measure was representative of the images in which the γ-tubulin signals were rarely found as distinct foci (Figure 4.5A). (+)-6-tuliposide A treated cells were different from those of other treatments, in which three peaks were detected. These data support the observation of distorted spindles and further distinguish the mitotic arrests induced by each of the three compounds.

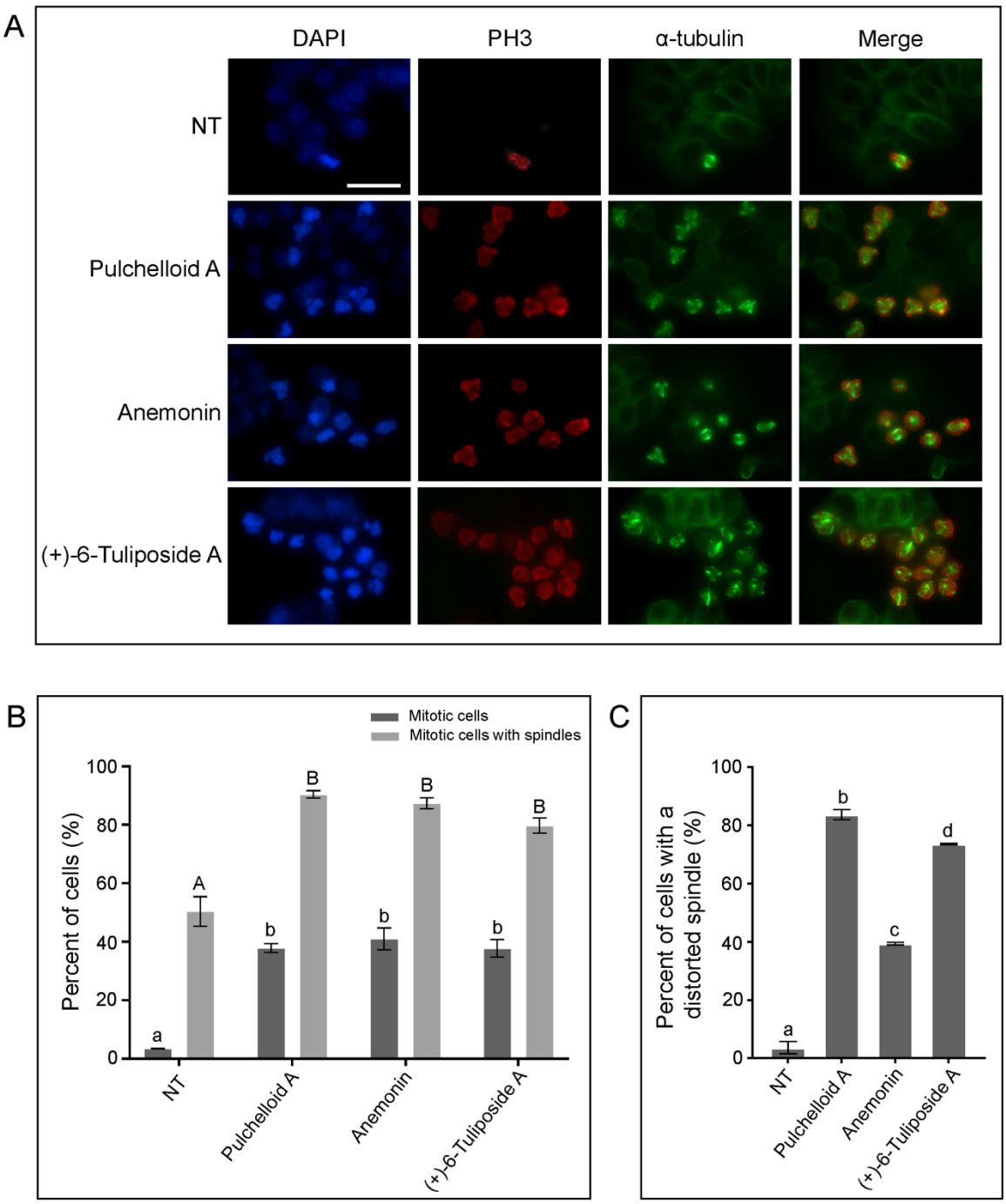
A
DAPI
PH3
α-tubulin
Merge
NT
Pulchelloid A
Anemonin
(+)-6-Tuliposide A
B
Mitotic cells
Mitotic cells with spindles
Percent of cells (%)
100
80
60
40
20
0
a
A
b
B
b
B
b
B
NT
Pulchelloid A
Anemonin
(+)-6-Tuliposide A
C
Percent of cells with a distorted spindle (%)
100
80
60
40
20
0
a
b
c
d
NT
Pulchelloid A
Anemonin
(+)-6-Tuliposide A

Figure 4.4. HT-29 cells treated with pulchelloid A, anemonin and (+)-6-tuliposide A each exhibited a phospho-histone H3 signal and a distorted mitotic spindle structure. **A.** HT-29 cells were either not-treated or treated with pulchelloid A, anemonin or (+)-6-tuliposide A for 18 h. Cells were analyzed by immunofluorescence microscopy where DNA was detected with DAPI (blue), phosphorylated histone H3 with anti-phospho-histone H3 antibodies (red) and tubulin with anti-α-tubulin antibodies (green). The merge column is the combination of phospho-histone H3 and α-tubulin staining. Scale bar represents 50 μm. **B.** The mean percentages of cells exhibiting a phospho-histone H3 signal (mitotic cells, dark grey) and mitotic cells with a spindle structure (light grey) after treatment. Error bars represent the SEM of at least three independent experiments. Statistical significance was determined using one-way ANOVA followed by Tukey's post hoc test ($p < 0.001$). Means that are significantly different from the mean of the not-treated control are represented with a different letter (a, b; A, B). **C.** The mean percentages of cells with a distorted (non-bipolar) spindle structure after treatment. Error bars represent the SEM of at least three independent experiments. Statistical significance was determined using one-way ANOVA followed by Tukey's post hoc test ($p < 0.005$). Means that are significantly different from each other are represented with a different letter (a, b, c, d).

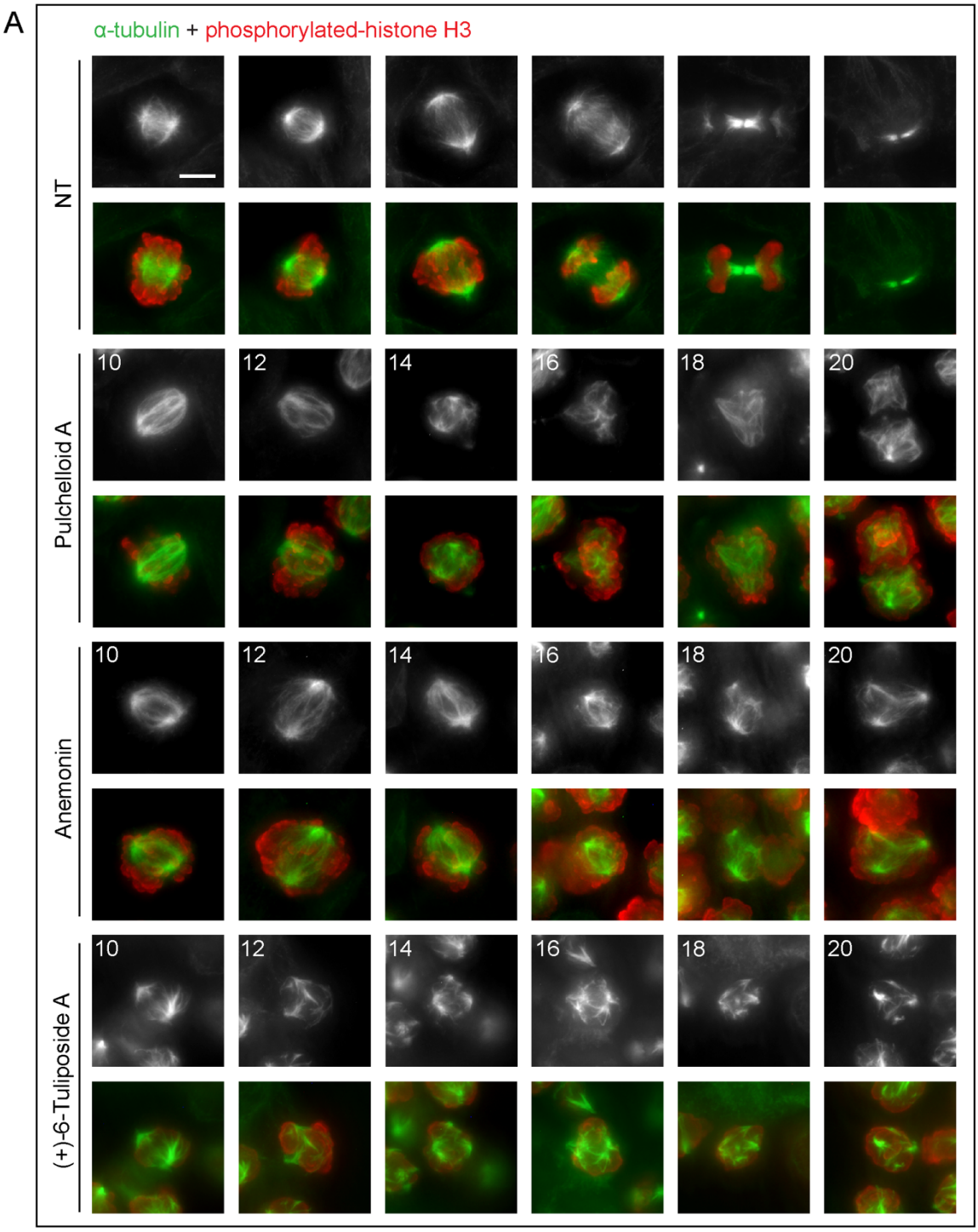
A
α-tubulin + phosphorylated-histone H3
NT
Pulchelloid A
Anemonin
(+)-6-Tuliposide A
10
12
14
16
18
20

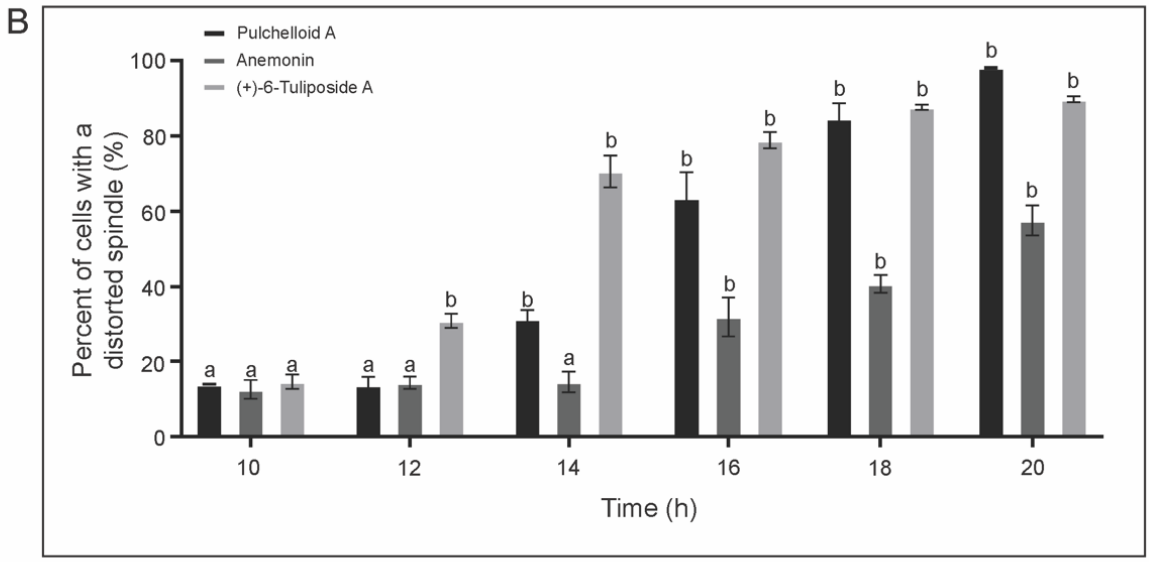

Figure 4.5. The percentage of cells with a distorted mitotic spindle structure increase over time after treatment with pulchelloid A, anemonin and (+)-6-tuliposide A. **A.** HT-29 cells were either not-treated and fixed at 18 h (asynchronous culture), or treated with pulchelloid A, anemonin or (+)-6-tuliposide A and fixed at various times (synchronous culture) for analysis by immunofluorescence microscopy. Representative images of each phase of the cell cycle are shown for not-treated cells. Tubulin was detected with anti-α-tubulin antibodies (grayscale/green), and phosphorylated histone H3 with anti-phospho-histone H3 antibodies (red). Scale bar represents 10 μm. **B.** The mean percentages of cells with a distorted (non-bipolar) spindle structure after treatment over time. Error bars represent the SEM of at least three independent experiments. Statistical significance was determined using one-way ANOVA followed by Tukey's post hoc test ($p < 0.05$). Means that are significantly different from the mean of the initial timepoint are represented with a different letter (a, b).

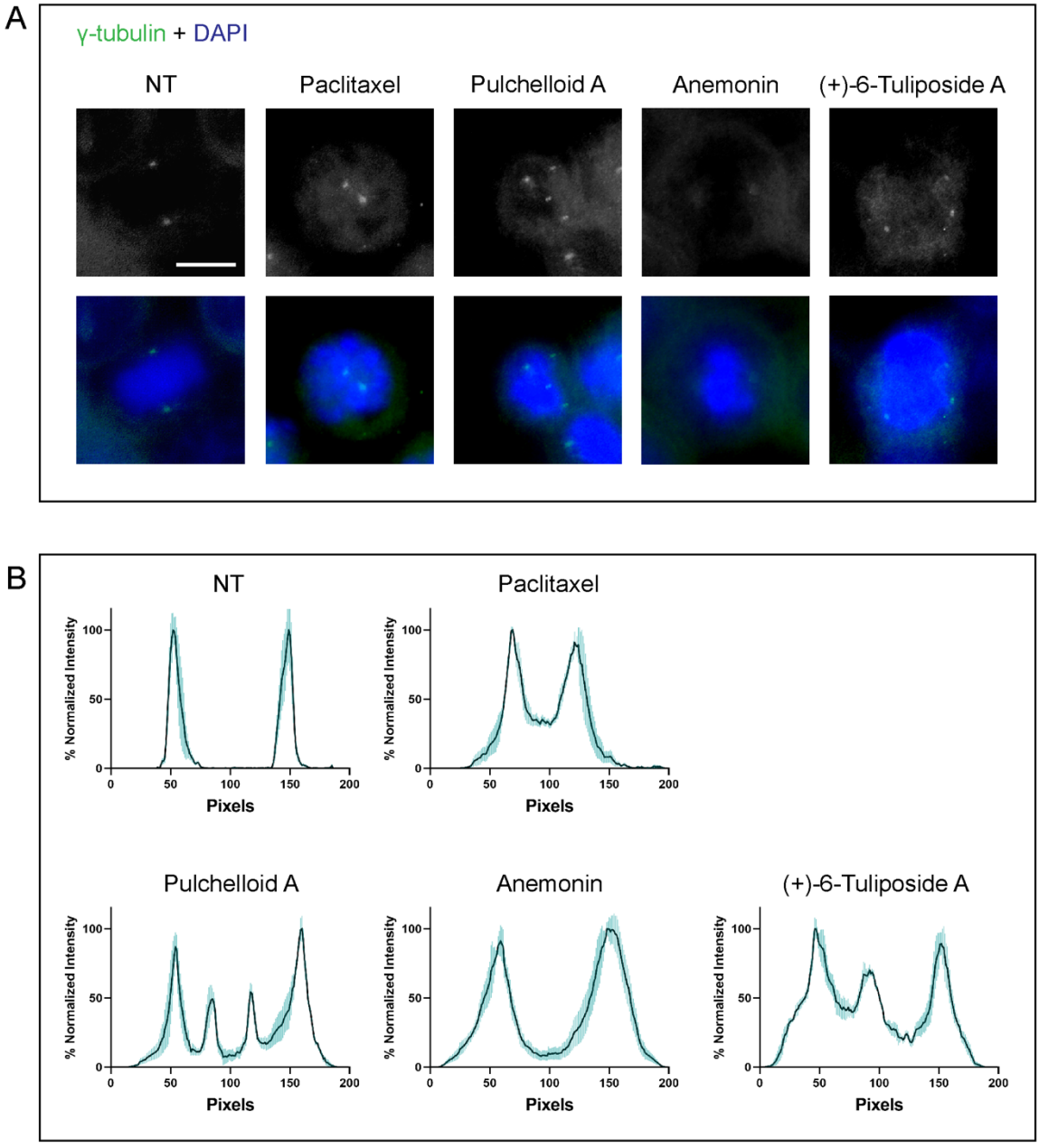

Figure 4.6. HT-29 cells treated with pulchelloid A, anemonin and (+)-6-tuliposide A exhibit irregular localization of γ-tubulin. **A.** HT-29 cells were either not-treated or treated with paclitaxel, pulchelloid A, anemonin or (+)-6-tuliposide A and fixed at 18 h for immunofluorescence microscopy. γ-tubulin was detected with anti-γ-tubulin antibodies (grayscale/green) and DNA was stained with DAPI (blue). Scale bar represents 10 μm. **B.** The intensity of γ-tubulin fluorescence was measured over the area of one cell. Measurements were normalized to cytoplasmic intensity and highest intensity across all treatments. Error bars represent the SEM of at least three independent experiments.

4.4.4 Pulchelloid A, anemonin and (+)-6-tuliposide A induced DNA damage correlated with spindle distortion

The disorganization of the mitotic spindle in treated cells led us to ask whether this might affect the structure of chromosomes. We used immunofluorescence microscopy and anti-γ-histone H2AX antibodies to evaluate cells that were not-treated, or treated with camptothecin (a genotoxic agent), pulchelloid A, anemonin, or (+)-6-tuliposide A for 18 h. We assessed if DNA was damaged by recording γ-histone H2AX signals in cells (Figure 4.6A). No γ-histone H2AX signals were observed in not-treated cells, whereas camptothecin (CPT) induced γ-histone H2AX signals in 99% of cells (Figures 4.6A, B). After treatment with pulchelloid A, 29 ± 2% of cells had γ-histone H2AX signals, whereas treatment with anemonin induced 15 ± 1% of cells with γ-histone H2AX signals and (+)-6-tuliposide A induced 37 ± 2% of cells with γ-histone H2AX signals (Figure 4.6B). Interestingly, the γ-histone H2AX signals were punctate, in contrast to the generalized staining observed by camptothecin treatment, and the signals induced by the three compounds were only observed in the mitotic cells with no signals observed in interphasic cells.

We reasoned that if there was a relationship between mitosis and DNA damage, then the duration of mitosis should increase the number of cells with damaged DNA. To test this, we applied pulchelloid A, anemonin, or (+)-6-tuliposide A to synchronized cells (Figure 4.7C) as described in experiments above. The number of cells with γ-histone H2AX signals increased between 10 and 20 h with (+)-6-tuliposide A inducing the greatest number of cells with damaged DNA (increasing from 34 ± 4% to 77 ± 3%) followed by pulchelloid

A (increasing from 27 ± 3% to 69 ± 1%) and anemonin (increasing from 22 ± 4% to 51 ± 5%).

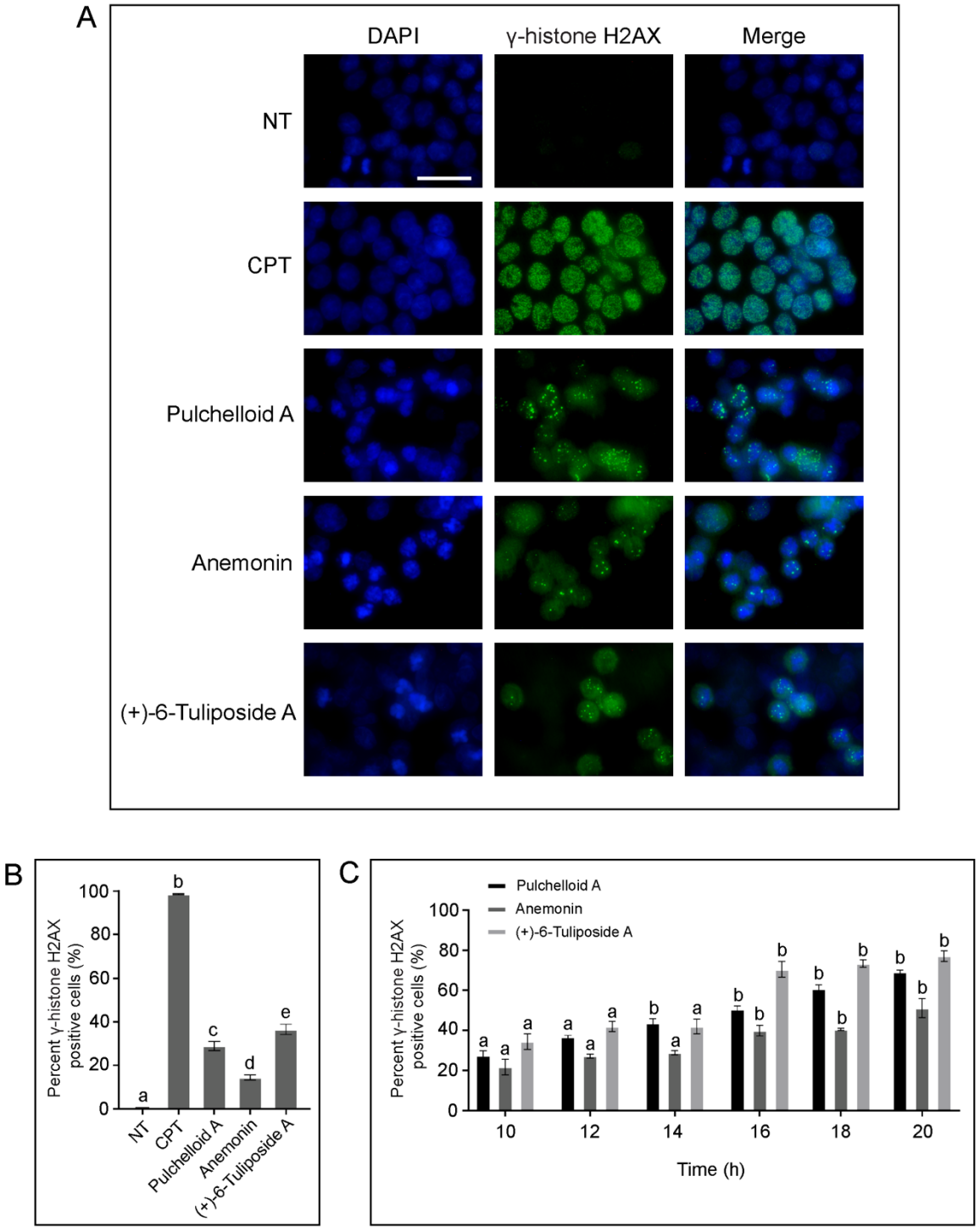

Figure 4.7. HT-29 cells treated with pulchelloid A, anemonin and (+)-6-tuliposide A acquired γ-histone H2AX foci. **A.** HT-29 cells were either not-treated or treated with camptothecin (CPT), pulchelloid A, anemonin or (+)-6-tuliposide A and fixed at 18 h for immunofluorescence microscopy. γ-histone H2AX foci were detected with anti-γ-histone H2AX antibodies (green) and DNA was stained with DAPI (blue). Scale bar represents 50 μm. **B.** The mean percentages of cells with greater than 5 γ-histone H2AX foci after treatment. Error bars represent the SEM of at least three independent experiments. Statistical significance was determined using one-way ANOVA followed by Tukey's post hoc test ($p < 0.05$). Means that are significantly different from each other are represented with a different letter (a, b, c, d, e). **C.** The mean percentages of cells with greater than 5 γ-histone H2AX foci after treatment over time. Synchronized HT-29 cells were either not-treated or treated with pulchelloid A, anemonin or (+)-6-tuliposide A and fixed at various times for analysis by immunofluorescence microscopy. Error bars represent the SEM of at least three independent experiments. Statistical significance was determined using one-way ANOVA followed by Tukey's post hoc test ($p < 0.05$). Means that are significantly different from the mean of the initial timepoint are represented with a different letter (a, b).

4.4.5 Pulchelloid A, anemonin and (+)-6-tuliposide A induced irregular localization and expression of kinetochore- and centrosome-associated proteins

We then investigated three proteins involved in the spindle assembly checkpoint (SAC) at the metaphase to anaphase transition. First, we examined centromere-associated protein E (CENP-E) a kinesin-like motor protein involved in the elongation of spindle fibres and chromosome movement. We used immunofluorescence microscopy and anti-CENP-E antibodies to evaluate cells that were either not-treated, or treated with paclitaxel, pulchelloid A, anemonin, or (+)-6-tuliposide A. CENP-E accumulates in the G2 phase of the cell cycle and associates with the kinetochores throughout mitosis, as shown in not-treated cells (Figure 4.8A). In nocodazole treated cells, CENP-E is distributed throughout the cell and associated with the kinetochores (Mirzaa et al., 2014). In paclitaxel treated cells, CENP-E is clustered to the hyper-polymerized tubulin and clustered chromosomes are observed. Pulchelloid A treated cells revealed a pattern of CENP-E distribution that was

irregular and distinct from either not-treated, nocodazole or paclitaxel treatments. Anemonin treated cell had few CENP-E foci, suggesting that CENP-E is either improperly localized or the protein has low levels of expression, whereas (+)-6-tuliposide A treated cells had irregular CENP-E localization that was similar to pulchelloid A treated cells.

We used western blotting to determine whether the changes in CENP-E signal intensity observed by immunofluorescence were due to changes in the levels of expression. Cells were either not-treated, or treated with nocodazole, paclitaxel, pulchelloid A, anemonin, or (+)-6-tuliposide A (Figure 4.8B). We separated the mitotic cells (Mit.) from interphase cells (Int.) using the mechanical shake-off technique. Cell extracts were separated by SDS-PAGE and their relative protein levels were standardized to actin. CENP-E expression was low in not-treated cells and high in cells arrested in mitosis by nocodazole and paclitaxel, as expected (Figure 4.8B). Of the three compounds of interest, CENP-E levels were highest in the mitotic cells induced by pulchelloid A similar to nocodazole and paclitaxel treated cells. CENP-E expression was low in all anemonin treated cells and not significantly different from the not-treated sample, whereas mitotic cells induced by (+)-6-tuliposide A had intermediate levels of CENP-E that were statistically different from the pulchelloid A and anemonin mitotic samples (Figure 4.8C). This aligns with the results of CENP-E immunofluorescence where we did not observe strong foci in anemonin treated cells (Figure 4.8A).

We then reasoned that if CENP-E signals were different in cells treated by the three compounds, then proteins that interact with CENP-E may also vary in signal intensity. We investigated budding uninhibited by benzimidazole-related 1 (BubR1) by immunofluorescence microscopy and anti-BubR1 antibodies in either not-treated cells or cells treated with nocodazole, paclitaxel, pulchelloid A, anemonin or (+)-6-tuliposide A

(Figure 4.9). In not-treated cells, BubR1 is present in prophase and metaphase followed by a sharp decline in intensity in anaphase. In nocodazole treated cells, BubR1 is distributed throughout the cell, whereas in paclitaxel treated cells, BubR1 is clustered in a manner similar to the distribution of CENP-E observed. In cells treated with pulchelloid A, the BubR1 signal was readily detectable; however, in contrast, in anemonin and (+)-6-tuliposide A, treated cells the BubR1 signals were weaker and similar to that of the CENP-E signals.

We then examined the status of the centrosomes by immunofluorescence microscopy and anti-PLK-1 antibodies in either not-treated cells or cells treated with nocodazole, paclitaxel, pulchelloid A, anemonin or (+)-6-tuliposide A (Figure 4.10). In not-treated cells, polo-like kinase 1 (PLK-1) associates with the centrosomes in the early stages of mitosis before translocating to the zone between the segregated chromosomes to accumulate in the midbody (Figure 4.10). Nocodazole treated cells had several PLK-1 foci of relatively lower intensity than the foci in paclitaxel treated cells. In pulchelloid A treated cells, the pattern of PLK-1 staining was similar to that of paclitaxel, with four intensely stained foci. Anemonin treated cells displayed two groups of PLK-1 foci, whereas in (+)-6-tuliposide A treated cells, we observed three groups of PLK-1 foci. The PLK-1 foci patterns in each of pulchelloid A, anemonin and (+)-6-tuliposide A treated cells align with the γ-tubulin foci observed (Figure 4.6). These results were consistent with the emerging patterns that compounds with methylene carbonyls may arrest cells in mitosis by different mechanisms.

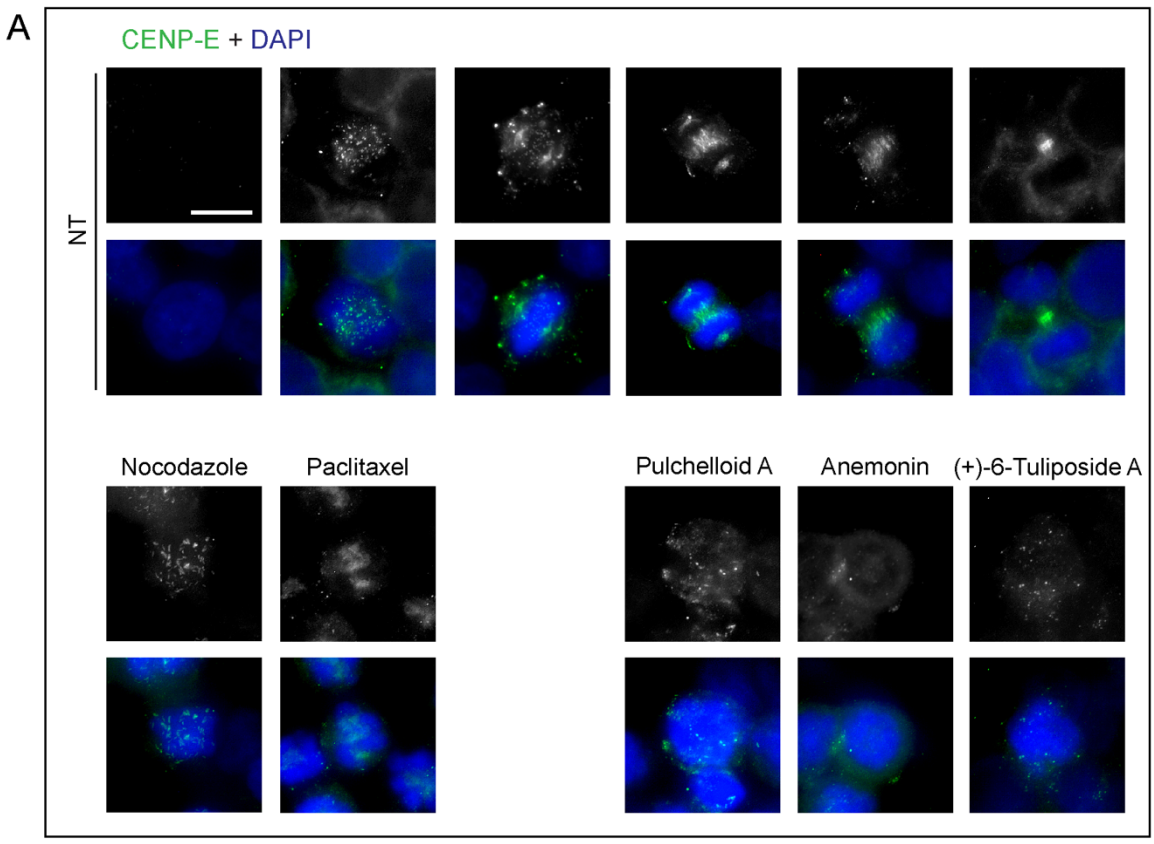
A
CENP-E + DAPI
NT
Nocodazole
Paclitaxel
Pulchelloid A
Anemonin
(+)-6-Tuliposide A

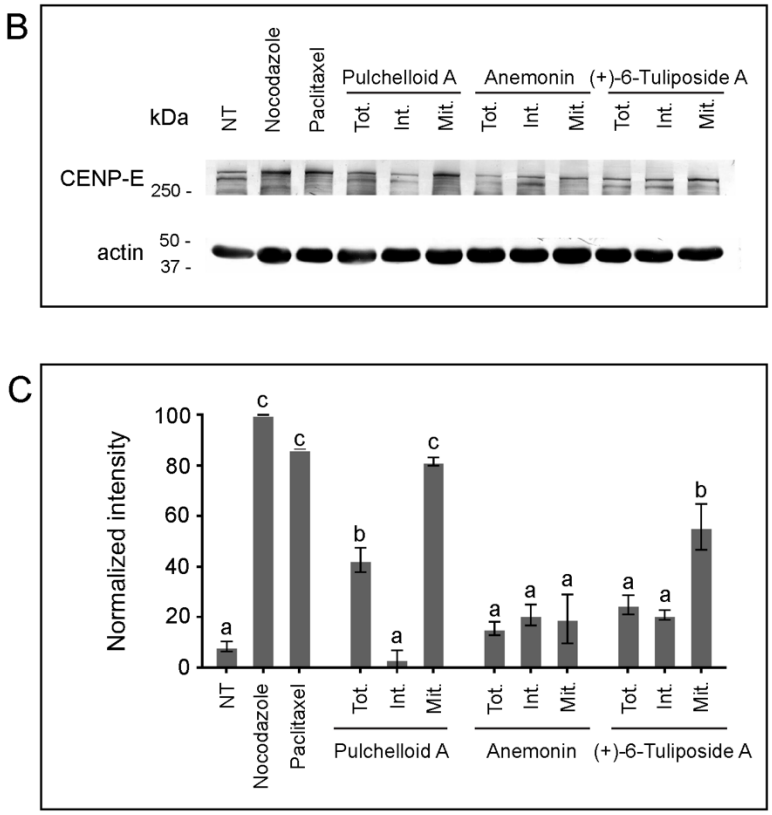

Figure 4.8. HT-29 cells treated with pulchelloid A exhibit irregular localization and high expression of CENP-E, anemonin treated cells exhibit poor localization and low expression, and (+)-6-tuliposide A treated cells exhibit irregular localization and intermediate expression. **A.** HT-29 cells were either not-treated or treated with nocodazole, paclitaxel, pulchelloid A, anemonin or (+)-6-tuliposide A for 18 h. Cells were analyzed by immunofluorescence microscopy where DNA was detected with DAPI (blue), and CENP-E with anti-CENP-E antibodies (grayscale/green). Representative images of each phase of the cell cycle are shown for not-treated cells. Scale bar represents 10 μm. **B.** HT-29 cells were either not-treated or treated with nocodazole, paclitaxel, pulchelloid A, anemonin or (+)-6-tuliposide A for 18 h. Cell extracts of total cell populations (Tot.) were collected by trypsinization. Mitotic cells (Mit.) were separated by mechanical shake-off from interphase cells (Int.). Cell extracts were separated by SDS-PAGE and analysed by western blotting for CENP-E. Protein levels were standardized to actin. **C.** Normalized band intensities of CENP-E western blots are shown. Error bars represent the SEM of at least three independent experiments. Statistical significance was determined using one-way ANOVA followed by Tukey's post hoc test ($p < 0.05$). Means that are significantly different from each other are represented with a different letter (a, b, c).

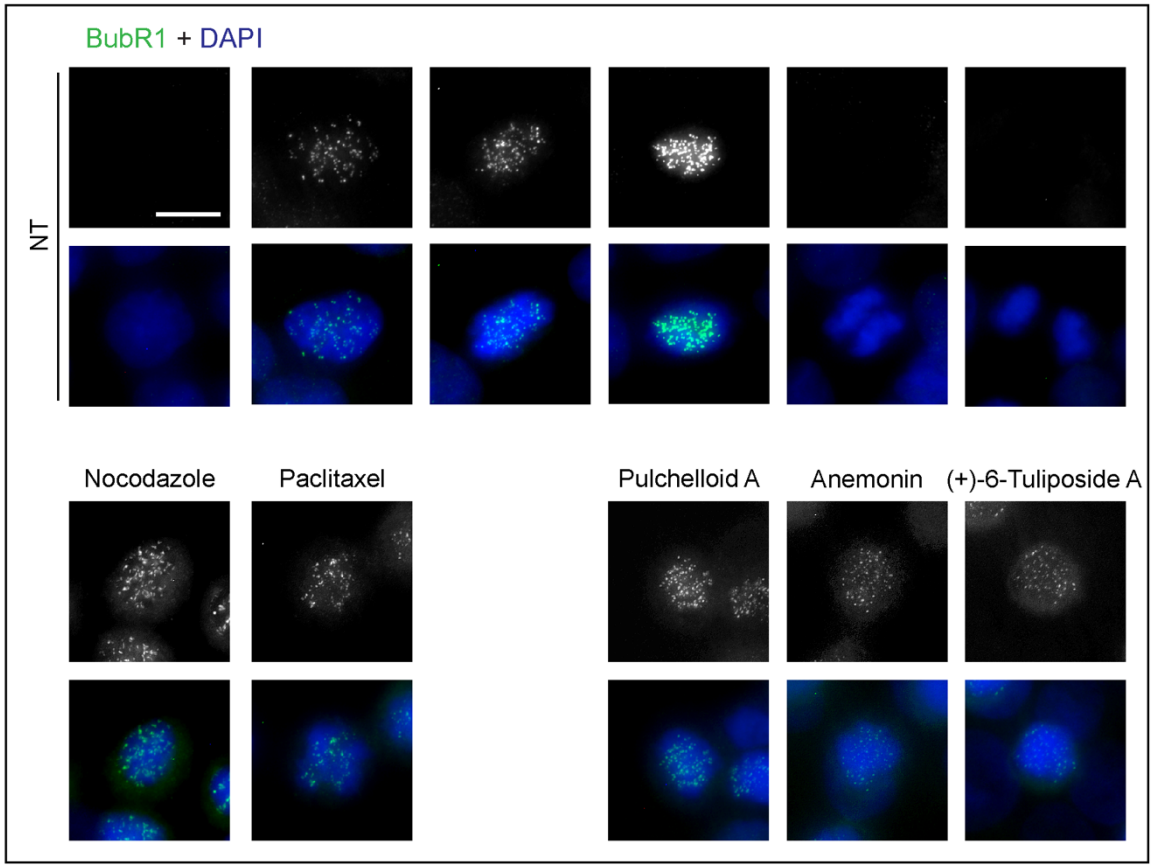

Figure 4.9. HT-29 cells treated with pulchelloid A, anemonin and (+)-6-tuliposide A each exhibit BubR1 signals. HT-29 cells were either not-treated or treated with nocodazole, paclitaxel, pulchelloid A, anemonin or (+)-6-tuliposide A for 18 h. Cells were analyzed by immunofluorescence microscopy where DNA was detected with DAPI (blue), and BubR1 with anti-BubR1 antibodies (grayscale/green). Representative images of each phase of the cell cycle are shown for not-treated cells. Scale bar represents 10 µm.

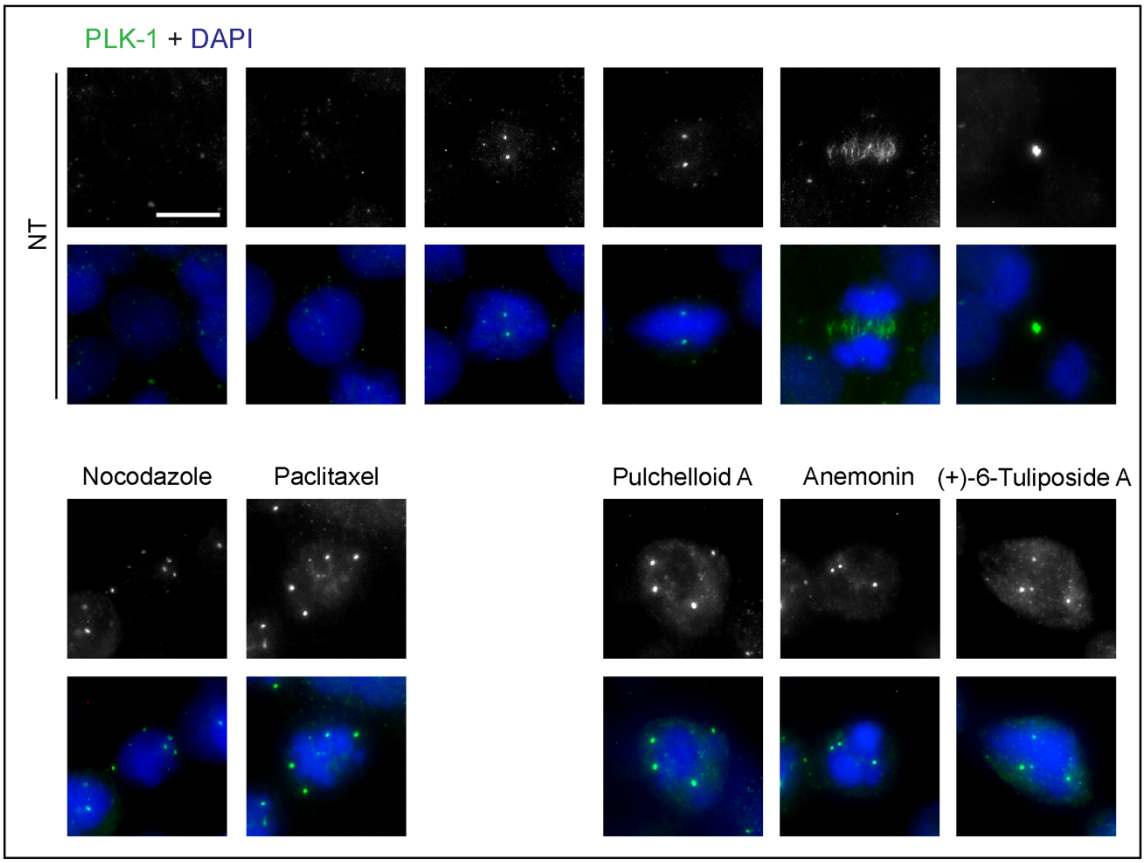

Figure 4.10. HT-29 cells treated with pulchelloid A, anemonin and (+)-6-tuliposide A each exhibit irregular localization of PLK-1. HT-29 cells were either not-treated or treated with nocodazole, paclitaxel, pulchelloid A, anemonin or (+)-6-tuliposide A for 18 h. Cells were analyzed by immunofluorescence microscopy where DNA was detected with DAPI (blue), and PLK-1 with anti-PLK-1 antibodies (grayscale/green). Representative images of each phase of the cell cycle are shown for not-treated cells. Scale bar represents 10 μm.

4.5 Discussion

This is the first report that differentiated the mitotic arrests induced by natural product compounds that share a methylene carbonyl moiety (pulchelloid A, anemonin, and (+)-6-tuliposide A) (Table 4.1). In our previous studies, we identified the anti-mitotic compounds anemonin from *Pulsatilla nuttalliana* (Chapter 2) and (+)-6-tuliposide A from *Erythronium grandiflorum* (Chapter 3). The mitotic arrests induced by these two compounds bore a striking resemblance to the anti-mitotic activities of pulchelloid A and hymenoratin, two sesquiterpene lactones identified by our laboratory from *Gaillardia aristata* (Bosco et al., 2021) and *Hymenoxys richarsonii* (Molina et al., 2021), respectively. The common features included a 40% rounded mitotic phenotype when applied to an asynchronous culture, distorted mitotic spindles, and chemical inactivation by β-ME reduction. Our findings, summarized in Table 4.1, indicate a distinct mitotic arrest profile for each compound, supporting the hypothesis that each targets a specific protein required for mitotic progression.

The so-called "40% mitotic arrest" prompted further investigation because it was less than the anti-mitotic compounds paclitaxel and nocodazole which induced nearly 100% cell rounding. When applied to a synchronized culture we observed that pulchelloid A, anemonin and (+)-6-tuliposide A induced prolonged mitotic arrests in nearly all cells, which eventually exit mitosis. In view of this result, a "40% mitotic arrest" in asynchronous cultures is consistent with a long mitotic delay effect in synchronized cultures, throughout which we observed distorted mitotic spindles and misaligned chromosomes.

Investigating γ-tubulin localization provided insight about the spindle distortion, especially in pulchelloid A and (+)-6-tuliposide A treated cells, which displayed an

abnormal number of γ-tubulin foci. Anemonin treated cells displayed two γ-tubulin peaks as found in a bipolar spindle structure, but the structures were not tightly organized, suggesting that the centrosomes were not properly functioning. Furthermore, there was a strong correlation between spindle distortion and damaged DNA, which was found only in mitotic cells. These results are similar to those in reports that any prolonged arrest can cause DNA damage (Dalton et al., 2007; Orth et al., 2012; Quignon et al., 2007) and that delayed mitosis is mediated by the spindle assembly checkpoint (SAC) (Rieder & Maiato, 2004; Shannon et al., 2002).

Narrowing the mitotic arrest to a pre-metaphase state guided the investigation to proteins involved in the mitotic checkpoint complex (MCC) of the SAC, which prevents the onset of anaphase until proper chromosome congression has occurred (Bolanos-Garcia, 2014; Lara-Gonzalez et al., 2021). In anemonin treated cell, the localization of CENP-E was difficult to detect, which was supported by the low expression of CENP-E in cell extracts, whereas pulchelloid A and (+)-6-tuliposide A treated cells displayed unequal distribution of CENP-E foci. Discrepancies in CENP-E distribution and expression may implicate kinetochore-chromosome attachment disruption, thus affecting proteins that regulate chromosome movement and alignment in prometaphase (Owa & Dynlacht, 2021). Non-essential kinetochore proteins are not strictly required for cell survival but play important roles in proper chromosome segregation during mitosis. If these proteins are targeted, either directly or indirectly, it can lead to mitotic arrest. Previous research has found that CENP-E disruption, through RNA interference or inhibition with the small molecule GSK923295, resulted in chromosome misalignment, increased mitotic arrest and

spindle disorganization (Fang et al., 2023; Ohashi et al., 2015; She et al., 2020; Xu et al., 2010).

BubR1 monitors the attachment of chromosomes to the mitotic spindle, delaying the initiation of anaphase until all chromosomes are correctly aligned and attached (H. Huang et al., 2008). The degradation of BubR1 is regulated by the anaphase-promoting complex/cyclosome (APC/C), an E3 ubiquitin ligase complex that ubiquitylates proteins, including BubR1, for degradation by the proteasome (Luna-Maldonado et al., 2021). We observed a BubR1 signal in all arrested cells which confirms the inability of cells to achieve SAC inactivation when treated with any of the three compounds. Finally, PLK-1 localization paralleled γ-tubulin localization suggesting PLK-1 was properly positioned to the centrosomes (Schmucker & Sumara, 2014) but may be dysfunctional if centrosomes are not organized correctly, as suggested by the abnormal numbers of γ-tubulin and PLK-1 foci. PLK-1 releases APC/C inhibition by phosphorylating Cdc20 (Jia et al., 2016) which triggers the targeted degradation of various proteins by the APC/C. Overall, these results provide support that these compounds inhibit proteins required for SAC silencing.

The methylene carbonyl functional group, especially when present as a butyrolactone, can react with sulfhydryl groups present in cysteine-containing polypeptides (Bailly, 2021; Berdan et al., 2019; Jackson et al., 2017; Lagoutte et al., 2016). Consistent with this possibility, all three compounds were inactivated by preincubation with β-ME. Therefore, we reasoned that removing the compound after treatment should produce the same result as continuous exposure if these compounds form covalent bonds with their targets. Of the three compounds, only pulchelloid A treated cultures maintained an arrest following removal of the compound. The profiles for anemonin and (+)-6-tuliposide A were

different from each other and from pulchelloid A, suggesting that each compound may target a different cysteine-containing polypeptide. The inability of anemonin and (+)-6-tuliposide A to provide a prolonged arrest under these conditions may suggest that their protein targets are more rapidly turned over than those of pulchelloid A. Alternatively, a ubiquitin ligase could be directly inhibited by these compounds resulting in the delay of protein degradation prolonging SAC activation. The mechanisms underlying these mitotic arrests likely involve complex interactions among multiple proteins and pathways in the SAC. Several factors that affect protein turnover dynamics may contribute, including cell cycle regulators, mitotic checkpoint proteins, DNA damage, and protein synthesis and degradation machinery (Luna-Maldonado et al., 2021).

These data illustrate the fundamental principle that structural differences in inhibitor chemistry underlie distinct biological functions, likely through different targets. Furthermore, the results of this study suggest that current descriptors like “cytotoxic” and “mitotic” might be too broad to categorize the multitude of natural products. Relying solely on cytotoxicity provides a limited view on the potential therapeutic impact of a compound, neglecting its specificity and mechanism of action. Our results emphasize the importance of persistent investigation into compounds inducing less than 100% arrest in asynchronous cultures since they may inhibit highly specialized mitotic mechanisms. This underscores their significance in identifying new drug targets for precision medicine, where many mitotic regulators lack known inhibitors. Further investigations are warranted to unveil precise and potentially novel targets for therapeutic advancement of these natural products.

Table 4.1. Comparing the characteristics of the mitotic arrests of pulchelloid A, anemonin and (+)-6-tuliposide A. A summary of the characteristics that distinguish the mitotic arrest of pulchelloid A, anemonin and (+)-6-tuliposide A through cell cycle analysis and mitotic proteins.

Characteristic	**Pulchelloid A**	**Anemonin**	**(+)-6-Tuliposide A**
Percent cell rounding	40%	40%	40%
Reduction by β-ME	+	+	+
Distorted spindle	+	+	+
DNA damage	+	+	+
Tightly organized γ-tubulin foci	+	-	+
Number of γ-tubulin foci	4	2	3
Length of mitotic arrest	9 h	8 h	11 h
Activity maintained after media replacement	+	-	-
CENP-E expression	++	-	+

CHAPTER 5

General Discussion

At the beginning of this project, our laboratory had previously identified two sesquiterpene lactones, pulchelloid A (Bosco et al., 2021) and hymenoratin (Molina et al., 2021), from species in the Asteraceae plant family that induced a mitotic arrest in cancer cells. This added to the small but growing repertoire of sesquiterpene lactones with anti-mitotic activity (Bosco & Golsteyn, 2017). Using a phenotypic morphology assay to screen extracts from our prairie plant library in the search for other anti-mitotic natural products, we identified *Pulsatilla nuttalliana* (Ranunculaceae) extracts that induced cell rounding. By biology-guided fractionation we purified anemonin as the active compound that induced a mitotic arrest, which expanded our list including pulchelloid A and hymenoratin (Chapter 2). Anemonin is structurally related, yet distinct from sesquiterpene lactones, which led us to hypothesize that phylogenetic distance and chemical diversity of anti-mitotic compounds are positively related. To test this, we selected *Erythronium grandiflorum* (Liliaceae), the most phylogenetically distant species in our library relative to *Gaillardia aristata* (Asteraceae, pulchelloid A) that induced a mitotic arrest. We identified (+)-6-tuliposide A as the active compound, which is structurally distinct from pulchelloid A yet has several critical functional groups. These data support our hypothesis affirming that an increase in phylogenetic distance fosters chemical diversity of anti-mitotic compounds (Chapter 3). Guided by the principle that structure and function are correlated, we predicted that the differences in chemical structure between these compounds would indicate different protein targets. We then asked if the mitotic arrests of pulchelloid A, anemonin and (+)-6-tuliposide A could be differentiated beyond their shared characteristics of 40% cell rounding in an asynchronous population, distorted mitotic spindles and inactivation by β-ME reduction.

Through a series of assays, we identified unique differences between their mitotic arrests, providing evidence that each compound targets a distinct protein (Chapter 4). This is the first report that anti-mitotic compounds with similar mitotic arrest phenotypes have been differentiated from one another.

5.1 Diverse chemical structures induce similar mitotic phenotypes

The diversity in chemical profiles between *G. aristata*, *P. nuttalliana* and *E. grandiflorum* was predicted based on the phylogenetic distance between them (Figure 1.4), resulting in three distinct active anti-mitotic compounds—pulchelloid A (**2**), anemonin (**13**) and (+)-6-tuliposide A (**14**). Despite their structural differences, they share an α,β-unsaturated carbonyl moiety, which we predicted would be reduced by incubation with β-ME and result in the inhibition of their activity. Furthermore, given the well documented role of the α-methylene-γ-butyrolactone as the active moiety of many sesquiterpene lactones (Cotugno et al., 2012; Sturgeon et al., 2005), this outcome was anticipated for pulchelloid A. However, these data provided insight into the activity of anemonin and (+)-6-tuliposide A. The α,β-unsaturated carbonyl takes the form of a butenolide in anemonin, whereas in (+)-6-tuliposide A the active moiety manifests as an α,β-unsaturated ester. This suggested that this anti-mitotic activity may be more broadly due to the presence of an α,β-unsaturated carbonyl in these compounds, rather than an α-methylene-γ-butyrolactone. Therefore, the deliberate choice of these compounds for comparison was rooted in their distinct arrangements of an α,β-unsaturated system: exocyclic in pulchelloid A, endocyclic in anemonin, and linear in (+)-6-tuliposide A (Figure 5.1).

The identification of anemonin and (+)-6-tuliposide A expands the class of compounds exhibiting this mitotic arrest phenotype beyond sesquiterpene lactones. Our findings suggest that this group may encompass a broader range of compounds sharing the common feature of α,β-unsaturated carbonyls. However, it is noteworthy that certain sesquiterpene lactones are not anti-mitotic even though they possess α,β-unsaturated carbonyls. These compounds have been found to either be inactive or exhibit different biological activities, such as anti-inflammatory, anti-viral and anti-malarial (Ho et al., 2014). This indicates the remainder of the chemical structure emerges as equally crucial, likely influencing target specificity, while the α,β-unsaturated carbonyl may engage in Michael addition reactions with cellular cysteines.

While the Asteraceae plant family has historically been a source of sesquiterpene lactones (Bosco & Golsteyn, 2017; Bosco et al., 2021; Molina et al., 2021), this chemical exploration has broadened our search parameters and increased the number of examples we can draw from the literature of compounds with similar mitotic phenotypes (Figure 5.2). Isolated from the African tree *Parinari curatellifolia* (Chrysobalanaceae), 13-hydroxy-15-oxozoapatlin (OZ) (**15**) was originally thought to induce a G2 phase arrest since microtubule polymerization was not inhibited (Lee et al., 1996). Later, OZ was found to induce a 30% mitotic arrest with distorted spindles and misaligned chromosomes (Rundle et al., 2001). They proposed that OZ may interact with a motor protein to inhibit chromosome congression. Another example is *ent*-15-oxokaurenoic acid (EKA) (**16**), an *ent*-kaurene diterpenoid isolated from a tropical Asteraceae plant that induced a 20-30% mitotic arrest with abnormal spindle morphology at 20 μM in HCT116 cells (Rundle et al., 2006). Utilising a biotinylated version of EKA, they found that EKA co-localized and

bound to RanBP2 during the mitotic arrest. They suggest that this resulted in CENP-E not associating with kinetochores and chromosomes failed to congress. While not a sesquiterpene lactone, EKA contains an α,β-unsaturated carbonyl, a characteristic akin to pulchelloid A (sesquiterpene lactone), as well as anemonin and (+)-6-tuliposide A (not sesquiterpene lactones).

Adopting the chemical genetic screen approach to identify EKA, another *ent*-kaurene diterpenoid, pharicin A (**17**), was isolated from *Isodon pharicus* and was found to induce mitotic arrest in leukemia cells with misaligned chromosomes (Xu et al., 2010). Intriguingly, pharicin A induced mitotic arrest in paclitaxel-resistant cells, making it a promising avenue for cancer therapies targeting resistant tumours. Following this discovery, pharicins C through W were isolated from *I. pharicus* and a subset were reported as cytotoxic (Hu et al., 2018). Of note, their findings corroborated that the α,β-unsaturated carbonyl accounted for the activity of sculponeatin A (**18**) since sculponeatin B (**19**), lacking a carbonyl in conjunction with the methylene, proved inactive. This aligns with our results, supported by the β-ME assay, that methylene reduction of an α,β-unsaturated carbonyl leads to compound inactivation.

Further expanding the repertoire of *ent*-kaurenes, kamebakaurin (**20**), isolated from *Isodon excia*, was reported to induce mitotic arrest with multiple spindle defects and misaligned chromosomes at 50 μM (Jiang et al., 2015). Interestingly, similar to the results of our study, kamebakaurin induced mitotic cells with diffuse and abnormal numbers of pericentrin foci, indicating potential disruption of centrosome function. Another compound, bubristatin-1 (BRT-1) (**21**) featuring an α,β-unsaturated carbonyl was selected from a diterpenoid library to target BubR1 (Huang et al., 2019). Utilizing a biotinylated probe,

researchers confirmed that BRT-1 binds to BubR1. Moreover, BRT-1 extended the duration of progression from prophase to the onset of anaphase in HeLa cells, along with inducing misaligned chromosomes—results mirroring those obtained by the three compounds in our study.

Jackson *et al.* (2017) reviews the reactivity of α,β-unsaturated carbonyls with thiols, many of which were reported to exhibit anti-proliferative activities. The authors discuss the binding affinity and stability of thiol adducts that can form through Michael addition reactions, shedding light on chemical protein interactions, initially driven by noncovalent binding affinity and subsequent covalent bond formation. They provide quantitative data to elucidate that the variance in reactivity is linked to the positioning of the α,β-unsaturated carbonyl and the arrangement of surrounding atoms in the chemical structure. The distinct arrangements of an α,β-unsaturated systems in pulchelloid A, anemonin and (+)-6-tuliposide A likely contributes to their difference in activity and mechanism of action.

A warhead hypothesis has been noted by others where the highly reactive nature of "warheads", the electrophilic functional group on a covalent inhibitor, such as α,β-unsaturated carbonyls, results in arbitrary selectivity in the reaction with nucleophilic residues of proteins risking off-target toxicity (Gehringer & Laufer, 2019; Huang et al., 2022). We provide evidence that the compounds investigated in this thesis exhibit specific anti-mitotic activities at precise concentrations without indiscriminately targeting all cysteine-containing proteins through cytotoxicity. This indicates that these compounds have a high enough degree of specificity to inhibit a protein and limit toxicity. Both our results and existing literature underscore the pivotal role of the entire chemical structure of

a compound in contributing to the specificity and potency of an α,β-unsaturated carbonyl active moiety, thereby challenging a warhead hypothesis.

Phylogenetic bioprospecting, as highlighted in numerous studies (Bay-Smidt et al., 2011; Culp et al., 2020; Guzman & Molina, 2018; Larsen et al., 2010; Liana & Rungsihirunrat, 2021; Pellicer et al., 2018), has emerged as an important tool in drug discovery. Many pathways in mitosis have no known inhibitors, therefore the search for specific inhibitors holds significant value, as seen in the selection of BRT-1 to target BubR1. Our β-ME assay serves as a means to identify α,β-unsaturated carbonyl functional groups within plant extracts through a biological lens, which can be subsequently confirmed through chemistry methods. This approach also allows for an expanded phylogenetic search to identify more diverse structures with similar mitotic arrest phenotypes. In the field of precision medicine, a broader spectrum of compounds provides increased options for the development of effective and personalized treatment plans.

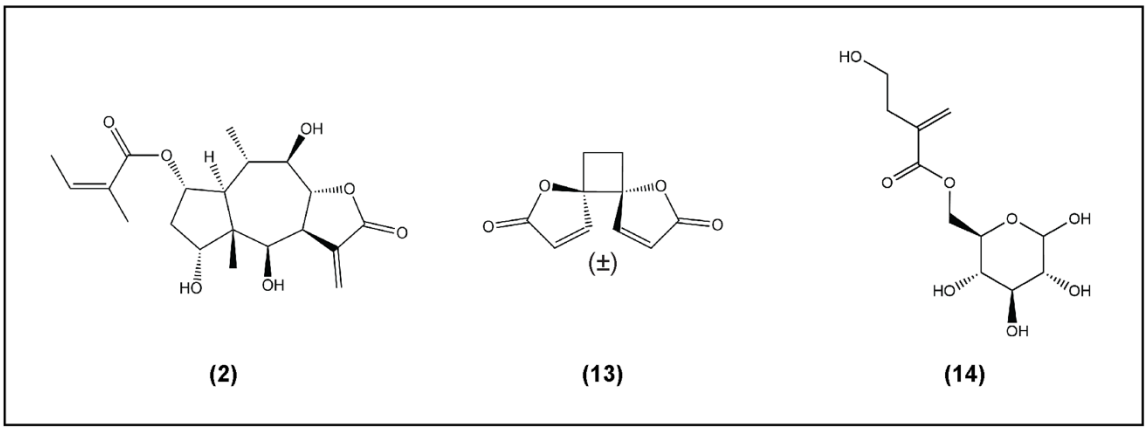

Figure 5.1. Chemical structures of the anti-mitotic compounds pulchelloid A **(2)**, anemonin **(13)** and (+)-6-tuliposide A **(14)**.

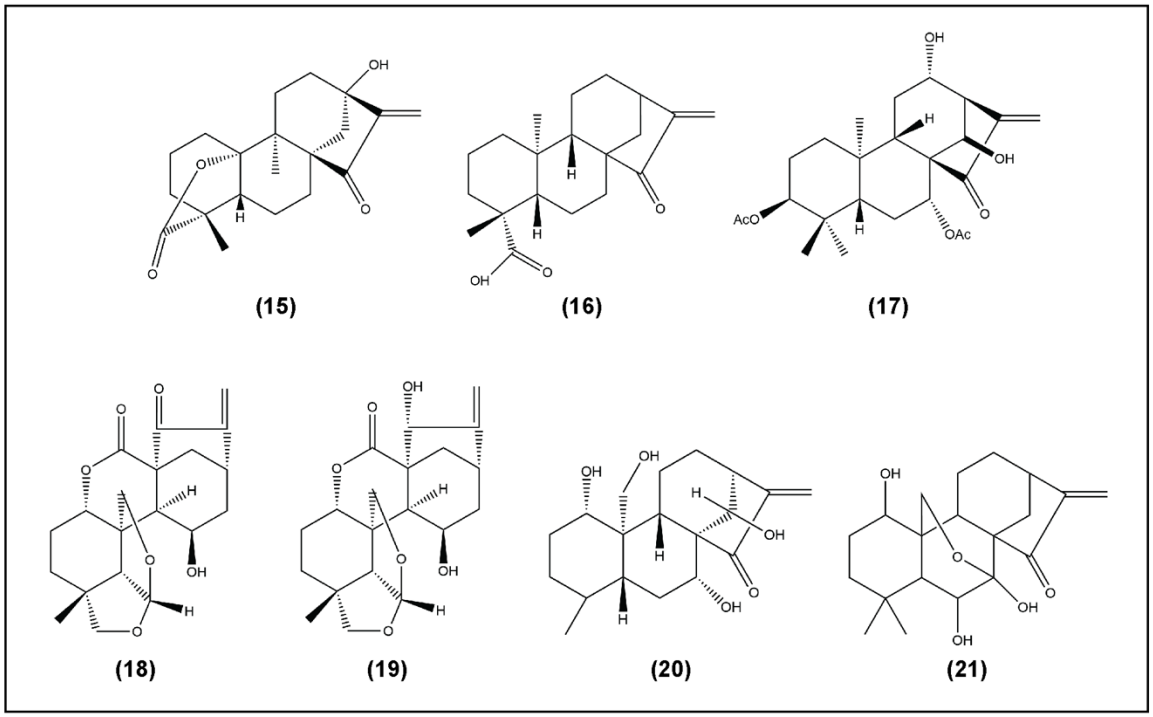

Figure 5.2. Compounds that induce similar mitotic phenotypes to pulchelloid A, anemonin and (+)-6-tuliposide A. 13-hydroxy-15-oxozoapatlin **(15)**, *ent*-15-oxokaurenoic acid **(16)**, pharicin A **(17)**, sculponeatin A **(18)**, sculponeatin B **(19)**, kamebakaurin **(20)**, and bubristatin-1 **(21)**.

5.2 Similar mitotic arrest phenotypes require further investigation to identify distinct mitotic profiles which provide evidence for different cellular protein targets

The concept that chemical structure is directly related to function implies that each compound will have a distinct protein target. The chemical structures of pulchelloid A, anemonin and (+)-6-tuliposide A suggest that they target different proteins and indicate that while their mitotic arrests have similarities, they are not identical. Pulchelloid A, anemonin, and (+)-6-tuliposide A each arrest mitosis in a manner such that chromosomes failed to congress, ultimately leading to a mitotic arrest. Upon further investigation, we identified distinct mitotic arrest profiles for the three compounds (Table 4.1), suggesting that each acts via a different mechanism. Based on these differences, we can suggest specific mitotic regulatory pathways that may be inhibited and guide research towards identifying the target of each compound.

Prometaphase is characterized by the critical process of chromosome congression, aligning the chromosomes along the metaphase plate in preparation for their subsequent segregation during mitosis. An integral aspect is the proper attachment of microtubules to kinetochores. Defects in this attachment can disrupt the tension necessary for proper chromosome alignment, contributing to misaligned chromosomes and distorted mitotic spindles, as observed in our study. Furthermore, incorrect attachment can damage DNA which further intensifies SAC signalling due to the activation of the DNA damage pathway (Guerrero et al., 2010). Incorrect attachment can occur during unperturbed mitoses, including monotelic, syntelic and merotelic attachment, however these events are typically corrected by proteins, such as Aurora kinase B, that regulate kinetochore-microtubule interactions. It is possible that the inhibition of these proteins results in failed chromosome congression followed by mitotic arrest.

The large family of centromere proteins (CENP) are essential for centromere function. One of the main drivers of chromosome congression is CENP-E, a kinesin motor protein regulated by post-translational modifications, such as farnesylation (Ashar et al., 2000) and SUMOylation (Dasso, 2008). BubR1 associates with CENP-E at the kinetochore until proper kinetochore-microtubule attachment is achieved, upon which the BubR1 signal is silenced (Mao et al., 2005). We observed sustained BubR1 signals and difference in CENP-E localization and expression in cells treated in our study with pulchelloid A, anemonin and (+)-6-tuliposide A, which suggest that CENP-E may not be functioning properly. Upstream proteins that are involved in the correct functioning of CENP-E could also be affected to cause this mitotic arrest. Aurora kinase B directs CENP-E to kinetochores (Ditchfield et al., 2003), and INCENP and RanBP2 are required for the activation and SUMOylation of Aurora kinase B to function properly in monitoring microtubule attachment to the HEC1 complex of the kinetochore (Di Cesare et al., 2023; Musacchio & Salmon, 2007; Samejima et al., 2015). RNAi depletion of RanBP2 results in mitotic cells with misaligned chromosomes, multipolar spindles, disruption of spindle poles and mislocalization of many kinetochore proteins, including CENP-E, CENP-F, and RanGAP1 (Joseph et al., 2004). Similarly, the depletion of HEC1 results in mitotic arrest due to unattached chromosomes (Martin-Lluesma et al., 2002) as with the inhibition of many kinetochore-associated proteins (Musacchio & Salmon, 2007). The *ent*-kaurene EKA was identified to bind RanBP2 and prevent the association of CENP-E with kinetochores to cause a prolonged prometaphase arrest with distorted spindle and misaligned chromosomes (Rundle et al., 2006), a mitotic phenotype similar to those obtained in our study of pulchelloid A, anemonin and (+)-6-tuliposide A.

Centrosome duplication and maturation have a significant influence on spindle formation and function during cell division. Multipolar spindles can emerge from either the overduplication of centrosomes or the abnormal separation of core centrosome proteins. Alternatively, pseudo bipolar spindles can occur by centrosome clustering after overduplication. Centrosomal abnormalities often result from the overexpression of centrosome-associated kinases, such as Aurora kinase B and PLK-4, which are integral to centrosome duplication, maturation, separation, and regulation of spindle assembly (Bühler & Stolz, 2022). PLK-4 auto-phosphorylates to signal its degradation by the E3 ubiquitin ligase SCF complex to prevent reduplication of centrioles (Holland et al., 2010; Wang et al., 2014). Interestingly, the sesquiterpene lactone 6-OAP has been reported to presumably bind Skp1, a component of the SCF complex, to induce a prometaphase arrest (Cheng et al., 2016; Liu et al., 2011; Liu et al., 2015). Although they report this chemical protein interaction does not involve cysteine chemistry, inhibition of the SCF complex can then lead to centriole accumulation, which impacts microtubule dynamics and chromosome stability. As previously mentioned, the *ent*-kaurene kamebakaurin induced a mitotic arrest with distorted spindles, misaligned chromosomes, and abnormal number of pericentrin foci (Jiang et al., 2015). In our study of pulchelloid A, anemonin and (+)-6-tuliposide A, we observed an increased number of y-tubulin and PLK-1 foci, suggesting an abnormal number of centrosomes formed, resulting in multipolar spindles. Like the eukaryotic cell cycle itself, the cycling of centrosomes involves many proteins each with regulatory enzymes to ensure accurate functionality and localization. Targeting these proteins or enzymes could lead to the mitotic arrest phenotype induced by the compounds researched in this study.

An additional level of complexity is added if we consider that proteins can have multiple roles in regulating mitosis. For example, BubR1 phosphorylates CENP-E, monitors the attachment of microtubules to kinetochores and is a part of the MCC (Huang et al., 2019), all of which are critical for ensuring the cell cycle only continues once chromosome congression has occurred properly. This emphasized the importance of identifying an inhibitor of BubR1, for which bubristatin-1 was selected and was affective in inducing a mitotic arrest (Huang et al., 2019). Another example of a multifaceted protein is CENP-F which is involved in kinetochore-microtube attachment, chromosomal stability, dynein activity and centrosome maturation. Like CENP-E, the proper localization of CENP-F is regulated by farnesylation (Hussein & Taylor, 2002; Vergnolle & Taylor, 2007) which presents an intriguing site for inhibition. Since farnesylation occurs at CAAX motifs (Hussein & Taylor, 2002), and our compounds of interest can be inactivated by β-ME reduction, our compounds may inhibit protein function by binding to cysteines in CAAX motifs, thus inhibiting farnesyl-mediated protein activation. Of interest, the farnesyltransferase inhibitor SCH66336 does not interfere with the localization of CENP-E and CENP-F to kinetochores but does impact the ability of CENP-E to associate with microtubules (Ashar et al., 2000), which is a possible explanation for the CENP-E observations in our study. Without post-translational modifications, mitotic regulatory proteins are unable to function properly and result in a prometaphase arrest, as observed in our study and many examples from the literature.

Mitosis is a highly regulated and intricate process that presents a vast number of protein targets for the inhibition of cellular proliferation. The cellular targets resulting in a prometaphase arrest could either be centromere- or kinetochore-associated proteins,

centrosomal proteins, or enzymes that regulate the function of these proteins (i.e., kinases, E3 ligases, farnesyl transferases). Additionally, transcription factors that regulate the expression of key mitotic regulatory proteins could be targeted by these compounds. It has been shown that sesquiterpene lactones target the transcription factor NF-κβ (nuclear factor κβ), as in the case of parthenolide and costunolide—compounds that induce mitotic arrests with chromosome congression defects (Berdan et al., 2019; Whipple et al., 2013). While the complexity of mitotic regulation presents challenges, it also offers numerous potential targets for intervention. Ultimately, understanding the precise targets of pulchelloid A, anemonin, and (+)-6-tuliposide A in the context of early mitotic events will contribute to the development of targeted therapies and enhance our knowledge of mitotic regulation.

5.3 Future Directions

We have expanded the number of natural products with which to inhibit mitosis and distinguished that each compound exhibits a distinct mitotic arrest profile, suggesting different mechanisms of action. Subsequent investigations should focus on identifying their precise protein targets. One strategy is to utilize click-chemistry, a technique by which a compound can be labelled and covalently bound to its target in native biological environments, such as cell cultures, followed by protein identification by mass spectrometry (Parker & Pratt, 2020). Previous researchers employing this approach have been successful in identifying the cellular targets for specific compounds (Banuelos et al., 2016; Do et al., 2021). In collaboration with Dr. Raymond Andersen at the University of British Columbia, our laboratory aims to identify the target of pulchelloid A (**2**). Modifying pulchelloid A by attaching an alkyne group (**22**) permits a copper (I)-catalyzed azide-alkyne

cycloaddition “click” reaction to biotin, from which the complex can be pulled down on a streptavidin column and proteins can be identified by mass spectrometry (Figure 5.3). Other researchers have had success in labelling small molecules directly with biotin to permit compound localization by immunofluorescence microscopy or protein identification through pull downs for mass spectrometry. However, the addition of an alkynyl group is designed to be sterically minimized compared to attaching biotin directly to the inhibitor. In parallel, chemical-genetic interaction screens can be used to identify genes that are positively or negatively corelated with the inhibitor. In collaboration with Dr. Charles Boone at the University of Toronto, we are conducting a chemical-genetic CRISPR screen in haploid human cells to identify genes that are positively and negatively correlated with cell viability after treatment with pulchelloid A. Identifying the precise cellular target of pulchelloid A will provide another manner to inhibit mitosis and may contribute to the development of a targeted medicine.

Natural products, including those identified in this thesis, stand out as exceptional source of anti-mitotic compounds, having evolved under ecological pressures and optimized to be compatible with biological pathways. Their tremendous potential as both scientific tools and novel therapies for precision medicine emphasizes the need for continued research in the field natural products. This highlights the importance of exploring natural products as a reservoir of biologically active compounds, particularly in under-investigated regions like the Canadian prairie, to uncover unique and diverse compounds. This thesis contributes to the broader landscape of natural product discovery and enhances our understanding of the intricate connections between nature and human health.

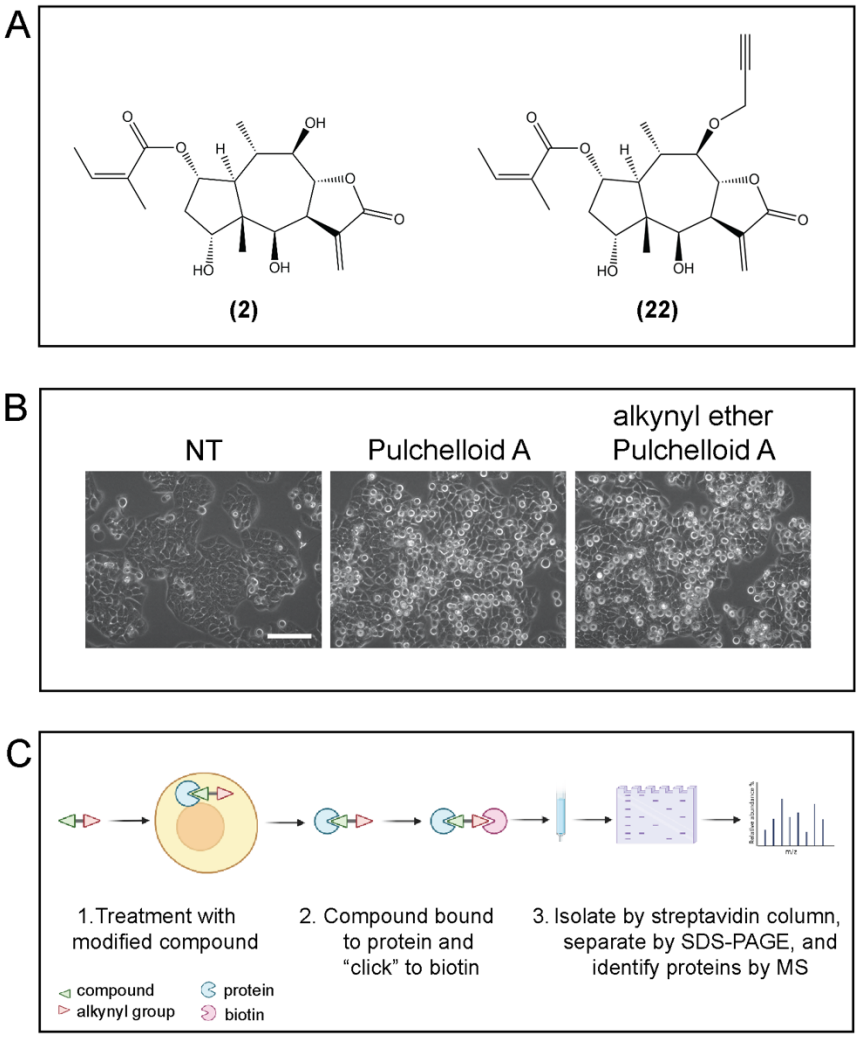

Figure 5.3. Click-chemistry approach to identify cellular targets. **A.** Pulchelloid A **(2)** and an alkynyl ether modified structure of pulchelloid A **(22)**. **B.** Pulchelloid A maintains its cell rounding activity when modified with an alkynyl group. Scale bar represent 100 µm. **C.** Click-chemistry protocol for identifying cellular targets of alkynyl ether modified structure of pulchelloid A.

REFERENCES

Ali, I., Khatoon, S., Amber, F., Abbas, Q., Ismail, M., Engel, N., & Ahmad, V. U. (2019). Isolation of anemonin from *Pulsatilla wallichiana* and its biological activities. *Journal of the Chemical Society of Pakistan*, *41*, 325-333.

Arakaki, M., Christin, P., Nyffeler, R., Lendel, A., Eggli, U., Ogburn, R. M., Spriggs, E., Moore, M. J., & Edwards, E. J. (2011). Contemporaneous and recent radiations of the world's major succulent plant lineages. *Proceedings of the National Academy of Sciences*, *108*, 8379-8384.

Ashar, H. R., James, L., Gray, K., Carr, D., Black, S., Armstrong, L., Bishop, W. R., & Kirschmeier, P. (2000). Farnesyl transferase inhibitors block the farnesylation of CENP-E and CENP-F and alter the association of CENP-E with the microtubules. *Journal of Biological Chemistry*, *275*, 30451-30457.

Bailly, C. (2021). Anticancer targets and signaling pathways activated by britannin and related pseudoguaianolide sesquiterpene lactones. *Biomedicines*, *9*, 1325-1343.

Bain, J., Flanagan, J., & Kuijt, J. (2014). *Common Coulee Plants of Southern Alberta*. University of Lethbridge.

Bak, D. W., Bechtel, T. J., Falco, J. A., & Weerapana, E. (2019). Cysteine reactivity across the subcellular universe. *Current Opinion in Chemical Biology*, *48*, 96-105.

Banuelos, C. A., Tavakoli, I., Tien, A. H., Caley, D. P., Mawji, N. R., Li, A., Wang, J., Yang, Y. C., Imanura, Y., Yan, L., Wen, J. G., Andersen, R. J., & Sadar, M. D. (2016). Sintokamide A is a novel antagonist of androgen receptor that uniquely binds activation function-1 in its amino-terminal domain. *Journal of Biological Chemistry*, *291*, 22231-22243.

Bay-Smidt, M. G. K., Jäger, A. K., Krydsfeldt, K., Meerow, A. W., Stafford, G. I., Van Staden, J., & Rønsted, N. (2011). Phylogenetic selection of target species in Amaryllidaceae tribe Haemantheae for acetylcholinesterase inhibition and affinity to the serotonin reuptake transport protein. *South African Journal of Botany*, *77*, 175-183.

Beaubien, E., & Hamann, A. (2011). Spring folwering response to climate change between 1936 and 2006 in Alberta, Canada. *BioScience*, *61*, 514-524.

Berdan, C. A., Ho, R., Lehtola, H. S., To, M., Hu, X., Huffman, T. R., Petri, Y., Altobelli, C. R., Demeulenaere, S. G., Olzmann, J. A., Maimone, T. J., & Nomura, D. K. (2019). Parthenolide covalently targets and inhibits focal adhesion kinase in breast cancer cells. *Cell Chemical Biology*, *26*, 1027-1035.

Bolanos-Garcia, V. M. (2014). Formation of multiprotein assemblies in the nucleus: the spindle assembly checkpoint. *International Review of Cell and Molecular Biology*, *307*, 151-174.

Bosco, A., & Golsteyn, R. M. (2017). Emerging anti-mitotic activities and other bioactivities of sesquiterpene compounds upon human cells. *Molecules*, *22*, 459-481.

Bosco, A., Molina, L., Kernéis, S. M., Hatzopoulos, G., Favez, T., Gonczy, P., Tantapakul, C., Maneerat, W., Yeremy, B., Williams, D. E., Andersen, R. J., & Golsteyn, R. M. (2021). Pulchelloid A, a sesquiterpene lactone from the Canadian prairie plant *Gaillardia aristata* inhibits mitosis in human cells. *Molecular Biology Reports*, *48*, 5459-5471.

Bühler, M., & Stolz, A. (2022). Estrogens—origin of centrosome defects in human cancer? *Cells*, *11*, 432-461.

Chadwick, M., Trewin, H., Gawthrop, F., & Wagstaff, C. (2013). Sesquiterpene lactones: benefits to plants and people. *International Journal of Molecular Science*, *14*, 12780-12805.

Chen, G., & Deng, X. (2018). Cell synchronization by double thymidine block. *Bio-Protocol*, *8*, 1-5.

Cheng, X., Liu, Y. Q., Wang, G. Z., Yang, L. N., Lu, Y. Z., Li, X. C., Zhou, B., Qu, L. W., Wang, X. L., Cheng, Y. X., Liu, J., Tao, S. C., & Zhou, G. B. (2016). Proteomic identification of the oncoprotein STAT3 as a target of a novel Skp1 inhibitor. *Oncotarget*, *8*, 2681-2693.

Christensen, L. P. (1995). Tuliposides from *Alstroemeria revoluta*. *Phytochemistry*, *38*, 1371-1373.

Costantino, V. V., Lobos-Gonzales, L., Ibañez, J., Fernandez, D., Cuello-Carrión, F. D., Valenzuela, M. A., Barbieri, M. A., Semina, S. N., Jahn, G. A., Quest, A. F. G., & Lopez, L. A. (2016). Dehydroleucodine inhibits tumour growth in a preclinical

melanoma model by inducing cell cycle arrest, senescence and apoptosis. *Cancer Letters*, *372*, 10-23.

Cotugno, R., Fortunato, R., Santoro, A., Gallotta, D., Braca, A., De Tommasi, N., & Belisario, M. A. (2012). Effect of sesquiterpene lactone coronopilin on leukaemia cell population growth, cell type-specific induction of apoptosis and mitotic catastrophe. *Cell Proliferation*, *45*, 53-65.

Cragg, G. M. (1998). Paclitaxel (Taxol): a success story with valuable lessons for natural product drug discovery and development. *Medical Research Reviews*, *18*, 315-331.

Culp, E. J., Waglechner, N., Wang, W., Fiebig-Comyn, A. A., Hsu, Y. P., Koteva, K., Sychantha, D., Coombes, B. K., Van Nieuwenhze, M. S., Brun, Y. V., & Wright, G. D. (2020). Evolution-guided discovery of antibiotics that inhibit peptidoglycan remodelling. *Nature*, *578*, 582-587.

Dalton, W. B., Nandan, M. O., Moore, R. T., & Yang, V. W. (2007). Human cancer cells commonly acquire DNA damage during mitotic arrest. *Cancer Research*, *67*, 11487-11492.

Dasso, M. (2008). Emerging roles of the SUMO pathway in mitosis. *Cell Division*, *3*, 5-16.

Desbène, S., & Giorgi-Renault, S. (2002). Drugs that inhibit tubulin polymerization: the particular case of podophyllotoxin and analogues. *Current Medicinal Chemistry*, *2*, 71-90.

Di Cesare, E., Moroni, S., Bartoli, J., Damizia, M., Giubettini, M., Koerner, C., Krenn, V., Musacchio, A., & Lavia, P. (2023). Aurora B SUMOylation is restricted to centromeres in early mitosis and requires RANBP2. *Cells*, *12*, 372-391.

Ditchfield, C., Johnson, V. L., Tighe, A., Ellston, R., Haworth, C., Johnson, T., Mortlock, A., Keen, N., & Taylor, S. S. (2003). Aurora B couples chromosome alignment with anaphase by targeting BubR1, Mad2, and Cenp-E to kinetochores. *The Journal of Cell Biology*, *161*, 267-280.

Do, Q., Huang, T., Liu, Y., Tai, J., & Chen, S. (2021). Identification of cytosolic protein target of catechol estrogens in breast cancer cells using a click chemistry-based workflow. *Journal of Proteome Research*, *20*, 624-633.

dos Santos, G. S., Teixeira, T. R., Colepicolo, P., & Debonsi, H. M. (2021). Natural products from the poles: structural diversity and biological activities. *Revista Brasileira de Farmacognosia*, *31*, 531-560.

Duan, H., Zhang, Y., Xu, J., Qiao, J., Suo, Z., Hu, G., & Mu, X. (2006). Effect of anemonin on NO, ET-1 and ICAM-1 production in rat intestinal microvascular endothelial cells. *Journal of Ethnopharmacology*, *104*, 362-366.

Erb, M., & Kliebenstein, D. J. (2020). Plant secondary metabolites as defenses, regulators, and primary metabolites: the blurred functional trichotomy. *Plant Physiology*, *184*, 39-52.

Fang, H., Zhang, Y., Lin, C., Sun, Z., Wen, W., Sheng, H., & Lin, J. (2023). Primary microcephaly gene CENPE is a novel biomarker and potential therapeutic target for non-WNT/non-SHH medulloblastoma. *Frontiers in Immunology*, *14*, 1227143-1227155.

Fonrose, X., Ausseil, F., Soleilhac, E., Masson, V., David, B., Pouny, I., Cintrat, J.-C., Rousseau, B., Barette, C., Massiot, G., & Lafanechère, L. (2007). Parthenolide inhibits tubulin carboxypeptidase activity. *Cancer Research*, *67*, 3371-3378.

Gallego-Jara, J., Lozano-Terol, G., Sola-Martínez, R. A., Cánovas-Díaz, M., & de Diego Puente, T. (2020). A compressive review about taxol: history and future challenges. *Molecules*, *25*, 5986-6010.

Gascoigne, K. E., & Taylor, S. S. (2008). Cancer cells display profound intra- and interline variation following prolonged exposure to antimitotic drugs. *Cancer Cell*, *14*, 111-122.

Gehringer, M., & Laufer, S. A. (2019). Emerging and re-emerging warheads for targetted covalent inhibitors: applications in medicinal chemistry and chemical biology. *Journal of Medicinal Chemistry*, *62*, 5673-5724.

Goto, H., Yasui, Y., Nigg, E. A., & Inagaki, M. (2002). Aurora-B phosphorylates histone H3 at serine28 with regard to the mitotic chromosome condensation. *Genes to Cells*, *7*, 11-17.

Guénard, D., Guéritte-Voegelein, F., & Potier, P. (1993). Taxol and taxotere: discovery, chemistry, and structure-activity relationships. *American Chemical Society*, *26*, 160-167.

Guerrero, A. A., Martinez, A. C., & van Wely, K. H. (2010). Merotelic attachments and non-homologous end joining are the basis of chromosomal instability. *Cell Division*, *5*, 13-21.

Guo, M., Jin, J., Zhao, D., Rong, Z., Cao, L. Q., Li, A. H., Sun, X. Y., Jia, L. Y., Wang, Y. D., Huang, L., Li, Y. H., He, Z. J., Li, L., Ma, R. K., Lv, Y. F., Shao, K. K., & Cao, H. L. (2022). Research advances on anti-cancer natural products. *Frontiers in Oncology*, *12*, 866154-866171.

Guzman, E., & Molina, J. (2018). The predictive utility of the plant phylogeny in identifying sources of cardiovascular drugs. *Pharmaceutical Biology*, *56*, 154-164.

Hanahan, D., & Weinberg, R. A. (2011). Hallmarks of cancer: the next generation. *Cell*, *144*, 646-674.

Hartmann, T. (1996). Diversity and variability of plant secondary metabolism: a mechanistic view. *Entomologia Experimentalis et Applicata*, *80*, 177-188.

Hendzel, M. J., Wei, Y., Mancini, M. A., Hooser, A. V., Ranalli, T., Brinkley, B. R., Bazett-Jones, D. P., & Allis, D. (1997). Mitosis-specific phosphorylation of histone H3 initiates primarily within pericentromeric heterochromatin during G2 and spreads in an ordered fashion coincident with mitotic chromosome condensation. *Chromosoma*, *106*, 348-360.

Ho, W. E., Peh, H. Y., Chan, T. K., & Wong, W. S. (2014). Artemisinins: pharmacological actions beyond anti-malarial. *Pharmacology & Therapeutics*, *142*, 126-139.

Hoffmann, T., Krug, D., Bozkurt, N., Duddela, S., Jansen, R., Garcia, R., Gerth, K., Steinmetz, H., & Müller, R. (2018). Correlating chemical diversity with taxonomic distance for discovery of natural products in myxobacteria. *Nature Communications*, *9*, 803-813.

Holland, A. J., Lan, W., Niessen, S., Hoover, H., & Cleveland, D. W. (2010). Polo-like kinase 4 kinase activity limits centrosome overduplication by autoregulating its own stability. *Journal of Cell Biology*, *188*, 191-198.

Holt, S. V., Vergnolle, M. A., Hussein, D., Wozniak, M. J., Allan, V. J., & Taylor, S. S. (2005). Silencing Cenp-F weakens centromeric cohesion, prevents chromosome alignment and activates the spindle checkpoint. *Journal of Cell Science*, *118*, 4889-4900.

Hu, Z. X., Liu, M., Wang, W. G., Li, X. N., Hu, K., Li, X. R., Du, X., Zhang, Y. H., Puno, P. T., & Sun, H. D. (2018). 7alpha,20-epoxy-ent-kaurane diterpenoids from the aerial parts of *Isodon pharicus*. *Journal of Natural Products*, *81*, 106-116.

Huang, A. C., & Osbourn, A. (2019). Plant terpenes that mediate below-ground interactions: prospects for bioengineering terpenoids for plant protection. *Pest Management Science*, *75*, 2368-2377.

Huang, F., Han, X., Xiao, X., & Zhou, J. (2022). Covalent warheads targetting cysteine residue: the promising approach in drug development. *Molecules*, *27*, 7728-7746.

Huang, H., Hittle, J., Zappacosta, F., Annan, R. S., Hershko, A., & Yen, T. J. (2008). Phosphorylation sites in BubR1 that regulate kinetochore attachment, tension, and mitotic exit. *Journal of Cell Biology*, *183*, 667-680.

Huang, Y., Lin, L., Liu, X., Ye, S., Yao, P. Y., Wang, W., Yang, F., Gao, X., Li, J., Zhang, Y., Zhang, J., Yang, Z., Liu, X., Yang, Z., Zang, J., Teng, M., Wang, Z., Ruan, K., Ding, X., . . . Yao, X. (2019). BubR1 phosphorylates CENP-E as a switch enabling the transition from lateral association to end-on capture of spindle microtubules. *Cell Research*, *29*, 562-578.

Huang, Y. H., Lee, T. H., Chan, K. J., Hsu, F. L., Wu, Y. C., & Lee, M. H. (2008). Anemonin is a natural bioactive compound that can regulate tyrosinase-related proteins and mRNA in human melanocytes. *Journal of Dermatological Science*, *49*, 115-123.

Hussein, D., & Taylor, S. S. (2002). Farnesylation of Cenp-F is required for G2/M progression and degradation after mitosis. *Journal of Cell Science*, *115*, 3403-3414.

Ibrahim, M. F., Hussain, F. H. S., Zanoni, G., & Vidari, G. (2017). The main constituents of *Tulipa systola* Stapf. roots and flowers; their antioxidant activities. *Natural Products Research*, *31*, 2001-2007.

Inayama, S., Harimaya, K., Ohkura, T., & Kawamata, T. (1982). Isolation and structures of Pulchelloid A and Pulchelloid B, new pseudoguaianolides from *Gaillardia pulchella*. *Heterocycles*, *17*, 219-223.

Isah, T., Umar, S., Mujib, A., Sharma, M. P., Rajasekharan, P. E., Zafar, N., & Frukh, A. (2018). Secondary metabolism of pharmaceuticals in the plant in vitro cultures: strategies, approaches, and limitations to achieving higher yield. *Plant Cell, Tissue and Organ Culture*, *132*, 239-265.

Jaakola, L., & Hohtola, A. (2010). Effect of latitude on flavonoid biosynthesis in plants. *Plant, Cell & Environment*, *33*, 1239-1247.

Jackson, P. A., Widen, J. C., Harki, D. A., & Brummond, K. M. (2017). Covalent modifiers: a chemical perspective on the reactivity of alpha,beta-unsaturated carbonyls with thiols via hetero-michael addition reactions. *Journal of Medicinal Chemistry*, *60*, 839-885.

Jia, L., Li, B., & Yu, H. (2016). The Bub1-Plk1 kinase complex promotes spindle checkpoint signalling through Cdc20 phosphorylation. *Nature Communications*, *7*, 10818-10832.

Jiang, L., Chi, C., Yuan, F., Lu, M. H., Hu, D., Wang, L., & Liu, X. (2022). Anti-inflammatory effects of anemonin on acute ulcerative colitis via targeted regulation of protein kinase C-θ. *Chinese Medicine*, *17*, 39-51.

Jiang, S., Du, J., Kong, Q., Li, C., Li, Y., Sun, H., Pu, J., & Mao, B. (2015). A group of *ent*-kaurane diterpenoids inhibit hedgehog signaling and induce cilia elongation. *Public Library of Science One*, *10*, 1371-1385.

Jie, Y., Yang, X., & Chen, W. (2022). *Pulsatilla decoction* combined with 5-fluorouracil triggers immunogenic cell death in the colorectal cancer cells. *Cancer Biotherapy & Radiopharmaceuticals*, *37*, 945-954.

Joglekar, A. P. (2016). A cell biological perspective on past, present and future investigations of the spindle assembly checkpoint. *Biology*, *5*, 44-63.

Johnson, L., Goping, I. S., Rieger, A., Mane, J. Y., Huzil, T., Banerjee, A., Luduena, R., Hassani, B., Winter, P., & Tuszynski, J. A. (2017). Novel colchicine derivatives and their anti-cancer activity. *Current Topics in Medicinal Chemistry*, *17*, 2538-2558.

Joseph, J., Liu, S. T., Jablonski, S. A., Yen, T. J., & Dasso, M. (2004). The RanGAP1-RanBP2 complex is essential for microtubule-kinetochore interactions in vivo. *Current Biology*, *14*, 611-617.

Kearns, C. M. (1997). Pharmacokinetics of the taxanes. *Pharmacotherapy*, *17*, 105S-109S.

Kernéis, S., Swift, L. H., Lewis, C. W., Bruyère, C., Oumata, N., Ruchaud, S., Bain, J., & Golsteyn, R. M. (2015). Natural product extracts of the Canadian prairie plant,

Thermopsis rhombifolia, have anti-cancer activity in phenotypic cell-based assays. *Natural Products Research*, *29*, 1026-1034.

Kershaw, L., & Allen, L. (2020). *Vascular Flora of Alberta: An illustrated guide*.

Kim, Y., Kim, S. B., You, Y. J., & Ahn, B. Z. (2002). Deoxypodophyllotoxin: the cytotoxic and antiangiogenic component from *Pulsatilla koreana*. *Planta Medica*, *68*, 271-274.

Kingston, D. G. I. (2021). My 60-year love affair with natural products. *Journal of Natural Products*, *84*, 932-948.

Kubara, P. M., Kernéis-Golsteyn, S., Studény, A., Lanser, B. B., Meijer, L., & Golsteyn, R. M. (2012). Human cells enter mitosis with damaged DNA after treatment with pharmacological concentrations of genotoxic agents. *Biochemical Journal*, *446*, 373-381.

Kuijt, J. (1982). *A Flora of Waterton Lakes National Park*. University of Alberta Press.

Lagoutte, R., Serba, C., Abegg, D., Hoch, D. G., Adibekian, A., & Winssinger, N. (2016). Divergent synthesis and identification of the cellular targets of deoxyelephantopins. *Nature Communications*, *7*, 12470-12481.

Lara-Gonzalez, P., Pines, J., & Desai, A. (2021). Spindle assembly checkpoint activation and silencing at kinetochores. *Seminars in Cell and Developmental Biology*, *117*, 86-98.

Larsen, M. M., Adsersen, A., Davis, A. P., Lledó, M. D., Jäger, A. K., & Rønsted, N. (2010). Using a phylogenetic approach to selection of target plants in drug discovery of acetylcholinesterase inhibiting alkaloids in Amaryllidaceae tribe Galantheae. *Biochemical Systematics and Ecology*, *38*, 1026-1034.

Łaska, G., Maciejewska-Turska, M., Sieniawska, E., Swiatek, L., Pasco, D. S., & Balachandran, P. (2021). Extracts from *Pulsatilla patens* target cancer-related signaling pathways in HeLa cells. *Scientific Reports*, *11*, 10654-10670.

Łaska, G., Sienkiewicz, A., Stocki, M., Zjawiony, J. K., Sharma, V., Bajguz, A., Piotrowska-Niczyporuk, A., Jacob, M., & Khan, S. (2019). Phytochemical

screening of *Pulsatilla* species and investigation of their biological activities. *Acta Societatis Botanicorum Poloniae*, *88*, 3613.

Lazzarotto, M., Hammerer, L., Hetmann, M., Borg, A., Schmermund, L., Steiner, L., Hartmann, P., Belaj, F., Kroutil, W., Gruber, K., & Fuchs, M. (2019). Chemoenzymatic total synthesis of deoxy-, *epi*-, and podophyllotoxin and a biocatalytic kinetic resolution of dibenzylbutyrolactones. *Angewandte Chemie International Edition*, *58*, 8226-8230.

Lee, I., Shamon, L. A., Chai, H., Chagwedra, T. E., Besterman, J. M., Farnsworth, N. R., Cordell, G. A., Pezzuto, J. M., & Kinghorn, A. D. (1996). Cell-cycle specific cytotoxicity mediated by rearranged *ent*-kaurene diterpenoids isolated from *Parinari curatellifolia*. *Chemico-Biological Interactions*, *99*, 193-204.

Lewis, C. W., & Golsteyn, R. M. (2016). Cancer cells that survive checkpoint adaptation contain micronuclei that harbor damaged DNA. *Cell Cycle*, *15*, 3131-3145.

Li, Y., Wang, S., Wei, X., Zhang, S., Song, Z., Chen, X., & Zhang, J. (2019). Role of inhibitor of yes-associated protein 1 in triple-negative breast cancer with taxol-based chemoresistance. *Cancer Science*, *110*, 561-567.

Li, Y. N., Ning, N., Song, L., Geng, Y., Fan, J. T., Ma, C. Y., & Jiang, H. Z. (2021). Derivatives of deoxypodophyllotoxin induce apoptosis through Bcl-2/Bax proteins expression. *Anti-Cancer Agents Medicinal Chemistry*, *21*, 611-620.

Liana, D., & Rungsihirunrat, K. (2021). Phytochemical screening, antimalarial activities, and genetic relationship of 16 indigenous Thai Asteraceae medicinal plants: A combinatorial approach using phylogeny and ethnobotanical bioprospecting in antimalarial drug discovery. *Journal of Advanced Pharmaceutical Technology & Research*, *12*, 254-260.

Lin, Z., Wu, C., Chuang, Y., & Chuang, W. (2013). Anti-cancer mechanisms of clinically acceptable colchicine concentrations on hepatocellular carcinoma. *Life Sciences*, *93*, 323-328.

Liu, Y., Chen, X. Q., Liang, H. X., Zhang, F. X., Zhang, B., Jin, J., Chen, Y. L., Cheng, Y. X., & Zhou, G. B. (2011). Small compound 6-O-angeloylplenolin induces mitotic arrest and exhibits therapeutic potentials in multiple myeloma. *Public Library of Science One*, *6*, e21930.

Liu, Y., Wang, X., Cheng, X., Lu, Y., Wang, G., Li, X., Zhang, J., Wen, Z., Huang, Z., Gao, Q., Yang, L., Cheng, Y., Tao, S., Liu, J., & Zhou, G. (2015). Skp1 in lung cancer: clinical significance and therapeutic efficacy of its small molecule inhibitors. *Ocotarget*, *6*, 34953-34967.

Lobanovska, M., & Pilla, G. (2017). Penicillin's discovery and antibiotic resistance: lessons for the future? *Yale Journal of Biology and Medicine*, *90*, 135-145.

Luna-Maldonado, F., Andonegui-Elguera, M. A., Diaz-Chavez, J., & Herrera, L. A. (2021). Mitotic and DNA damage response proteins: maintaining the genome stability and working for the common good. *Frontiers in Cell and Developmental Biology*, *9*, 700162-700178.

Maiato, H., Gomes, A. M., Sousa, F., & Barisic, M. (2017). Mechanisms of chromosome congression during mitosis. *Biology*, *6*, 13-69.

Malumbres, M. (2014). Cyclin-dependent kinases. *Genome Biology*, *15*, 122-132.

Mao, Y., Desai, A., & Cleveland, D. W. (2005). Microtubule capture by CENP-E silences BubR1-dependent mitotic checkpoint signaling. *Journal of Cell Biology*, *170*, 873-880.

Martin-Lluesma, S., Stucke, V. M., & Nigg, E. A. (2002). Role of Hec1 in spindle checkpoint signaling and kinetochore recruitment of Mad1/Mad2. *Science*, *297*, 2267-2270.

Miller, J. S. (2011). The discovery of medicines from plants: a current biological perspective. *Economic Botany*, *65*, 396-407.

Mimaki, Y., Yokosuka, A., Kuroda, M., & Sashida, Y. (2001). Cytotoxic activities and structure-cytotoxic relationships of steroidal saponins. *Biological and Pharmaceutical Bulletin*, *24*, 1286-1289.

Mirzaa, G. M., Vitre, B., Carpenter, G., Abramowicz, I., Gleeson, J. G., Paciorkowski, A. R., Cleveland, D. W., Dobyns, W. B., & O'Driscoll, M. (2014). Mutations in CENPE define a novel kinetochore-centromeric mechanism for microcephalic primordial dwarfism. *Human Genetics*, *133*, 1023-1039.

Moerman, D. E. (2009). *Native American Medicinal Plants: An Ethnobotanical Dictionary*. Timber Press, Inc.

Moffat, J. G., Vincent, F., Lee, J. A., Eder, J., & Prunotto, M. (2017). Opportunities and challenges in phenotypic drug discovery: an industry perspective. *Nature Reviews Drug Discovery*, *16*, 531-543.

Molina, L., Allard, H. K., Kernéis, S. M., & Golsteyn, R. M. (2022). Connecting plant species and natural products from the Canadian prairie ecological zone to biomedical knowledge. *Botany*, *100*, 231-245.

Molina, L., Williams, D. E., Andersen, R. J., & Golsteyn, R. M. (2021). Isolation of a natural product with anti-mitotic activity from a toxic Canadian prairie plant. *Heliyon*, *7*, e07131.

Moriarty, R. M., Romain, C. R., Karle, I. L., & Karle, J. (1965). The structure of anemonin. *Journal of the American Chemical Society*, *87*, 3251-3252.

Moss, E. H., & Packer, J. G. (1983). *Flora of Alberta: A manual of flowering plants, conifers, ferns, and fern allies found growing without cultivation in the province of Alberta, Canada*. University of Toronto Press.

Mosyakin, S. L. (2016). Nomenclature notes on North American taxa of Anemonastrum and *Pulsatilla* (Ranunculaceae), with comments on the circumscription of *Anemone* and related genera. *Phytoneuron*, *79*, 1-12.

Musacchio, A., & Salmon, E. D. (2007). The spindle-assembly checkpoint in space and time. *Nature Reviews Molecular Cell Biology*, *8*, 379-393.

Newman, D. J. (2022). Natural products and drug discovery. *National Science Review*, *9*, 206-227.

Newman, D. J., & Cragg, G. M. (2020). Natural products as sources of new drugs over the nearly four decades from 01/1981 to 09/2019. *Journal of Natural Products*, *83*, 770-803.

Ning, Z., Hu, B., Sun, Y. Y., Ding, J. F., Han, X. Y., Lu, X. L., Yin, Z. F., He, Y., Jiao, B. H., Yu, H. B., & Liu, X. Y. (2024). Eutypellaolides A-J sesquiterpene diversity

expansion of the polar fungus *Eutypella* sp. D-1. *Frontiers in Microbiology*, *15*, 1349151-1349162.

Ninkuu, V., Zhang, L., Yan, J., Fu, Z., Yang, T., & Zeng, H. (2021). Biochemistry of terpenes and recent advances in plant protection. *International Journal of Molecular Science*, *22*, 5710-5732.

Ohashi, A., Ohori, M., Iwai, K., Nambu, T., Miyamoto, M., Kawamoto, T., & Okaniwa, M. (2015). A novel time-dependent CENP-E inhibitor with potent antitumor activity. *Public Library of Science One*, *10*, e0144675.

Orth, J. D., Loewer, A., Lahav, G., & Mitchison, T. J. (2012). Prolonged mitotic arrest triggers partial activation of apoptosis, resulting in DNA damage and p53 induction. *Molecular Biology of the Cell*, *23*, 567-576.

Owa, M., & Dynlacht, B. (2021). A non-canonical function for centromere-associated protein-E controls centrosome integrity and orientation of cell division. *Communications Biology*, *4*, 358-370.

Park, B. H., Jung, K. H., Son, M. K., Seo, J. H., Lee, H. S., Lee, J. H., & Hong, S. S. (2013). Antitumor activity of *Pulsatilla koreana* extract in anaplastic thyroid cancer via apoptosis and anti-angiogenesis. *Molecular Medicine Reports*, *7*, 26-30.

Parker, C. G., & Pratt, M. R. (2020). Click chemistry in proteomic investigations. *Cell*, *180*, 605-632.

Pavarini, D. P., Pavarini, S. P., Niehues, M., & Lopes, N. P. (2012). Exogenous influences on plant secondary metabolite levels. *Animal Feed Science and Technology*, *176*, 5-16.

Pellicer, J., Saslis-Lagoudakis, C. H., Carrió, E., Ernst, M., Garnatje, T., Grace, O. M., Gras, A., Mumbrú, M., Vallès, J., Vitales, D., & Rønsted, N. (2018). A phylogenetic road map to antimalarial *Artemisia* species. *Journal of Ethnopharmacology*, *225*, 1-9.

Perron-Sierra, F. M., Kucharkzyk, N., Boucley, C., Guyard-Daumas, C., Sciberras, S., Fouache, F., Plantier, S., Studeny, A., Bossard, C., Casara, P. J., & Golsteyn, R. M. (2012). Synthesis of cis-fused pyran indolocarbazole derivatives that inhibit FLT3 kinase and the DNA damage kinase, checkpoint kinase 1. *Anti-Cancer Agents in Medicinal Chemistry*, *12*, 194-201.

Prosser, S. L., & Pelletier, L. (2017). Mitotic spindle assembly in animal cells: a fine balancing act. *Nature Reviews Molecular Cell Biology*, *18*, 187-201.

Quignon, F., Rozier, L., Lachages, A. M., Bieth, A., Simili, M., & Debatisse, M. (2007). Sustained mitotic block elicits DNA breaks: one-step alteration of ploidy and chromosome integrity in mammalian cells. *Oncogene*, *26*, 165-172.

Ren, Y., Yu, J., & Kinghorn, A. D. (2016). Development of anticancer agents from plant-derived sesquiterpene lactones. *Current Medicinal Chemistry*, *23*, 2397-2420.

Rieder, C. L., & Maiato, H. (2004). Stuck in division or passing through: what happens when cells cannot satisfy the spindle assembly checkpoint. *Developmental Cell*, *7*, 637-651.

Rogakou, E. P., Pilch, D. R., Orr, A. H., Ivanova, V. S., & Bonner, W. M. (1998). DNA double-stranded breaks induce histone H2AX phosphorylation on serine 139. *Journal of Biological Chemistry*, *273*, 5858-5868.

Rundle, N. T., Nelson, J., Flory, M. R., Joseph, J., Th'ng, J., Aebersold, R., Dasso, M., Andersen, R. J., & Roberge, M. (2006). An *ent*-kaurene that inhibits mitotic chromosomes movement and binds the kinetochore protein ran-binding protein 2. *American Chemical Society Chemical Biology*, *1*, 443-450.

Rundle, N. T., Xu, L., Andersen, R. J., & Roberge, M. (2001). G2 DNA damage checkpoint inhibition and antimitotic activity of 13-hydroxy-15-oxozoapatlin. *Journal of Biological Chemistry*, *276*, 48231-48236.

Saidi, R., Ghrab, F., Kallel, R., El Feki, A., Boudawara, T., Chesné, C., Ammar, E., & Mezghani Jarraya, R. (2018). Tunisian *Clematis flammula* essential oil enhances wound healing: GC-MS analysis, biochemical and histological assessment. *Journal of Oleo Science*, *67*, 1483-1499.

Samejima, K., Platani, M., Wolny, M., Ogawa, H., Vargiu, G., Knight, P. J., Peckham, M., & Earnshaw, W. C. (2015). The inner centromere protein (INCENP) coil is a single alpha-helix (SAH) domain that binds directly to microtubules and is important for chromosome passenger complex (CPC) localization and function in mitosis. *Journal of Biological Chemistry*, *290*, 21460-21472.

Santucci, B., Picardo, M., Iavarone, C., & Trogolo, C. (1985). Contact dermatitis to Alstroemeria. *Contact Dermatitis*, *12*, 215-219.

Saslis-Lagoudakis, C. H., Savolainen, V., Williamson, E. M., Forest, F., Wagstaff, S. J., Baral, D. R., Watson, M. F., Pendry, C. A., & Hawkins, J. A. (2012). Phylogenies reveal predictive power of traditional medicine in bioprospecting. *Proceedings of the National Academy of Sciences*, *109*, 15835-15840.

Scaria, B., Sood, S., Raad, C., Khanafer, J., Jayachandiran, R., Pupulin, A., Grewal, S., Okoko, M., Arora, M., Miles, L., & Pandey, S. (2020). Natural health products (NHP's) and natural compounds as therapeutic agents for the treatment of cancer; mechanisms of anti-cancer activity of natural compounds and overall trends. *International Journal of Molecular Science*, *21*, 8480-8512.

Schiff, P. B., Fant, J., & Horwitz, S. B. (1979). Promotion of microtubule assembly *in vitro* by taxol. *Nature*, *277*, 665-667.

Schmucker, S., & Sumara, I. (2014). Molecular dynamics of PLK1 during mitosis. *Molecular & Cellular Oncology*, *1*, e954507.

Seaman, F. C. (1982). Sesquiterpene lactones as taxonomic characters in the Asteraceae. *The Botanical Review*, *48*, 121-592.

Shannon, K. B., Canman, J. C., & Salmon, E. D. (2002). Mad2 and BubR1 function in a single checkpoint pathway that responds to a loss of tension. *Molecular Biology of the Cell*, *13*, 3706-3719.

She, Z. Y., Yu, K. W., Zhong, N., Xiao, Y., Wei, Y. L., Lin, Y., Li, Y. L., & Lu, M. H. (2020). Kinesin-7 CENP-E regulates chromosome alignment and genome stability of spermatogenic cells. *Cell Death Discovery*, *6*, 25-42.

Son, M. K., Jung, K. H., Hong, S., Lee, H., Zheng, H., Choi, M., Seo, J. H., Suh, J., & Hong, S. S. (2013). SB365, *Pulsatilla* saponin D suppresses the proliferation of human colon cancer cells and induces apoptosis by modulating the AKT/mTOR signalling pathway. *Food Chemistry*, *136*, 26-33.

Sotillo, W. S., Villagomez, R., Smiljanic, S., Huang, X., Malakpour, A., Kempengren, S., Rodrigo, G., Almanza, G., Sterner, O., & Oredsson, S. (2017). Anti-cancer stem cell activity of a sesquiterpene lactone isolated from *Ambrosia arborescens* and of a synthetic derivative. *Public Library of Science One*, *12*, e0184304.

Spasevska, I., Ayoub, A. T., Winter, P., Preto, J., Wong, G. K., Dumontet, C., & Tuszynski, J. A. (2017). Modeling the *Colchicum autumnale* tubulin and a comparison of its

interaction with colchicine to human tubulin. *International Journal of Molecular Science*, *18*, 1676-1690.

Srivastava, S., Misra, A., Shukla, P. K., Kumar, B., Lata, S., & Rawat, A. K. S. (2014). A validated over pressured layered chromatography (OPLC) method for separation and quantification of colchicine in *Gloriosa superba* (L.) tubers from different geographical regions. *Royal Society of Chemistry*, *4*, 60902-60906.

Sturgeon, C. M., Craig, K., Brown, C., Rundle, N. T., Andersen, R. J., & Roberge, M. (2005). Modulation of the G2 cell cycle checkpoint by sesquiterpene lactones psilostachyins A and C isolated from the common ragweed *Ambrosia artemisiifolia*. *Planta Medica*, *71*, 938-943.

Swift, L. H., & Golsteyn, R. M. (2016). Development of anticancer agents from plant-derived sesquiterpene lactones. *Biology of the Cell*, *108*, 127-148.

Swift, L. H., & Golsteyn, R. M. (2018). Experimental determination of checkpoint adaptation by mitotic shake-off and microscopy. *Methods in Molecular Biology*, *1769*, 159-168.

Swinney, D. C., & Anthony, J. (2011). How were new medicines discovered? *Nature Reviews Drug Discovery*, *10*, 507-519.

Szenteczki, M. A., Godschalx, A. L., Gauthier, J., Gibernau, M., Rasmann, S., & Alvarez, N. (2022). Transcriptomic analysis of deceptively pollinated *Arum maculatum* (Araceae) reveals association between terpene synthase expression in floral trap chamber and species-specific pollinator attraction. *Genes Genomes Genetics*, *12*, 175-189.

Tannas, K. (2004). *Common Plants of the Western Rangelands: Forbs*. Alberta Agriculture, Food and Rural Development.

Thornburg, C. C., Britt, J. R., Evans, J. R., Akee, R. K., Whitt, J. A., Trinh, S. K., Harris, M. J., Thompson, J. R., Ewing, T. L., Shipley, S. M., Grothaus, P. G., Newman, D. J., Schneider, J. P., Grkovic, T., & O'Keefe, B. R. (2018). NCI program for natural product discovery: a publicly-accessible library of natural product fractions for high-throughput screening. *American Chemical Society Chemical Biology*, *13*, 2484-2497.

Tietje, M., Antonelli, A., Baker, W. J., Govaerts, R., Smith, S. A., & Eiserhardt, W. L. (2022). Global variation in diversification rate and species richness are unlinked in plants. *Proceedings of the National Academy of Sciences*, *119*, e2120662119.

Tietje, M., Antonelli, A., Forest, F., Govaerts, R., Smith, S. A., Sun, M., Baker, W. J., & Eiserhardt, W. L. (2023). Global hotspots of plant phylogenetic diversity. *New Phytologist*, *240*, 1636-1646.

Tuescher, J. M. (2018). *Extracts from the prairie plant Symphoricarpos occidentalis or the natural product, Pheophorbide A, induce light-dependent vacuolation of human cells* University of Lethbridge].

Tuescher, J. M., Beck, C. R., Spencer, L., Yeremy, B., Shi, T., Andersen, R. J., & Golsteyn, R. M. (2021). Extracts prepared from a Canadian toxic plant induce light-dependent perinuclear vacuoles in human cells. *Toxins*, *13*, 138-153.

Tuescher, J. M., Tailfeathers, D., Kernéis, S. M., Baratte, B., Ruchaud, S., Bach, S., Batut, M., Pouny, I., Sautel, F., & Golsteyn, R. M. (2020). The Canadian prairie plant *Thermopsis rhombifolia* contains luteolin, a flavone that inhibits cyclin dependent kinase 9 and arrest cells in the G1-phase of the cell cycle. *Journal of Natural Health Product Research*, *2*, 1-14.

Ulloa, C. U., Acevedo-Rodríguez, P., Beck, S., Belgrano, M. J., Bernal, R., Berry, P. E., Brako, L., Celis, M., Davidse, G., Forzza, R. C., Gradstein, S. R., Hokche, O., León, B., León-Yánez, S., Magill, R. E., Neill, D. A., Nee, M., Raven, P. H., Stimmel, H., . . . Jørgensen, P. M. (2017). An integrated assessment of the vascular plant species of the Americas. *Science*, *358*, 1614-1617.

van Vugt, M. A., van de Weerdt, B. C., Vader, G., Janssen, H., Calafat, J., Klompmaker, R., Wolthuis, R. M., & Medema, R. H. (2004). Polo-like kinase-1 is required for bipolar spindle formation but is dispensable for anaphase promoting complex/Cdc20 activation and initiation of cytokinesis. *Journal of Biological Chemistry*, *279*, 36841-36854.

Vergnolle, M. A., & Taylor, S. S. (2007). Cenp-F links kinetochores to Ndel1/Nde1/Lis1/dynein microtubule motor complexes. *Current Biology*, *17*, 1173-1179.

Vermeulen, K., Van Bockstaele, D. R., & Berneman, Z. N. (2003). The cell cycle: a review of regulation, deregulation and therapeutic targets in cancer. *Cell Proliferation*, *36*, 131-149.

Wang, G., Jiang, Q., & Zhang, C. (2014). The role of mitotic kinases in coupling the centrosome cycle with the assembly of the mitotic spindle. *Journal of Cell Science*, *127*, 4111-4122.

Wang, Z., Huang, J., Zhou, S., Luo, F., Xu, W., Wang, Q., Tan, Q., Chen, L., Wang, J., Chen, H., Chen, L., Xie, Y., & Du, X. (2017). Anemonin attenuates osteoarthritis progression through inhibiting the activation of the IL-1B/NF-κB pathway. *Journal of Cellular and Molecular Medicine*, *21*, 3231-3243.

Wani, M. C., Taylor, H. L., Wall, M. E., Coggon, P., & McPhail, A. T. (1971). The isolation and structure of taxol, a novel antileukemic and antitumor from *Taxus brevifolia*. *American Chemical Society*, *93*, 2325-2327.

Whipple, R. A., Vitolo, M. I., Boggs, A. E., Charpentier, M. S., Thompson, K., & Martin, S. S. (2013). Parthenolide and costunolide reduce microtentacles and tumor cell attachment by selectively targeting detyrosinated tubulin independent from NF-κB inhibition. *Breast Cancer Research*, *15*, 83-95.

Wikström, N., Savolainen, V., & Chase, M. W. (2001). Evolution of the angiosperms: calibrating the family tree. *Proceedings of the Royal Society of London*, *268*, 2211-2220.

Williams, D. E., & Andersen, R. J. (2020). Biologically active marine natural products and their molecular targets discovered using a chemical genetic approach. *Natural Products Reports*, *37*, 617-633.

Wilson, B. A. P., Thornburg, C. C., Henrich, C. J., Grkovic, T., & O'Keefe, B. R. (2020). Creating and screening natural product libraries. *Natural Products Reports*, *37*, 893-918.

Wink, M. (2003). Evolution of secondary metabolites from an ecological and molecular phylogenetic perspective. *Phytochemistry*, *64*, 3-19.

Wu, R., Xi, Z., Liu, M., Ren, H., Dai, R., Jiang, X., Nik Nabil, W. N., Wang, Y., Feng, J., Chai, Q., Dong, Q., & Xu, H. (2023). *Pulsatilla decoction* and its bioactive component beta-peltatin induce G2/M cell cycle arrest and apoptosis in pancreatic cancer. *Chinese Medicine*, *18*, 61-74.

Xu, H. Z., Huang, Y., Wu, Y. L., Zhao, Y., Xiao, W. L., Lin, Q. S., Sun, H. D., Dai, W., & Chen, G. Q. (2010). Pharicin A, a novel natural *ent*-kaurene diterpenoid, induces

mitotic arrest and mitotic catastrophe of cancer cells by interfering with BubR1 function. *Cell Cycle*, *9*, 2897-2907.

Yeshi, K., Crayn, D., Ritmejerytė, E., & Wang, P. (2022). Plant secondary metabolites produced in response to abiotic stress has potential application in pharmaceutical product development. *Molecules*, *27*, 313-344.

Yu, K. W., Zhong, N., Xiao, Y., & She, Z. Y. (2019). Mechanisms of kinesin-7 CENP-E in kinetochore-microtubule capture and chromosome alignment during cell division. *Biology of the Cell*, *111*, 143-160.

Zwicker, P., Schultze, N., Niehs, S., Methling, K., Wurster, M., Albrecht, D., Bernhardt, J., Wachlin, G., Lalk, M., Lindequist, U., & Haertel, B. (2016). A proteomic approach for the identification of immunotoxic properties of tulipalin A. *Proteomics*, *16*, 2997-3008.

APPENDIX I – Supplementary Material for Chapter 2:

Two anti-mitotic activities are present in extracts from the Canadian Prairie Crocus,

Pulsatilla nuttalliana

Supplemental Figure 2.1

Anemonin (1): Isolated as an off-white solid; ^{1}H NMR (DMSO-d_6, 500 MHz): δ 8.28 (2H, d, J = 5.7 Hz, H-3 and H-8), 6.32 (2H, d, J = 5.7 Hz, H-2 and H-9), 2.62 (2H, m, H-5' and H-6'), 2.26 (2H, m, H-5 and H-6) ppm; ^{13}C NMR (DMSO-d_6, 125 MHz) δ 171.41 (C-1 and C-10), 156.14 (C-3 and C-8), 119.71 (C-2 and C-9), 89.98 (C-4 and C-7), 22.82 (C-5 and C-6) ppm.

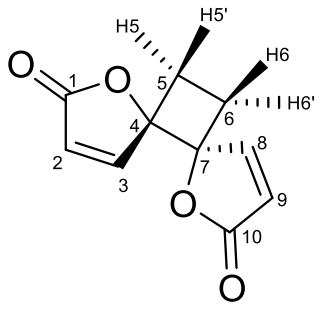

1

Supplemental Figure 2.2

^{1}H NMR Spectrum of Anemonin (**1**) recorded at 500 MHz in DMSO-d_6

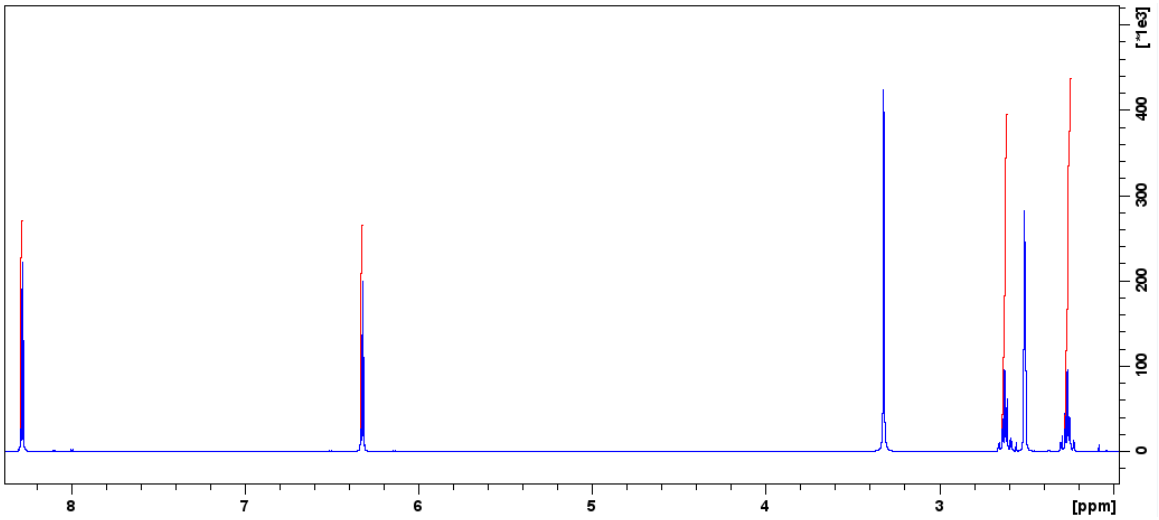

Supplemental Figure 2.3

^{13}C NMR Spectrum of Anemonin (**1**) recorded at 125 MHz in DMSO-d_6

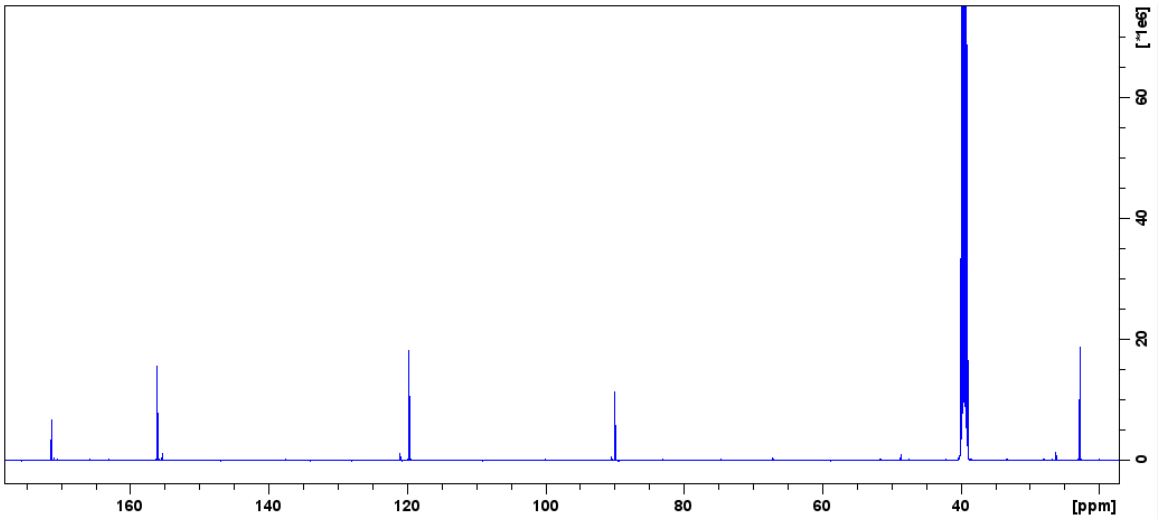

APPENDIX II – Supplementary Material for Chapter 3:

An anti-mitotic compound, (+)-6-tuliposide A, isolated from the Canadian Glacier Lily, *Erythronium grandiflorum*

Supplemental Figure 3.1

(+)-6-Tuliposide A (1): Isolated as a colourless viscous oil; $[\alpha]^{25}_{D}$ +44° (c 0.6, MeOH), see Ibrahim et al., 2017; ^{1}H NMR, see Christensen, 1995 and Santucci, 1985; ^{13}C NMR (D_2O, compare to Christensen, 1995 and Santucci et al., 1985) δ 169.53/169.52 (C-1'), 137.12 (C-2'), 129.88/129.84 (C-3'), 60.86 (C-5'), 35.00 (C-4') ppm; α-D-glucose: 93.02 (C-1), 72.30 (C-2), 73.47 (C-3), 70.13 (C-4), 70.59 (C-5), 64.48 (C-6) ppm; β-D-glucose: 96.88 (C-1), 74.93 (C-2), 76.42 (C-3), 70.48 (C-4), 74.31 (C-5), 64.44 (C-6) ppm; ^{13}C NMR (DMSO-d_6) δ 166.35/166.34 (C-1'), 137.47/137.42 (C-2'), 124.43/126.37 (C-3'), 59.48/59.47 (C-5'), 34.97/34.94 (C-4') ppm; D-glucose: 96.92 (C-1), 92.30 (C-1), 76.37, 74.70, 73.45, 72.82, 72.18, 70.48, 70.08, 69.15, 64.19 (C-6), 64.14 (C-6) ppm; positive ion HRESIMS $[M+Na]^+$ *m/z* 301.0905 (calcd for $C_{11}H_{18}O_8Na$, 301.0894).

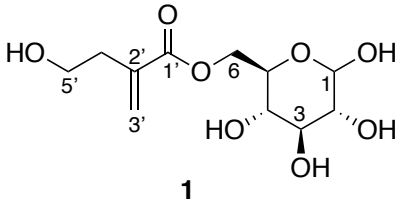

1

Supplemental Figure 3.2

^{1}H NMR Spectrum of (+)-6-Tuliposide A (**1**) recorded at 600 MHz in D_2O

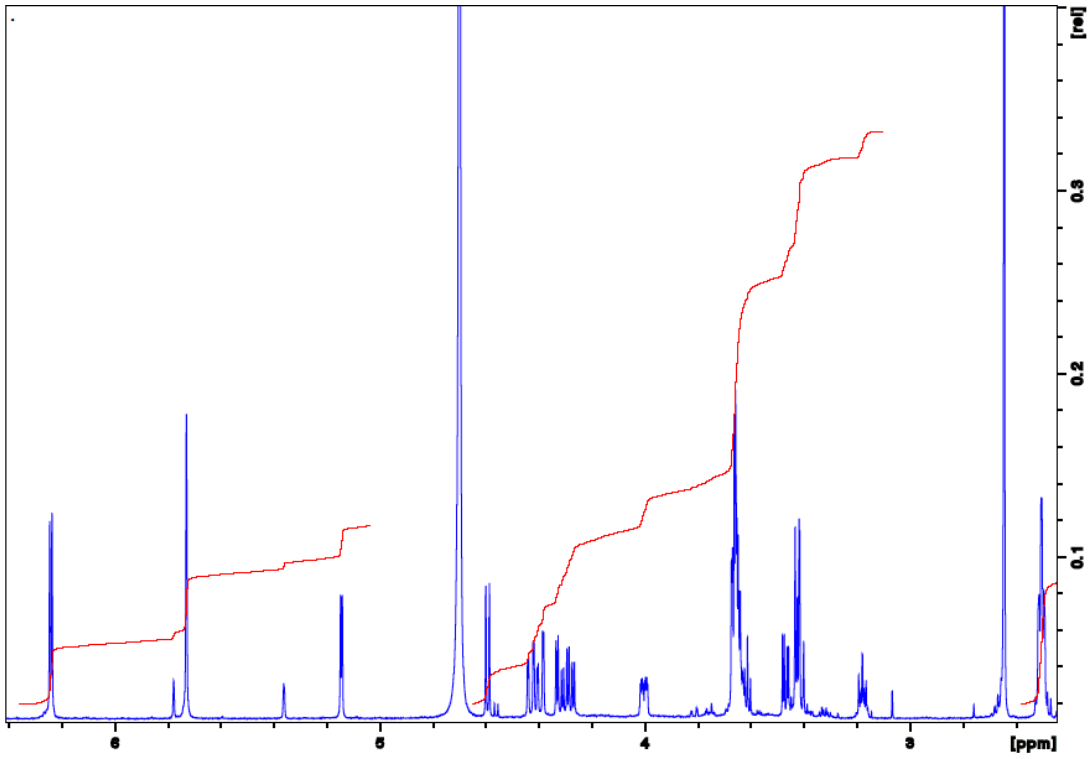

Supplemental Figure 3.3

^{1}H NMR Spectrum of (+)-6-Tuliposide A (**1**) recorded at 600 MHz in DMSO-d_6

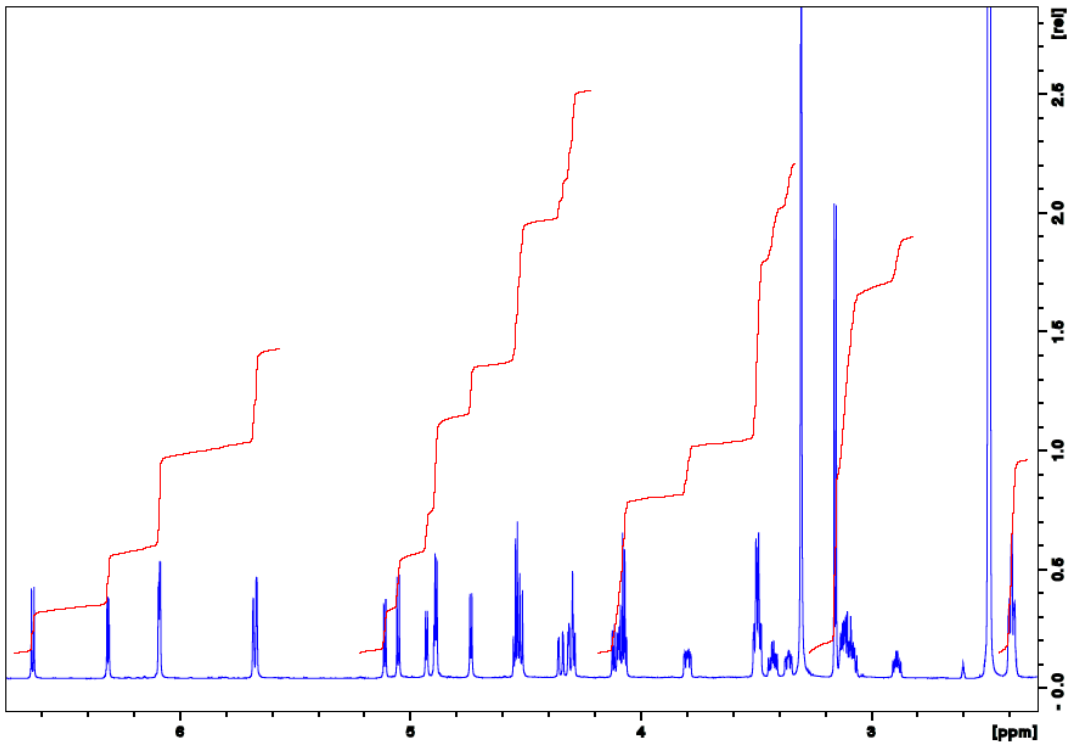

Supplemental Figure 3.4

^{13}C NMR Spectrum of (+)-6-Tuliposide A (**1**) recorded at 150 MHz in D_2O

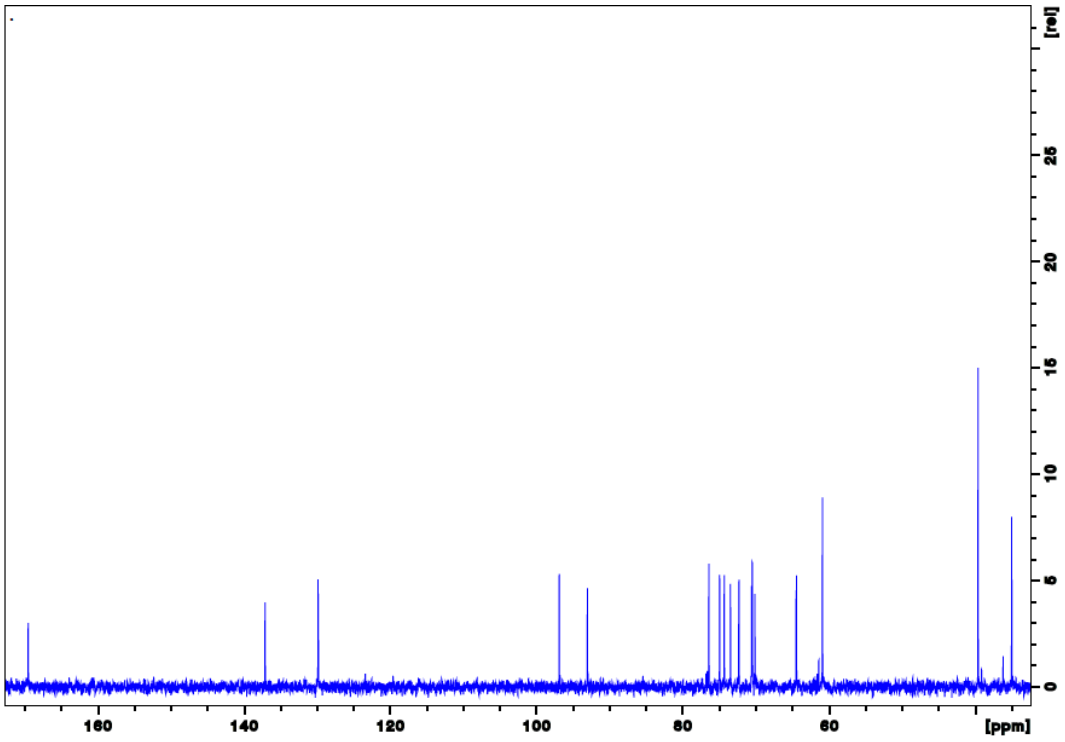

Supplemental Figure 3.5

^{13}C NMR Spectrum of (+)-6-Tuliposide A (**1**) recorded at 150 MHz in DMSO-d_6